WORKING PAPER · NO. 2024-77

Is Workplace Temperature a Valuable Job Amenity? Implications for Climate Change

Ashwin Rode, Rachel E. Baker, Tamma Carleton, Anthony Louis D'Agostino, Michael Delgado, Timothy Foreman, Diana R. Gergel, Michael Greenstone, Trevor Houser, Solomon Hsiang, Andrew Hultgren, Amir Jina, Robert E. Kopp, Steven B. Malevich, Kelly E. McCusker, Ishan Nath, Matthew Pecenco, James Rising, Jiacan Yuan

JULY 2024 (UPDATED OCTOBER 2024)

EPIC
ENERGY POLICY INSTITUTE
AT THE UNIVERSITY OF CHICAGO

An Affiliated Center of
Becker Friedman Institute

5757 S. University Ave.
Chicago, IL 60637
Main: 773.702.5599
bfi.uchicago.edu

Is workplace temperature a valuable job amenity? Implications for climate change*

Ashwin Rode, Rachel E. Baker, Tamma Carleton, Anthony Louis D'Agostino, Michael Delgado, Timothy Foreman, Diana R. Gergel, Michael Greenstone, Trevor Houser, Solomon Hsiang, Andrew Hultgren, Amir Jina, Robert E. Kopp, Steven B. Malevich, Kelly E. McCusker, Ishan Nath, Matthew Pecenco, James Rising, Jiacan Yuan*

*Rode: University of Chicago (email: aarode@uchicago.edu); Baker: Brown University (email: rachel_e_baker@brown.edu); Carleton: University of California, Berkeley, and NBER (email: tcarleton@berkeley.edu); D'Agostino: Mathematica (email: ADagostino@mathematica-mpr.com); Delgado: Rhodium Group (email: mdelgado@rhg.com); Foreman: International Institute for Applied Systems Analysis (email: foreman@iiasa.ac.at); Gergel: RWE AI Research Lab (email: diana.gergel@rwe.com); Greenstone: University of Chicago and NBER (email: mgreenst@uchicago.edu); Houser: Rhodium Group (email: tghouser@rhg.com); Hsiang: Stanford University, and NBER (email: solhsiang@stanford.edu); Hultgren: University of Illinois Urbana-Champaign (email: ahultgr@illinois.edu); Jina: University of Chicago and NBER (email: amirjina@uchicago.edu); Kopp: Rutgers University (email: robert.kopp@rutgers.edu); Malevich: Climate Impact Lab (email: smalevich@impactlab.org); McCusker: Climate Impact Lab (email: kmccusker@impactlab.org); Nath: Federal Reserve Bank of San Francisco (email: Ishan.Nath@sf.frb.org); Pecenco: Brown University (email: matthew_pecenco@brown.edu); Rising: University of Delaware (email: jrising@udel.edu); Yuan: Fudan University (email: jcyuan@fudan.edu.cn). This project is an output of the Climate Impact Lab consortium that received funding from the Energy Policy Institute of Chicago (EPIC), the Alfred P. Sloan Foundation, the Carnegie Corporation, the International Growth Centre, King Philanthropies, the Ray and Dagmar Dolby Fund, the Skoll Global Threats Fund, the Tata Center for Development, and the US National Science Foundation. Tamma Carleton acknowledges funding from the U.S. Environmental Protection Agency Science To Achieve Results Fellowship (no. FP91780401). James Rising acknowledges funding from the H2020-MSCA-RISE project GEMCLIME-2020 GA number 681228. We are grateful for the support of the University of Chicago's Research Computing Center for assistance with the calculations carried out in this work. We thank David Card, Jisung Park, and numerous workshop participants at IZA, the Federal Reserve Bank of San Francisco, UCLA, UC Santa Barbara, AERE, NBER Summer Institute, Toulouse School of Economics, London School of Economics, and Princeton University. We thank Laura Alcocer, Thomas Bearpark, Kate Champion, Trinetta Chong, Delgerzaya Delgerjargal, Greg Dobbels, Ruozhou Du, Rebecca Frost, Jonah Gilbert, Radhika Goyal, Simon Greenhill, Dylan Hogan, Azhar Hussain, Theodor Kulczycki, Ruixue Li, Maya Norman, Sebastien Phan, Christina Schwarz, Nishka Sharma, Justin Simcock, Emile Tenezakis, Yuqi Song, Jingyuan Wang, and Jong-kai Yang for invaluable research assistance during all stages of this project, and we thank Samantha Anderson, Jack Chang, Megan Landín, and Terin Mayer for excellent project management. We acknowledge the World Climate Research Programme's Working Group on Coupled Modeling, which is responsible for CMIP, and we thank the climate modeling groups for producing and making available their model output. For CMIP, the U.S. Department of Energy's Program for Climate Model Diagnosis and Intercomparison provides coordinating support and led development of software infrastructure in partnership with the Global Organization for Earth System Science Portals. Any views expressed in this paper are those of the authors and do not necessarily represent the views of the Federal Reserve System or its staff. This version: Thursday 3rd October, 2024.

Abstract

Using data representing one-third of the world's population, we find that extreme hot and cold days cause substantial labor supply declines for weather-exposed workers, but not for weather-protected workers. With these results and a simple theoretical framework, we calculate that the value of a weather-protected job's thermal comfort varies widely globally but is worth 2.9% of annual income on average. We project that climate change will increase worker thermal discomfort by 1.8% of global GDP in 2099 under a very high emissions scenario and 0.5% under an intermediate scenario, demonstrating the importance of this new category of climate damages.

I Introduction

Willingness-to-pay for goods that lack an explicit market is a topic of considerable interest to economists and policymakers. An area of particular interest has been workplace amenities. It is widely recognized that a worker derives well-being not only from a job's wage compensation, but also from its non-wage amenities, which include predictable working hours, a comfortable work environment, and safety from health hazards, including mortality risk. At least since Smith (1776) and more formally in Rosen's (1974) seminal work, the "compensating differentials" theory has posited that jobs with unpleasant working conditions must offer a wage premium over similar jobs with more pleasant working conditions. However, despite its theoretical grounding, decisive field evidence has been challenging to marshal due to the potential for confounding the impact of the target job amenity with others that are unobserved, and endogenous sorting such that higher ability workers have jobs with better unobserved amenities (Lavetti, 2023). As a result of these challenges, the value workers place on workplace amenities remains poorly understood, with credible empirical studies typically confined to selected settings (Greenberg et al., 2021; Kolstad and Kowalski, 2016; Mas and Pallais, 2017; Wissmann, 2022).

One potentially important job amenity that, to the best of our knowledge, has not been studied previously is thermal comfort or temperature-induced labor disutility. As climate change is causing new temperature records to be set regularly and policymakers grapple with the appropriate ways to protect workers,[1] the importance of worker thermal discomfort is becoming apparent. Although it is commonly understood that extreme hot or cold temperatures make people uncomfortable, irritable, and generally unhappy, the magnitude of workers' willingness-to-pay for thermal discomfort is unknown. Because globally over 60% of prime age adults work, even small influences of temperature on individual workers have the potential to accumulate into large effects in aggregate. Importantly, the willingness-to-pay for thermal comfort on the job is distinct from temperatures' effects on labor supply and productivity, which have both been the subject of well developed literatures (e.g., Graff Zivin and Neidell (2014), Somanathan et al. (2018)).[2] However, no existing study quantifies willingness-to-pay (WTP) to avoid temperature-induced labor disutility.

This paper has three main parts that together demonstrate that worker disutility from extreme temperatures is an imporant non-wage workplace amenity and projects that it

[1] See President Biden's recent announcement described here: https://www.reuters.com/world/us/dangerous-us-heat-wave-pushes-eastward-capping-globes-record-july-2023-07-27/.

[2] Building on a century of laboratory, factory, and military experiments (Bell and Watts, 1971; Glazer, 2005; Hancock, Ross, and Szalma, 2007; Huntington, 1922; Parsons, 2014; Pilcher, Nadler, and Busch, 2002; Ramsey, 1995; Seppanen, Fisk, and Lei, 2006; Vaile et al., 2008; Wyon, 2001), Graff Zivin and Neidell (2014) and Garg, Gibson, and Sun (2019) provide estimates for the effect of temperature on labor supply using time use survey data from the US and China respectively, while macroeconomic analyses suggest that labor productivity effects are a channel through which temperature affects economic output (Burke, Hsiang, and Miguel, 2015; Deryugina and Hsiang, 2014; Heal and Park, 2013; Hsiang, 2010; Zhang et al., 2018).

will become a substantial share of the costs of climate change. The first part develops a simple approach to recover an expression of workers' WTP for thermal comfort. The key insight is that the workers optimal condition for time spent at work equates the marginal disutility of labor with the wage. Practically, we embed this idea in a framework where wages are set periodically (i.e., annually), labor supply is determined daily, and the amenity (e.g., temperature) arrives daily. Workers choose their labor supply in response to the wage they earn and the disutility they experience while working, which varies with temperature.

The model allows us to derive a expression for the WTP for thermal comfort that we use throughout the analysis. Specifically, this expression is equal to the change in labor supply due to the temperature change multiplied by the ratio of the wage rate and the elasticity of labor supply with respect to wages, holding the marginal utility of wealth constant (i.e., the Frisch elasticity of labor supply). In many respects, our approach is the obverse of the canonical compensating differentials literature for estimating the value of non-pecuniary job characteristics (Rosen, 1986; Thaler and Rosen, 1976), because we assume that wages are fixed and labor supply is elastic while that approach assumes that workers supply labor inelastically and that wages are flexible. We believe that our approach is better suited for daily amenities, like daily temperatures, while the canonical one is better suited for more permanent amenities.

The second part of the paper quantifies the current value of workplace thermal comfort at high spatial resolution globally using a novel dataset on individuals' labor supply and historical weather data. We constructed a data set containing daily or weekly minutes worked for over 6 million individual workers by harmonizing disparate time use and labor force surveys from seven countries representing nearly a third of the world's population (i.e., Brazil, France, India, Mexico, Spain, UK, USA). These data are complemented with daily, $0.25° \times 0.25°$ globally harmonized historical climate data.

We find an inverse-U relationship between weekly minutes worked for workers in high-risk, weather-exposed industries (i.e., agriculture, mining, construction, and manufacturing), with a daily high temperature of 40° C (104° F) leading to 29 fewer minutes worked, relative to a 27° C (81° F) day. It is noteworthy that there is effectively no relationship between time spent working and daily high temperatures for workers in the rest of the economy, which we consider low risk for weather exposure. This finding is presumably due to indoor cooling and heating. These results are derived from rich econometric models that exploit within-location daily variation in weather to identify plausibly causal effects.

With these results and the paper's theoretical framework, we estimate the global average value of thermal comfort provided by a low-risk job relative to a high-risk job as equal to 2.9% of annual income. It is noteworthy that the WTP for a low-risk job is substantially larger in regions that frequently experience either extremely hot (e.g., it is 8.3% in Baghdad) or cold (e.g., 6.8% in Oslo) temperatures. Thus, this workplace amenity appears comparable in magnitude in utility terms to previously studied ones, including observed differences in on-the-job mortality risk (Greenberg et al., 2021), a

smoke-free workplace (Wissmann, 2022), and employer-sponsored health insurance (Kolstad and Kowalski, 2016).

The third part applies the economic model and estimated labor supply-temperature relationships to project the increase in worker disutility from predicted temperature change due to climate change. Specifically, we calculate the compensating variation necessary to offset the change in the utility value of workers' thermal comfort caused by projected climate change. Importantly, the projections account for predicted evolutions in the shares of high- and low-risk workers regionally as economies develop and the climate warms (e.g., the share of high-risk workers is lower in wealthier locations). The broad approach to estimating these costs of climate change follows the one outlined in Rode et al. (2021), Carleton et al. (2022), Hultgren et al. (2022), and Depsky et al. (2023).

We find that end-of-century global labor disutility costs due to projected climate change amount to roughly 1.8% of 2099 global GDP under a very high emissions scenario and fall to about 0.5% under an intermediate emissions scenario, demonstrating the benefits of mitigation.[3] The costs are highly heterogeneous with a substantially higher burden in the parts of the world that are poorer and hotter today. Additionally, the net present value of the global welfare costs due to labor disutility from the release of an additional ton of CO_2, which we refer to as the labor disutility "partial" social cost of carbon (SCC), is a substantial share of the *total* SCC (i.e., all measureable climate damages). For example, the United States Government used this working paper's research to include the labor disutility costs in its 2023 updating of the SCC; its inclusion increased the SCC by \$38.50, raising it by 25% (from \$151.10 to \$189.60), making apparent the importance of this new category of climate damages.[4]

The rest of the paper is organized as follows: Section II develops a theoretical framework to understand how a change in temperature can affect workers and firms; Section III details the data sources used in this analysis, which include work hours data, historical and projected future climate data, and socioeconomic covariates; Section IV explains the econometric approach for estimating the impact of temperature on labor supply on high-and low-risk workers; Section V presents the results of the econometric analysis and calculates the hedonic value of thermal comfort in a low-risk job; Section VI describes the projected impacts of future climate change on worker disutility; Section VII explores the robustness of our results to alternative assumptions about labor markets, including allowing for wages to adjust daily and possible heterogeneity within risk groups; Section VIII contains a concluding discussion.

[3]Throughout this paper, we use the terms "very high" and "intermediate" to refer to the RCP8.5 and RCP4.5 emissions scenarios, analogous to the terminology in IPCC (2021).

[4]Other points of comparison that underscore the importance of labor disutility are that the Obama Administraton's total SCC was \$51, and the DICE model's recent baseline estimate is \$61 (Barrage and Nordhaus, 2023).

II A stylized model of labor demand and supply under extreme temperatures

To characterize specific ways through which temperature affects social welfare via labor markets, we develop a stylized model of labor supply and demand under extreme temperatures. Extreme temperatures impact both firm output and worker disutility. While a number of previous studies deal with impacts on output (Adhvaryu, Kala, and Nyshadham, 2020; Burke, Hsiang, and Miguel, 2015; Cachon, Gallino, and Olivares, 2012; Deryugina and Hsiang, 2014; Heal and Park, 2013; Hsiang, 2010; Nath, 2020; Somanathan et al., 2018; Zhang et al., 2018), no study thus far has quantified the impacts on worker disutility.

To infer how the disutility of work varies with temperature, we use a revealed preference approach inspired by Rosen-style hedonic models (Rosen, 1986). In the canonical version of these models, workers supply their labor inelastically and receive a wage premium for more arduous work conditions that allows homogeneous workers to work in different sectors in equilibrium. However, there exist many settings in which wages are rigid but labor is supplied elastically, making the standard hedonic model ill-suited. In principle, discomfort from daily variation in temperature, air pollution, or noise pollution may cause workers to change their labor supply, even if wages do not adjust on a daily basis.

There are several reasons why fixed daily wages may be an empirically valid assumption. Many workers are compensated by a salary that only varies annually, and non-salaried workers are often employed under contracts that pre-determine their wage rate over long time horizons (e.g., annual). Moreover, even in contexts in which wages can vary at high frequency, the empirical labor economics literature suggests that in practice they are relatively inflexible and, in particular, do not adjust based on changing daily or weekly conditions (Akerlof et al., 1996; Barattieri, Basu, and Gottschalk, 2014; Dickens et al., 2007; Grigsby, Hurst, and Yildirmaz, 2021; Kahn, 1997). Perhaps most relevant to this study, Kaur (2019) finds that weather shocks with large negative productivity effects do not affect the wages of agricultural day labor in India.[5]

This paper's modeling insight is that when wage rates cannot adjust, there must exist a different margin of adjustment to guarantee an equilibrium. Given that workers dislike working in uncomfortable conditions, the predominant margin of adjustment in these settings is likely to be labor supply. This section outlines a model of the labor market that can be combined with the empirical relationship between labor supply and temperature that we estimate below to compute the worker disutility costs of extreme temperature.

The central feature of the model is that workers face disutility when working and

[5]While there exists considerable evidence that wages are inflexible over short time horizons, we nevertheless conduct a robustness check in Section VII.A that explores the sensitivity of our disutility estimates to relaxing this assumption.

the disutility varies with daily temperature. Worker productivity also varies with daily temperature. We assume there exists an optimal daily temperature T_{opt} where disutility is minimized and productivity is maximized at any given labor supply.[6] Furthermore, the marginal disutility of labor is also minimized, and marginal product of labor maximized, at T_{opt}.[7]

In the exposition that follows, we define the *climate* as the joint probability distribution of possible daily temperatures that can be expected to occur over a year. Let $\boldsymbol{\tau}$ be a vector of parameters describing the entire joint probability distribution over daily temperatures. A daily temperature realization for day d, T_d, is randomly drawn from a distribution characterized by $\boldsymbol{\tau}$. We express this random draw as $T_d(\boldsymbol{\tau})$.

The economy in our model consists of two sectors- "high-risk" (h) and "low-risk" (l) -producing distinct goods indexed 1 and 2, respectively. High-risk jobs (e.g., agriculture) are completely exposed to the daily outdoor temperature, $T_d(\boldsymbol{\tau})$. In contrast, low-risk jobs (e.g., services) offer a partly protected work environment with a less extreme temperature, $\widetilde{T}_d(\boldsymbol{\tau})$, where $\widetilde{T}_d(\boldsymbol{\tau}) \equiv \gamma T_{opt} + (1-\gamma)T_d(\boldsymbol{\tau})$. The temperature $\widetilde{T}_d(\boldsymbol{\tau})$ is thus a weighted average between T_{opt} and $T_d(\boldsymbol{\tau})$, with respective weights γ and $1-\gamma$ that the worker and firm take as exogenous. The technological parameter $\gamma \in (0,1)$ captures the degree of insulation from the outdoor temperature, with a γ value near zero representing almost no insulation, and a γ value near one representing almost perfect maintainance of T_{opt}.

At the beginning of the year, before daily temperatures are realized, firms specify their wage rate and workers optimally choose in which of the two sectors to work. Thereafter, upon each daily realization of temperature, workers choose how many hours to work in their chosen sector. At the end of the year, firms realize output as a function of total worker hours and the full sequence of realized daily temperatures over the year, $\boldsymbol{T}(\boldsymbol{\tau}) \equiv \{T_d(\boldsymbol{\tau})\}_{d=1}^{365}$, and workers choose how much to consume of each good based on realized annual income and prices.[8] In the context of this model, we derive an expression for workers' willingness to pay for a change in the climate $\boldsymbol{\tau}$ and illustrate that the disutility costs of extreme temperatures can be expressed as a function of estimable terms.

II.A Worker and firm sectoral choice and wage determination

Prior to the realization of daily temperatures, a representative worker faces a choice of whether to work in the high-risk or low-risk sector, which offer wages ω^h and ω^l, respectively. In addition to labor income, the worker receives asset income, κ, from holding shares in the high- and low-risk firms. The worker gains utility from consumption of the two goods, C_1 (produced in high-risk sector, sold for price p) and C_2 (produced in

[6]For this purpose, we assume the disutility-minimizing and productivity-maximizing temperature, T_{opt}, is constant, regardless of the level of labor supply.

[7]In other words, the marginal disutility of labor is increasing in temperature for $T > T_{opt}$, but decreasing in temperature for $T < T_{opt}$, while the marginal product of labor is decreasing in temperature for $T > T_{opt}$, but increasing in temperature for $T < T_{opt}$.

[8]In other words, workers consume hand-to-mouth on an annual basis.

low-risk sector, with price normalized to 1). Workers face disutility from working and the disutility varies with daily temperature, as experienced in each sector of employment.

The climate, described by $\boldsymbol{\tau}$, affects worker disutility through its influence on the realized daily temperature draws, $\boldsymbol{T} \equiv \{T_d\}_{d=1}^{365}$. We assume that workers are homogeneous in their preferences and productivity in each sector. Because the daily temperatures are not yet realized at the time of the worker's sectoral choice, and the price p and amount of asset income κ will depend on their realized values, a worker chooses the sector $s \in \{l, h\}$ that yields the higher expected utility given wages ω^h and ω^l, conditional on the climate $\boldsymbol{\tau}$.

Each firm hires one worker and operates in one of the two sectors, producing either good 1 (high risk) or good 2 (low risk). For reasons of simplicity and conciseness, we assume that the production technology of all firms producing good 1 is identical and that the technology for producing good 2 is also homogeneous. Let L_d^h and L_d^l denote the number of hours worked on day d by a high- and low-risk worker, respectively. Annual output of good 1 is produced according to the production function $af^1(\sum_{d=1}^{365} L_d^h, \boldsymbol{T})$, while for good 2 it is produced according to the production function $af^2(\sum_{d=1}^{365} L_d^l, \widetilde{\boldsymbol{T}})$, where $\widetilde{\boldsymbol{T}} \equiv \{\widetilde{T}_d\}_{d=1}^{365}$. Both production functions are increasing and concave in the annual hours that a worker works. Furthermore, at any given labor supply, output of each good and the marginal product of labor is maximized when the daily temperature on day d is T_{opt}, irrespective of the temperature on all other days in the year. The parameter a represents a productivity factor common to both sectors of the economy.

Although low-risk firms are exposed to less extreme temperatures, $\widetilde{T}_d$, as defined above, the benefits of the less extreme temperature come at a cost. We define β_j as the fixed cost for firm j to protect itself from extreme temperature and operate in the low-risk sector. The probability density function $g(\cdot)$ and cumulative distribution function $G(\cdot)$ specify the distribution of β_j values across firms.

Prior to the realization of daily temperatures, a firm j faces a choice of which sector to operate in and the wage rate to offer in that sector. Firm j's expected profit maximization problem is thus a wage offer decision nested within a sectoral choice decision, where the wage offer decision is subject to a participation constraint that the worker does not choose the other sector. Because the daily temperatures are not yet realized at this stage, and the price p and number of hours worked by high- and low-risk workers (L^h, L^l) will depend on their realized value, the firms make their sectoral and wage offer decisions to maximize expected profits, conditional on $\boldsymbol{\tau}$. Importantly, in deciding the wage within a sector, the firm takes into account its expected effect on the worker's labor supply.

II.B Worker labor supply decision

Having earlier accepted employment in a given sector at a specified wage, workers decide how much labor to supply each day after the daily temperature is realized. For a given day of the year $d = \underline{d}$, a high-risk worker's labor supply decision is thus:

$$\max_{L^h_{\underline{d}}} \mathbb{E}_{\boldsymbol{T}_{d>\underline{d}}}\Big[U(C^h_1, C^h_2) \;\Big|\; \boldsymbol{\tau}\Big] - D(L^h_{\underline{d}}, T_{\underline{d}}),$$

$$\text{such that } p(\boldsymbol{T}(\boldsymbol{\tau}))C^h_1(\boldsymbol{T}(\boldsymbol{\tau})) + C^h_2(\boldsymbol{T}(\boldsymbol{\tau})) = \omega^h\Big[\sum_{d=1}^{\underline{d}} L^h_d + \sum_{d=\underline{d}+1}^{365} L^h_d(T_d(\boldsymbol{\tau}))\Big] + \kappa(\boldsymbol{T}(\boldsymbol{\tau})), \tag{1}$$

where utility U is increasing and concave in each good, and disutility, D, is increasing and convex in daily labor supply. Furthermore, both disutility and the marginal disutility of labor are increasing in temperature for $T > T_{opt}$, but decreasing in temperature for $T < T_{opt}$. A low-risk worker's daily labor supply decision is the same as that of a high-risk worker, except that the low-risk worker is exposed to daily temperatures $\widetilde{T}_d$ instead of T_d. In choosing daily labor supply, workers thus trade off labor disutility against the wage earned from working.

Because workers choose how much of each good to consume at the end of the year, based on annual income and prices, the labor supply decision on day $\underline{d}$ is based on the expected utility of consumption. The expectation is taken over the vector of daily temperatures in the year after day $\underline{d}$ ($\boldsymbol{T}_{d>\underline{d}} \equiv \{T_d\}_{d=\underline{d}+1}^{365}$), which have yet to be realized.[9]

II.C Equilibrium conditions

Prior to the realization of daily temperatures, the climate $\boldsymbol{\tau}$ influences both the equilbrium wages and composition of the economy across sectors by affecting expected disutility and output in the two sectors. Equilibrium wages in the two sectors ($\omega^{h*}(\boldsymbol{\tau})$ and $\omega^{l*}(\boldsymbol{\tau})$) reflect a compensating differential of higher wages for workers at high-risk firms (Rosen, 1974, 1986). The equilibrium shares of employment in each sector are determined by the distribution across firms of the β_j costs of protection from extreme temperatures. Letting $\Delta^*(\boldsymbol{\tau})$ denote the equilibrium difference between low- and high-risk risk sector expected profit, only firms with $\beta_j < \Delta^*(\boldsymbol{\tau})$ will choose to operate in the low-risk sector. Thus the equilibrium shares of employment in the low- and high-risk sectors are respectively $G(\Delta^*(\boldsymbol{\tau}))$ and $1 - G(\Delta^*(\boldsymbol{\tau}))$.

After the realization of each day's temperature, workers choose daily labor supply in each sector ($L^{l*}_d(T_d)$ and $L^{h*}_d(T_d)$) such that the marginal disutility of labor equals the pre-determined wage in that sector. At the end of the year, the equilibrium relative price ($p^*(\boldsymbol{T})$) clears the markets for the two goods, and firms in each sector realize zero profits after payments to shareholders (i.e., workers, who own the firms). Detailed derivations of equilibrium conditions are shown in Appendix A.

[9] Similarly, the budget constraint reflects that daily labor supply decisions after $\underline{d}$ are yet to be made and will depend on the daily temperature realizations.

II.D Deriving an expression for temperature's welfare effects on workers and firms

This subsection derives an expression for workers' willingness-to-pay (WTP) for a change in the climate. The starting point is that a change in the climate $\boldsymbol{\tau}$, through altering daily temperature realizations T_d, affects worker disutility and firm productivity in the high- and low-risk sectors. Moreover, changes in the climate also affect the sectoral composition of the economy through changing expectations about daily temperatures. The expression for WTP accounts for all these changes and is built on the expected indirect utility functions of high- and low-risk workers.

The expression for WTP for a change in $\boldsymbol{\tau}$ is the negative of the total derivative of indirect utility with respect to $\boldsymbol{\tau}$. This expression is divided by the marginal utility of income (i.e., the marginal utility of the numeraire good, C_2) to convert it from utils to money, and its expected value is taken over the distribution of daily temperatures over the year, $\boldsymbol{T}$, conditional on $\boldsymbol{\tau}$. The total WTP is obtained by summing across high- and low-risk workers, using the sectoral shares, $1 - G(\Delta^*(\boldsymbol{\tau}))$ and $G(\Delta^*(\boldsymbol{\tau}))$, evaluated at the new, post-change $\boldsymbol{\tau}$.

Using the budget constraints, market clearing conditions, and the envelope theorem, we can express the total WTP as follows (see Appendix A for details):

$$
\begin{aligned}
\textit{Total WTP} = & \underbrace{(1 - G(\Delta^*(\boldsymbol{\tau})))\mathbb{E}_{\boldsymbol{T}}\Big[- p^* a f_T^1(\sum_{d=1}^{365} L_d^{h*}, \boldsymbol{T})\frac{\partial \boldsymbol{T}}{\partial \boldsymbol{\tau}} - \sum_{d=1}^{365}\Big(p^* a f_L^1(\sum_{d=1}^{365} L_d^{h*}, \boldsymbol{T}) - \omega^{h*}\Big)\frac{\partial L_d^{h*}}{\partial T_d}\frac{\partial T_d}{\partial \boldsymbol{\tau}} \;\Big|\; \boldsymbol{\tau}\Big]}_{\text{(A) Output loss for high-risk sector (good 1)}} \\
& + \underbrace{G(\Delta^*(\boldsymbol{\tau}))\mathbb{E}_{\boldsymbol{T}}\Big[- (1-\gamma) a f_T^2(\sum_{d=1}^{365} L_d^{l*}, \widetilde{\boldsymbol{T}})\frac{\partial \boldsymbol{T}}{\partial \boldsymbol{\tau}} - \sum_{d=1}^{365}\Big(a f_L^2(\sum_{d=1}^{365} L_d^{l*}, \boldsymbol{T}) - \omega^{l*}\Big)\frac{\partial L_d^{l*}}{\partial T_d}\frac{\partial T_d}{\partial \boldsymbol{\tau}} \;\Big|\; \boldsymbol{\tau}\Big]}_{\text{(B) Output loss for low-risk sector (good 2)}} \\
& + \underbrace{(1 - G(\Delta^*(\boldsymbol{\tau})))\mathbb{E}_{\boldsymbol{T}}\Big[\sum_{d=1}^{365}\frac{D_T(L_d^{h*}, T_d)}{U_2(C_1^{h*}, C_2^{h*})}\frac{\partial T_d}{\partial \boldsymbol{\tau}} \;\Big|\; \boldsymbol{\tau}\Big]}_{\text{(C) Disutility effects for high-risk workers}} + \underbrace{G(\Delta^*(\boldsymbol{\tau}))\mathbb{E}_{\boldsymbol{T}}\Big[(1-\gamma)\sum_{d=1}^{365}\frac{D_T(L_d^{l*}, \widetilde{T}_d)}{U_2(C_1^{l*}, C_2^{l*})}\frac{\partial T_d}{\partial \boldsymbol{\tau}} \;\Big|\; \boldsymbol{\tau}\Big]}_{\text{(D) Disutility effects for low-risk workers}}.
\end{aligned}
\tag{2}
$$

Equation 2 reveals two channels through which climate affects welfare.[10] The first, captured in parts (A) and (B) of Equation 2, is the impact to output that has been estimated previously at both microeconomic (Adhvaryu, Kala, and Nyshadham, 2020; Cachon, Gallino, and Olivares, 2012; Somanathan et al., 2018; Zhang et al., 2018) and macroeconomic scales (Burke, Hsiang, and Miguel, 2015; Deryugina and Hsiang, 2014;

[10] It is important to note that Equation 2 does not include climate-induced changes in prices (i.e., $\frac{\partial p^*}{\partial \boldsymbol{T}}\frac{\partial \boldsymbol{T}}{\partial \boldsymbol{\tau}}$, $\frac{\partial \omega^{h*}}{\partial \boldsymbol{\tau}}$, $\frac{\partial \omega^{l*}}{\partial \boldsymbol{\tau}}$), as these amount to transfers between workers and the firms they own and thus have no net effect on total WTP. Moreover, while Equation 2 reflects the fact that a change in climate alters the sectoral shares of the economy, $1 - G(\Delta^*(\boldsymbol{\tau}))$ and $G(\Delta^*(\boldsymbol{\tau}))$, the total WTP expression does not include changes in the low-risk sector's total protection costs, as these are exactly offset by changes in total profit due to the sectoral reallocation. See Appendix A for the detailed derivation.

Heal and Park, 2013; Hsiang, 2010; Nath, 2020). Here, climate-induced changes to productivity affect output in the high-risk sector and also in the low-risk sector, to the extent that it is vulnerable to the outdoor temperature (as captured by the parameter γ).[11] Given the extensive literature and the limitations of our data, which do not include measures of output, this paper does not directly estimate the productivity impacts of temperature changes.

The second channel, captured in parts (C) and (D) of Equation 2, constitutes the direct impact to worker disutility, and it is this paper's primary focus. The core insight is that work is less pleasant at high and low temperatures (i.e., when $T_d \neq T_{opt}$) and this is captured by the $D_T(L_d^{l*}, T_d)$ and $D_T(L_d^{l*}, \widetilde{T}_d)$ terms. We are unaware of previous efforts to quantify D_T, so there is no clear guidance on this channel's share of total WTP for a change in climate. The practical challenge is that the disutility of work is not directly observable in data. This paper's aim is to use a revealed preference-style approach to infer how the disutility of work varies with temperature and to develop empirical estimates of this second channel. Specifically, we derive an estimable expression for the wage change necessary to keep worker utility constant, given a change in labor disutility caused by a marginal change in daily temperature, holding all else equal.

For a high-risk worker on day d, we denote this compensatory wage change $\frac{\partial \omega^{h*}}{\partial T_d}\frac{\partial T_d}{\partial \boldsymbol{\tau}}\big|_{V_0^h}$, where V_0^h represents the initial, pre-temperature change utility level. The compensatory wage change is obtained by taking the total derivative of the high-risk worker's indirect utility with respect to $\boldsymbol{\tau}$, while holding constant all other prices and income, and setting this derivative equal to zero. This results in the following expression:

$$\frac{D_T(L_d^{h*}, T_d)}{U_2(C_1^{h*}, C_2^{h*})}\frac{\partial T_d}{\partial \boldsymbol{\tau}} = L_d^{h*}\Big[\frac{\partial \omega^{h*}}{\partial T_d}\frac{\partial T_d}{\partial \boldsymbol{\tau}}\Big|_{V_0^h}\Big]. \tag{3}$$

The object $\frac{D_T(L_d^{h*}, T_d)}{U_2(C_1^{h*}, C_2^{h*})}$ is the key element of part (C) in the total WTP expression (Equation 2), representing the WTP to avoid the disutility effects of daily temperature on high-risk workers. The expression is very similar to the measure of WTP that would be derived from canonical Rosen-style hedonic models where workers supply their labor inelastically and wage differentials guarantee an equilibrium (Rosen, 1986). However, in our context, we assume that labor supply does adjust and the wage rate does not adjust in response to the realization of a given day's temperature.

To express Equation 3 in terms of objects we can estimate with the data in this context, we therefore need to rewrite the right hand side in terms of changes in daily labor supply ($\frac{\partial L_d^{h*}}{\partial T_d}\frac{\partial T_d}{\partial \boldsymbol{\tau}}$), rather than changes in wages ($\frac{\partial \omega^{h*}}{\partial T_d}\frac{\partial T_d}{\partial \boldsymbol{\tau}}$). To do so, we rely on the elasticity of

[11] The effects on output consist of direct effects (i.e., $p^* a f_T^1(\sum_{d=1}^{365} L_d^{h*}, \boldsymbol{T})$ and $(1-\gamma) a f_T^2(\sum_{d=1}^{365} L_d^{l*}, \widetilde{\boldsymbol{T}})$ for high- and low-risk sectors, respectively) and effects mediated through changes in labor supply (i.e., $\Big(p^* a f_L^1(\sum_{d=1}^{365} L_d^{h*}, \boldsymbol{T}) - \omega^{h*}\Big)\frac{\partial L_d^{h*}}{\partial T_d}$ and $\Big(a f_L^2(\sum_{d=1}^{365} L^{l*}, \widetilde{\boldsymbol{T}}) - \omega^{l*}\Big)\frac{\partial L_d^{l*}}{\partial T_d}$ for high- and low-risk sectors, respectively). Applying the envelope theorem does not eliminate the latter due to the timing of the wage decision and also due to worker participation constraints in the firms' profit maximization problem. See Appendix A for a detailed derivation.

labor supply with respect to wage, holding the marginal utility of wealth constant. This elasticity is often referred to as the Frisch elasticity of labor supply, and we denote it as ϵ. With some manipulation, we can write:

$$\frac{D_T(L_d^{h*}, T_d)}{U_2(C_1^{h*}, C_2^{h*})} \frac{\partial T_d}{\partial \boldsymbol{\tau}} = \frac{\omega^{h*}\left(\frac{\partial L_d^{h*}}{\partial T_d}\frac{\partial T_d}{\partial \boldsymbol{\tau}}\right)}{\epsilon}. \tag{4}$$

This rearrangement provides an expression of the disutility costs to high-risk workers in terms of changes in daily high-risk labor supply, an object we estimate in this paper. A similar expression can be derived for low-risk workers:

$$(1-\gamma)\frac{D_T(L_d^{l*}, \widetilde{T}_d)}{U_2(C_1^{l*}, C_2^{l*})} \frac{\partial T_d}{\partial \boldsymbol{\tau}} = \frac{\omega^{l*}\left(\frac{\partial L_d^{l*}}{\partial T_d}\frac{\partial T_d}{\partial \boldsymbol{\tau}}\right)}{\epsilon}. \tag{5}$$

Thus given a change in the distribution of daily temperatures ($\frac{\partial T_d}{\partial \boldsymbol{\tau}}$), equations 4 and 5 reveal that it is possible to develop estimates of the value of labor disutility (left-hand side). Specifically, the value of disutility is equal to the product of the change in daily work time due to changing temperatures and the wage, divided by the Frisch elasticity of labor supply (right-hand side).

Figure 1 illustrates these disutility costs in the context of a daily labor market equilibrium. The worker's daily labor supply curve is specified by her marginal disutility of labor, while the firm's daily labor demand curve is specified by the marginal product of labor. The intersection of these two curves determines the number of hours worked, shown in Figure 1A for a daily temperature T_{opt}. In our framework, the wage rate, ω^*, is fixed at the beginning of the year and does not adjust in response to daily temperature variation. Extreme temperatures do however, cause disutility to increase, both overall and on the margin. Thus a rise in the temperature from T_{opt} to a more extreme, hot temperature of T_+ resets the equilibrium to a lower number of hours worked, while the wage remains fixed (Figure 1B). The gridded region in Figure 1B represents the increase in worker disutility from the temperature increase — the object we estimate in this paper.

Importantly, our method to infer a change in disutility from a change in daily labor supply assumes that wage rates do not adjust on a day-to-day basis in response to changing work conditions. If instead wage rates do adjust daily, then our estimated change in disutility will either be an underestimate or an overestimate, depending on whether the relative elasticities and shifts in labor supply and demand cause the wage to increase or decrease. Section VII.A describes both these cases and assesses the extent of the potential under- or overestimate under a range of scenarios.[12]

The approach developed here enables us to monetize various forms of temperature-induced disutility faced by workers by applying Equations 4 and 5. For instance, comparing labor supply losses of high- and low-risk workers in the face of extreme temperatures

[12]Section VII also considers the sensitivity of our estimates to other assumptions about the labor market.

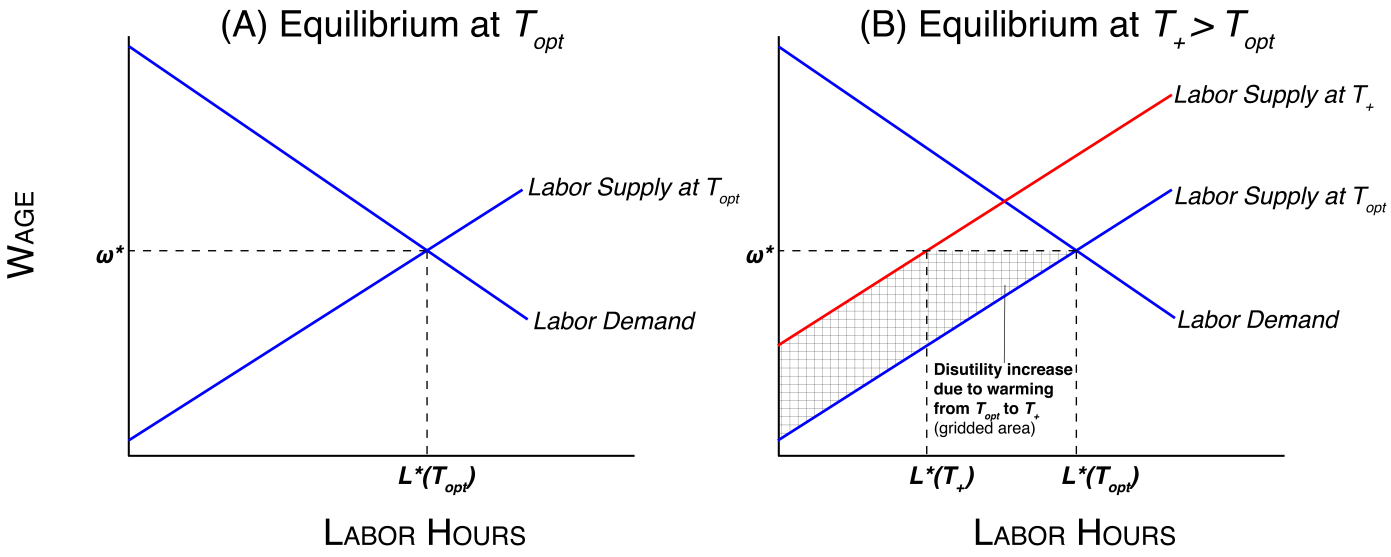

Figure 1: Effects of a temperature increase on labor supply and disutility. Intersection of upward-sloping marginal disutility of labor (labor supply) and downward-sloping marginal product of labor (labor demand) determines the equilibrium labor hours at a given temperature. Figure 1A illustrates the equilibrium under the optimal temperature T_{opt} (intersection of blue curves). Figure 1B illustrates the new equilibrium when the temperature increases from T_{opt} to T_+ (intersection of red supply curve and wage ω^*), with the old T_{opt} equilibrium also shown for comparison. The gridded region corresponds to the increased disutility faced by workers due to the temperature increase— the object we estimate in this paper.

can provide a way to characterize the hedonic value of thermal comfort offered by a low-risk job. The same procedure can also be used to calculate the disutility to high- and low-risk workers due to future climate change. We present these applications in Sections V and VI.

III Data

As described in the previous section, our approach to monetizing temperature-induced worker disutility relies on variation in daily labor supply in response to temperature exposure. For this purpose, we have assembled the most comprehensive dataset ever compiled on historical daily or weekly labor supply, workforce composition, climate, and weather data. We add to these data local future projections of climate, population, and income until 2100. Section III.A describes the historical data we use to estimate the relationship between labor supply and temperature. The results from this estimation are used to project how workers will be impacted under future climate change, accounting for changes in workforce composition in the future. Section III.B outlines the data we use for these projections. Appendix B provides a more extensive description of all of these data sources.

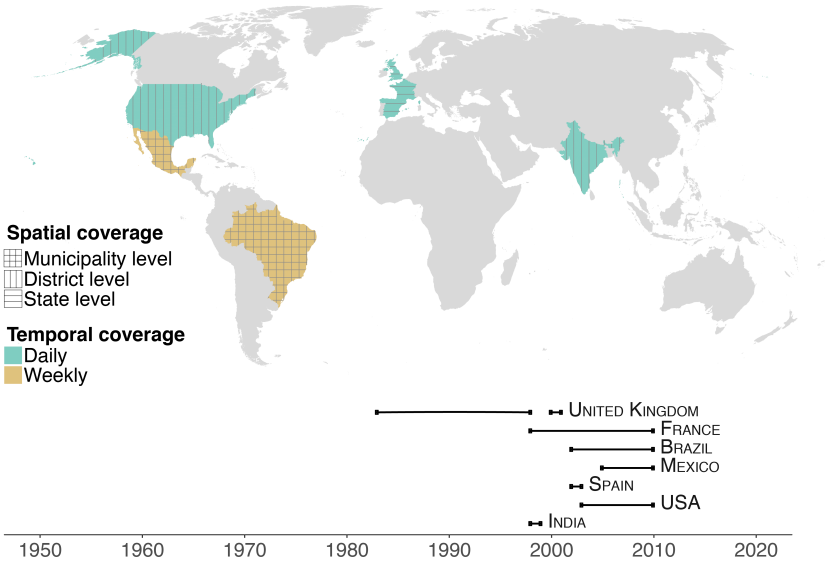

Figure 2: Labor statistics used to estimate the labor supply-temperature relationship. Map shows the spatial distribution and resolution of labor statistics from all countries used to generate regression estimates of the labor supply-temperature relationship. Temporal coverage for each country is shown under the map.

III.A Data to estimate the labor supply-temperature relationship

1. *Labor supply data.* We identified 7 countries for which representative labor or time-use survey data were available and could be used to analyze the relationship between daily temperature and labor supply. Specifically, for inclusion in our analysis, we required that the datasets could be harmonized (i.e., the questions regarding time spent working were similar across all included countries) and that they identify respondents' subnational geographic location (e.g., a county in the United States), their industry of employment, and the exact calendar date(s) on which work hours were measured. Datasets meeting these requirements were acquired for Brazil, France, India, Mexico, Spain, the United Kingdom, and the United States, which together had a population of 2.2 billion in 2020. The years of coverage vary across the countries but in total range from 1983 to 2010.[13] Spatial and temporal coverage and resolution are shown in Figure 2A.

The estimation sample comprises over 6.5 million observations, where an observation is a person-day or person-week. This sample is restricted to persons in the labor force who are between the ages of 15 and 65. We classify all workers as high risk or low risk according to the likelihood their industry requires a large share of the day to be spent outdoors, or leaves them weather-exposed because of workplace conditions. Specifically, we define workers in the agriculture, mining, construction, and manufacturing industries as high risk.[14] This categorization allows us to explore the differential effects of temperature by

[13]Some of the datasets include more recent years. However we constrain our analysis to end in 2010 in order to maintain consistency between historical and future climate datasets (see Appendix Section B.2.2).

[14]The practical details of how workers are labeled high risk and low risk for each country's dataset

type of labor activity (high-risk vs. low-risk). Each data source is summarized in Table 1.

2. *Historical climate and weather data.* Historical data on daily maximum temperature and precipitation are obtained from the Global Meteorological Forcing Dataset, v1 (GMFD) (Sheffield, Goteti, and Wood, 2006), a global gridded ($0.25° \times 0.25°$) daily weather record available from 1948 to 2010. We link climate and labor supply data by aggregating gridded daily data to the temporal and spatial resolution provided in the labor supply records. Appendix B.2.3 details the procedure for this linkage; importantly, it preserves the full distribution of temperature exposures that makes it possible to recover daily, grid-cell level nonlinearities in the labor supply-temperature relationship regardless of the spatial and temporal resolution of the labor supply data. This is discussed further in Section IV. We define weather as daily realizations of temperature and precipitation and climate as longer run averages.

Country	No. observations	Spatial scale	Years	Temporal scale	Data source	Labor supply	Percent high-risk	Mean age	Percent male	Mean household size (persons)
Brazil	3,519,564	municipality	2002-2010	weekly	labor force survey	356.64	30.76	36.6	55%	3.75
France	5,325	NUTS2	1998-1999	daily	time use survey	444.23	30.67	40.2	56%	3.10
India	48,646	district	1998-1999	daily	time use survey	369.26	82.68	35.2	57%	4.75
Mexico	2,947,406	municipality	2005-2010	weekly	labor force survey	376.07	43.47	36.2	63%	4.64
Spain	13,060	NUTS2	2002-2003	daily	time use survey	470.19	31.83	39.7	60%	3.61
UK	11,714	NUTS1	1983-2001	daily	time use survey	416.47	18.70	38.2	53%	3.19
USA	53,673	county	2003-2010	daily	time use survey	425.23	22.22	40.6	52%	3.41
All Countries	**6,599,388**	–	–	–	–	**366.45**	**36.82**	**36.51**	**59%**	**4.16**

Notes: Labor supply is recorded in minutes per day, averaged across the sample. In the Spatial scale column, municipalities, counties, and districts refer to second administrative level divisions (ADM2) in their respective countries; NUTS2 refers to the Nomenclature of Territorial Units for Statistics 2^{nd} level, which is specific to the European Union (EU) and falls between first and second administrative levels; and NUTS1 refers to the Nomenclature of Territorial Units for Statistics 1^{st} level, which is also specific to the European Union (EU) and falls between the first administrative level and country. As a point of reference, a United States state corresponds to a first administrative level and a U.S. county to a second administrative level.

Table 1: Labor supply data

III.B Data for projecting the labor disutility costs of climate change

1. *Climate and socioeconomic projections.* To project the impacts of future climate change, we use the infrastructure developed in Rode et al. (2021) and Carleton et al. (2022). Damages from climate change are computed for each of 24,378 globally comprehensive geographic regions (hereafter, *impact regions*),[15] using an ensemble of 33 climate

are in Appendix B.1. In addition, in Appendix D.2 we employ alternative classifications that take into account occupation.

[15]Impact regions are constructed such that they are either identical to, or are a union of, existing administrative regions. They (i) respect national borders, (ii) are roughly equal in population across regions (approximately 300,000 persons in 2015), and (iii) display approximately homogenous within-region climatic conditions. The algorithm used to create impact regions is detailed in Carleton et al. (2022).

projections that provide global gridded ($0.25° \times 0.25°$) daily temperature through the year 2100 (Taylor, Stouffer, and Meehl, 2012; Thrasher et al., 2012) under two standardized emissions scenarios: Representative Concentration Pathways 4.5 (RCP4.5, an emissions stabilization scenario) and 8.5 (RCP8.5, a scenario with high growth in fossil fuel emissions) (Thomson et al., 2011; Van Vuuren et al., 2011). Full details on the climate projection data are in Appendix B.2.2. Projections of population and income are also an essential ingredient in our computation of climate change's influence on labor supply and the share of high risk workers. For the projections of these variables, we rely on the Shared Socioeconomic Pathways (SSPs), which describe a set of plausible scenarios of socioeconomic development over the 21st century.[16] Full details on the income and population projection data are in Appendix B.3.3 and B.3.4.

2. *Projections of workforce composition.* We empirically uncover substantial heterogenity in the labor supply-temperature relationship based on whether workers are employed in high- or low-risk jobs. To account for this heterogeneity in future projections of climate change impacts, we first use historical data to estimate how the share of high-risk workers in a given population depends on two key covariates: long-run average temperature and income per capita. The share of high-risk workers (i.e., the dependent variable in this regression) is obtained from census data covering every ADM1 unit (first-level administrative unit, e.g. state) in 48 countries (Minnesota Population Center, 2019).[17] The explanatory variables are also measured at the ADM1 unit level and come from GMFD for climate data and Penn World Tables (PWT) and Gennaioli et al. (2014) for income data.[18] We then use the estimated historical relationship between high-risk workforce share and income and climate to project an impact region- and year-specific workforce composition for all future years through 2100 by relying on the climate and income projections described above.

IV Empirical approach

This section presents the regression equation used to recover the causal effect of daily temperature realizations on labor supply of high- and low-risk workers. Specifically, we exploit variation in daily weather to identify the response of labor supply to temperature, estimating the following equation on the pooled sample from 7 countries:

[16] See Hsiang and Kopp (2018) for a description of these scenarios. Specifically, we use SSP2, SSP3, and SSP4, which provide emissions in the absence of mitigation policy that fall between RCP4.5 and RCP8.5 in integrated assessment modeling exercises (Riahi et al., 2017). National population projections (IIASA Energy Program, 2016) and national income per capita projections (Dellink et al., 2015; IIASA Energy Program, 2016) are allocated to impact regions based respectively on current satellite-based within-country population distributions from Bright et al. (2012) (see Appendix B.3.4) and current nighttime light satellite imagery from the NOAA Defense Meteorological Satellite Program (DMSP) (see Appendix B.3.3).

[17] This data source is described in Appendix B.3.1.

[18] The construction of the income variable requires an estimation procedure to downscale to ADM1 level, details of which are provided in Appendix B.3.2.

$$Labor_{i,r,j,t} = f_r(\boldsymbol{T}_{j,t}) + g_r(\boldsymbol{P}_{j,t}) + \lambda_r \boldsymbol{X}_i + \alpha_{j,r} + \psi_{k,y,r} + \delta_{k,w,r} + \phi_{d,r} + \epsilon_{i,j,r,t}, \quad (6)$$

where i indexes a person, r denotes person i's risk group (*high*, *low*), j denotes person i's subnational location,[19] and t is the date of the observation, indexing either a day or a week depending on the temporal resolution of the labor supply data. Thus, $Labor_{i,r,j,t}$ is the number of minutes worked by person i of risk group r, in subnational location j, at date t, modeled as a function f_r of a temperature vector ($\boldsymbol{T}_{j,t}$) and function g_r of precipitation vector ($\boldsymbol{P}_{j,t}$). We control for a vector of individual-level covariates ($\boldsymbol{X}_i$) that consist of age, age-squared, gender, and household size. The final term, $\epsilon_{i,j,r,t}$, denotes the stochastic error term.

We interpret the estimated effect of temperature on labor supply as plausibly causal, because the specification includes a rich set of fixed effects so that the identifying variation is restricted to weather shocks. Specifically, we include a series of risk group-specific fixed effects for subnational location ($\alpha_{j,r}$), country k × year y ($\psi_{k,y,r}$), country k × week-of-year w ($\delta_{k,w,r}$), and day-of-week d ($\phi_{d,r}$). The fixed effects for subnational locations isolate within-location variation in labor supply and temperature exposure, and the country × year and country × week-of-year fixed effects flexibly account for long-term trends and seasonality, respectively, at the national level. Additionally, the day-of-week fixed effects allow for differences in work patterns throughout the week.[20] The result is that we believe it is valid to assume that the labor supply response to temperature is identified from the plausibly random daily variation in temperature.

Our focus in Equation 6 is the effect of temperature on labor supply, represented by the response function $f_r(\cdot)$, which varies by risk group. Before describing the functional form of this response, we note that the temperature data are provided at the grid-cell-by-day level, and grid cells are much smaller than the subnational location units in the labor supply data. To align these two datasets, we first take nonlinear functions of grid-level daily maximum temperature (and in the case of weekly labor supply observations, sum these values across days in the week). We then collapse across grid cells within each subnational unit using population weights in order to represent temperature exposure for the average person within a unit (see Appendix B.2.3 for details). This approach to aggregation ensures that we accurately represent temperature extremes at the grid-cell-by-day level.

We thus construct the daily (or weekly), subnational unit-level vector $\boldsymbol{T}_{j,t}$ and choose $f_r(\cdot)$ to be a linear function of the nonlinear elements of $\boldsymbol{T}_{j,t}$. This construction allows us to estimate a linear regression model while preserving the nonlinear relationship between labor supply and temperature that takes place at the grid-cell-by-day level (Hsiang, 2016).

[19] For France and Spain, j denotes a NUTS2 unit, while for the UK j denotes a NUTS1 unit. For all other countries, j denotes a second-level administrative unit (e.g., county). See Table 1.

[20] A separate fixed effect is included to indicate weekly observations, which span all days of the week.

The nonlinear transformations captured by $\boldsymbol{T}_{j,t}$ determine, through their linear combination in $f_r(\cdot)$, the functional form of the labor supply-temperature response function.

In our main specification, $\boldsymbol{T}_{j,t}$ is a three-knot restricted cubic spline in daily maximum temperatures.[21] Thus, we use 4 parameters to flexibly capture the relationship between labor supply and daily temperature. We emphasize results from the restricted cubic spline because it captures important nonlinearities while being relatively parsimonious. Results for alternative functional form specifications are similar to the restricted cubic spline and are provided in Appendix D.1. The r subscript on $f_r(\cdot)$ and all the paramaters indicates that Equation 6 allows all parameters to vary for high- and low-risk workers, although it is estimated in a single equation.

Analogous to temperature, we summarize daily grid-level precipitation in the subnational unit-level vector $\boldsymbol{P}_{j,t}$. We construct $\boldsymbol{P}_{j,t}$ as a second-order polynomial of daily precipitation,[22] and estimate a linear function of this vector, represented by $g_r(\cdot)$.

In addition to aligning the resolution of the historical weather data with the outcome data, we also implement a series of adjustments to all variables so that data at both daily and weekly temporal resolutions can be pooled in a single regression. Specifically, for daily observations, we include within-week values of temperature and precipitation in the regression and also rescale the values of outcome, weather, and person-level control variables by a factor of $\sqrt{7}$. These adjustments are necessary for our estimates to have a consistent interpretation across different timescales, and are detailed in Appendix C. Thus, for example, it is appropriate to interpret the parameters associated with temperature as the impact of a day's temperature on the number of minutes worked in a week.

We fit the multi-country pooled model in Equation 6 using weighted least squares, so that the coefficients correspond to the average person in the relevant risk group. Within each country, observations are weighted by the sample weights specified in that country's survey, while across countries, observations are differentially weighted according to the country's total population of workers in the particular risk group. This is necessary to ensure that our results are representative for the average person, and not simply driven by country datasets with the largest number of observations.[23] Standard errors are clustered at the ADM1 $\times$ month-of-sample level to account for spatial as well as temporal correlation in error structure.[24]

An alternative approach would be to allow the labor supply-temperature response of each risk group to vary across locations based on their income and climate, thus allowing for differential adaptation choices.[25] Such an approach has been used in other studies in

[21] In the case of weekly observations, these terms are summed across days in the week.

[22] In the case of weekly observations, the polynomial terms are summed across days in the week.

[23] The highly unequal sample sizes of the country surveys is reported in Table 1.

[24] In the case of France and Spain, we cluster at NUTS2 $\times$ month-of-sample, while for the UK, we cluster by NUTS1 $\times$ month-of-sample (Table 1).

[25] For instance, the labor supply of workers in poorer locations may be more sensitive to temperature than that of workers in richer locations, as greater wealth can afford workers and firms more access to protective technologies (e.g., air-conditioning). Additionally, whether a location is warm or cold on average may shape the degree to which hot or cold temperatures affect workers, because local long-

the climate-economy literature (Carleton et al., 2022; Rode et al., 2021), but we do not emphasize it here due to data and statistical limitations in this context. An important data limitation is that some of the time use and labor force surveys are not representative at subnational geographies.[26] Nevertheless, Appendix G reports estimates from an individual level labor supply model that includes interactions of daily temperature with measures of income per capita and climate at the level that the surveys are representative. Further, Section VII reports on how allowing for these interactions influences the hedonic value of thermal comfort and the impacts of climate change.

V Estimates of the disutility of labor under extreme temperatures

The revealed-preference style framework developed in Section II.D infers changes in disutility based on observed changes in labor supply in response to daily temperatures. As described in Equations 4 and 5, calculating the value of disutility requires multiplying labor supply changes by a wage rate and dividing by the Frisch elasticity of labor supply. This section estimates how high-risk and low-risk workers respond to daily temperature by altering their labor supply. It then uses these estimates to calculate the value of temperature-induced disutility in a high-risk job relative to a low-risk job, or equivalently, the hedonic value of thermal comfort offered by a low-risk job.

V.A Labor supply-temperature relationship: High- and low-risk workers

Figure 3 reports the results from estimating versions of Equation 6 where temperature is modeled with a restricted cubic spline in daily maximum temperature with knots at 27° C, 37° C, and 39° C.[27] Panel A graphically illustrates the response function from the global sample of all workers. Panels B and C plot the response functions that result from estimating the equation separately for low-risk and high-risk workers. In these figures, a day with a maximum temperature of 27° C is treated as the reference. Thus, each point along the function reveals the effect of a day at the relevant temperature on weekly minutes worked, relative to a 27° C day. Finally, the histograms at the bottom of these figures reveal the distribution of daily maximum temperatures in the relevant samples, with the differences in B and C reflecting differences in the geographic distribution of

run climatic conditions can influence heat- and cold-related adaptation choices (e.g., the availability of air-conditioning and heating, protective clothing).

[26] Surveys for the United States, the United Kingdom, and France are only representative at the national level, while surveys from Brazil, Mexico, India, and Spain are representative at the ADM1 level (e.g., state).

[27] Appendix D describes the procedure through which the knot locations were selected.

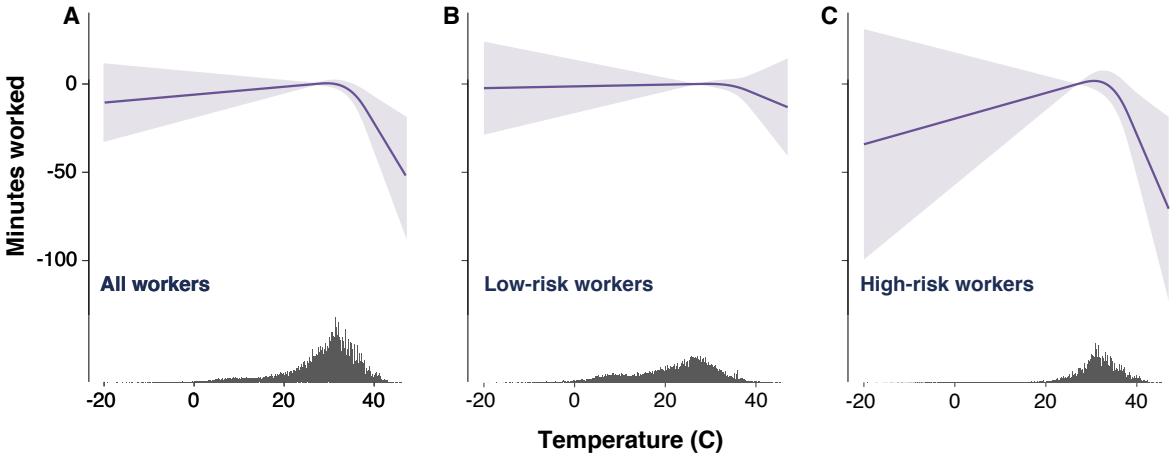

Figure 3: Changes in weekly minutes worked per person due to daily temperature. Labor supply-temperature response functions are estimated for all workers (A), low-risk workers (B), and high-risk workers (C), corresponding to Columns 1, 2, and 3 in Table 2, respectively. Points along each curve represent the effect on weekly labor supply of a single day at the daily maximum temperature value shown on the x-axis, relative to a day with a maximum temperature of 27°C (81°F). Shaded areas indicate 95% confidence intervals. Histograms show the distribution of daily maximum temperatures in each sample.

high- and low-risk workers.[28]

In the global sample, there is an inverted U-shaped response of labor supply to temperature that is consistent with prior literature from individual countries (Garg, Gibson, and Sun, 2019; Graff Zivin and Neidell, 2014). However, this relationship is almost entirely driven by workers in high-risk industries; for example, these workers work about 30 minutes less per week for each day when the temperature is 40° C or -10° C (although the latter is estimated somewhat imprecisely), both relative to a day with a maximum of 27° C. Perhaps the most striking finding is that the low-risk response function is essentially flat over the full range of observed temperatures. It is noteworthy that the higher end of the temperatures in the response function plots is within the sample.[29]

Table 2 reports on some key features of these response functions, providing marginal effects at various temperatures. Specifically, the estimates represent the change in weekly minutes worked per worker resulting from one additional day at a given temperature, compared to a reference day at 27° C. Column 1 reports estimates from the full sample of workers, while columns 2 and 3 provide estimates from the low-risk and high-risk subsamples, respectively. Finally, column 4 has results from estimating a version of Equation 6 that tests whether the effects of temperature are different for high-risk workers.

The data statistically confirm that extreme temperature days affect high-risk workers. Examining Column 1, we find that a day at 40° C, leads to a decrease in labor supply of

[28]The distribution shown in the histograms is weighted in the same manner as the regression. Within each country, observations are weighted by the sample weights specified in that country's survey, while across countries, observations are differentially weighted according to the country's total population of workers in the particular risk group (see Section IV).

[29]The range of temperatures in sample is -19.2° C to 46.1° C for high-risk workers and -17.3° C to 45.7° C for low-risk workers.

22.3 minutes per worker, relative to a day at 27° C. However, this pooled response masks substantial heterogeniety across low- and high-risk workers, with virtually the entire effect occuring among high-risk workers (see columns 3 and 4). We also note that even at 45° C, the effect for high-risk workers is statistically significant and larger, with a weekly decline in labor supply of almost 1 hour. High-risk workers are also affected at the other end of the temperature distribution, with a day at -10° C leading to reduced labor supply of about 30 minutes per worker compared to a day at 27° C, although the cold day estimates would not be considered statistically signifcant by conventional criteria. As with the hot days, there is virtually no response to a cold day for low-risk workers. Finally, the response functions of high- and low-risk workers differ significantly ($p = 9.8\%$).

	Weekly minutes worked per worker			
	(1)	(2)	(3)	(4)
Daily maximum temperature	All workers	Low-risk workers	High-risk workers	High minus Low
45°	-43.5	-11.0	-58.6	-47.6
	(14.1)	(11.8)	(22.4)	(26.4)
40°	-22.3	-5.7	-28.7	-23.0
	(7.4)	(6.2)	(12.1)	(14.2)
35°	-4.5	-1.2	-3.8	-2.6
	(2.2)	(2.1)	(4.9)	(5.4)
27°	–	–	–	–
	–	–	–	–
10°	-3.8	-0.9	-12.3	-11.5
	(4.0)	(4.9)	(12.0)	(13.0)
5°	-4.9	-1.1	-16.0	-14.9
	(5.1)	(6.3)	(15.6)	(16.8)
0°	-6.1	-1.3	-19.6	-18.3
	(6.3)	(7.7)	(19.1)	(20.7)
-5°	-7.2	-1.6	-23.2	-21.6
	(7.5)	(9.2)	(22.7)	(24.5)
-10°	-8.3	-1.8	-26.9	-25.0
	(8.7)	(10.6)	(26.2)	(28.3)
Overall significance of $\boldsymbol{T}_{j,t}$	$p = 10.0\%$	$p = 17.3\%$	$p = 11.1\%$	$p = 9.8\%$
Adj R-squared	0.56	0.56	0.56	0.56
N	6,599,335	4,175,377	2,423,958	6,599,335

Table 2: Weekly labor supply response to temperature. Column 1 of this table shows estimates for a single labor supply-temperature response function estimated using all worker observations. In this regression, observations within each country are weighted by the sample weights specified in that country's survey, while across countries, observations are differentially weighted according to the country's total population. Columns 2 and 3 show estimates for labor supply-temperature responses that differ for low- and high-risk workers respectively, as specified in Equation 6. In this regression, observations within each country are weighted by the sample weights specified in that country's survey, while across countries, observations are differentially weighted according to the country's total population of workers in the particular risk group. Column 4 shows estimates of the difference between the high- and low-risk responses (Column 3 minus Column 2). All regression estimates are from a restricted cubic spline in daily maximum temperature. Point estimates indicate the effect on weekly labor supply of a single day at each daily maximum temperature value shown, relative to a day with a maximum temperature of 27°C (81°F). Standard errors (in parentheses) are clustered at the ADM1 (e.g., state) × month-of-sample level.

We probed these results in several ways and two qualitative findings emerged. First, the evidence of an inverted U-shape response function for high-risk workers and little evidence of a response among low-risk workers is broadly consistent across alternative specifications of temporal controls in the estimating equation (Table 3) as well as to alternative functional forms (i.e., different nonlinear functions of $\boldsymbol{T}_{j,t}$), including a non-parametric binned regression (Appendix D.1). Second, there is only quite modest evidence of heterogeneity along observable dimensions. For example, we fail to reject that the labor supply response to daily temperatures varies by either income or climate among low-risk workers (Appendix Table G.1). Additionally for high-risk workers, we fail to reject that the response to daily temperatures varies by climate, though do find, with borderline statistical significance, that labor supply is less sensitive to daily temperatures in richer locations than in poorer locations.

Lastly, in Appendix D.2, we show that the results are robust to alternative classifications of high- and low-risk workers that take into account occupation rather than just industry. However, because our projection of the disutility costs of climate change relies on an industry-based classification of high- and low-risk workers,[30] we focus on the industry-based classification in the subsequent analysis.

V.B Temperature-induced disutility in a high-risk job, relative to a low-risk job

Section II.D outlined a revealed-preference approach to inferring changes in labor disutility from observed changes in labor supply in response to daily temperatures. This subsection develops estimates of the value of temperature-induced disutility in a high-risk job relative to a low-risk job, or the hedonic value of thermal comfort in a low-risk job. Importantly, because locations vary in their distribution of the differences between daily temperatures and T_{opt} over the year, the hedonic value of thermal comfort in a low-risk job will vary by location. In the extreme case of a location in which the temperature is exactly T_{opt} on every day of the year, the hedonic value of thermal discomfort will be exactly zero for both high-risk and low-risk workers. By contrast, in a location where daily temperatures are far from T_{opt}, this hedonic value will be large because of the shapes of the low-risk (flat) and high-risk (inverted U) response functions.

To characterize the temperature-induced disutility in a high-risk job relative to a low-risk job, in impact region c on a typical calendar date t (e.g., a typical January 23), we first calculate how much each type of worker's labor supply changes when experiencing region c's long-run average maximum temperature for date t, relative to experiencing the optimum temperature. In implementing this calculation, we use the empirically determined optimum temperatures for high- and low-risk labor supply, which are $T_{opt}^{high} = 30.6°C$ and

[30] This is because the census data sources used to estimate and project how the share of high-risk workers is related to a location's income and climate only contain detailed occupation information for a limited set of countries.

	Weekly minutes worked per worker							
	Low-risk workers				High-risk workers			
Daily maximum temperature	(1)	(2)	(3)	(4)	(5)	(6)	(7)	(8)
45°	-8.4	-9.4	-4.3	-11.0	-50.4	-50.8	-48.0	-58.6
	(11.6)	(11.8)	(11.4)	(11.8)	(23.8)	(23.6)	(21.8)	(22.4)
40°	-4.5	-4.9	-2.0	-5.7	-24.9	-25.2	-25.4	-28.7
	(6.1)	(6.2)	(6.0)	(6.2)	(12.6)	(12.5)	(11.8)	(12.1)
35°	-1.3	-1.2	-0.2	-1.2	-3.7	-3.8	-6.2	-3.8
	(2.0)	(2.0)	(2.0)	(2.1)	(5.0)	(4.8)	(5.0)	(4.9)
27°	–	–	–	–	–	–	–	–
	–	–	–	–	–	–	–	–
10°	0.4	-0.1	-1.2	-0.8	-9.2	-9.1	-0.6	-12.3
	(4.5)	(4.5)	(4.8)	(4.9)	(12.8)	(12.2)	(12.3)	(12.0)
5°	0.6	-0.2	-1.6	-1.1	-12.0	-11.8	-0.7	-16.0
	(5.8)	(5.8)	(6.2)	(6.3)	(16.6)	(15.8)	(15.9)	(15.6)
0°	0.7	-0.2	-2.0	-1.3	-14.7	-14.5	-0.9	-19.6
	(7.2)	(7.2)	(7.6)	(7.7)	(20.4)	(19.4)	(19.5)	(19.1)
-5°	0.8	-0.3	-2.3	-1.6	-17.4	-17.2	-1.1	-23.2
	(8.5)	(8.5)	(9.0)	(9.2)	(24.2)	(23.0)	(23.1)	(22.7)
-10°	0.9	-0.3	-2.7	-1.8	-20.1	-19.9	-1.2	-26.9
	(9.8)	(9.8)	(10.4)	(10.6)	(27.9)	(26.6)	26.7	(23.2)
Adj R-squared	0.56	0.56	0.56	0.56	0.56	0.56	0.56	0.56
N	4,175,377	4,175,377	4,175,377	4,175,377	2,423,958	2,423,958	2,423,958	2,423,958
Subnational location FE	Yes	Yes	Yes	Yes	Yes	Yes	Yes	Yes
Country × Year FE	Yes	–	–	Yes	Yes	–	–	Yes
ADM1 × Year FE	–	–	Yes	–	–	–	Yes	–
Country × Month-of-year FE	Yes	–	–	–	Yes	–	–	–
Country × Week-of-year FE	–	–	Yes	Yes	–	–	Yes	Yes
Country × Month × Year	–	Yes	–	–	–	Yes	–	–

Table 3: Labor supply response to temperature: Alternative specifications of temporal controls. This table shows estimates for labor supply-temperature responses that differ for low-risk (Columns 1-3) and high-risk (Columns 4-6) workers. All regression estimates are from a restricted cubic spline in daily maximum temperature; observations within each country are weighted by the sample weights specified in that country's survey, while across countries, observations are differentially weighted according to the country's total population of workers in the particular risk group. Point estimates indicate the effect on weekly labor supply of a single day at each daily maximum temperature value shown, relative to a day with a maximum temperature of 27°C (81°F). Standard errors (in parentheses) are clustered at the ADM1 (e.g., state) × month-of-sample level. Each column shows estimates using a different specification of temporal controls. Columns 4 and 8 employ the temporal controls specified in Equation 6 (i.e., country × year fixed effects, country × week-of-year fixed effects). Columns 1 and 5 employ country × year fixed effects along with country × month-of-year fixed effects; Columns 2 and 6 employ country × month × year fixed effects; Columns 3 and 7 employ ADM1 × year fixed effects along with country × week-of-year fixed effects. All regressions employ subnational location fixed effects and day-of-week fixed effects.

$T_{opt}^{low} = 29.3°C$.[31] Let $\overline{\boldsymbol{T}}_{c,t}$ represent region c's 1950-2010 average temperature vector for each calendar date t, and let $\boldsymbol{T}_{opt}^{r}$ denote the temperature vector corresponding to daily temperature T_{opt}^{r} for $r \in \{high, low\}$.[32] For a worker in risk group r, the annual difference in average minutes worked per worker relative to a year where every day's temperature is T_{opt}^{r} is:

$$\sum_{t} \Big[\widehat{f}_r(\overline{\boldsymbol{T}}_{c,t,y}) - \widehat{f}_r(\boldsymbol{T}_{opt}^{r})\Big], \tag{7}$$

where $\widehat{f}_r(\cdot)$ denote estimates of the temperature response functions from Equation 6. The additional change in minutes worked by a high-risk worker relative to a low-risk worker is thus:

$$\sum_{t} \Big(\Big[\widehat{f}_{high}(\overline{\boldsymbol{T}}_{c,t,y}) - \widehat{f}_{high}(\boldsymbol{T}_{opt}^{high})\Big] - \Big[\widehat{f}_{low}(\overline{\boldsymbol{T}}_{c,t,y}) - \widehat{f}_{low}(\boldsymbol{T}_{opt}^{low})\Big]\Big). \tag{8}$$

Valuing the temperature-induced disutility in a high-risk job relative to a low-risk job requires us to multiply the labor supply change from Equation 8 by a wage rate and divide by the Frisch elasticity of labor supply. We construct a wage rate for each impact region (ω_c) based on its average per capita income in 2010,[33] and following Chetty et al. (2011), we use a Frisch elasticity (ϵ) of 0.5.[34] The annual disutility of a high-risk job in impact region c is thus:

$$\frac{\omega_c}{\epsilon} \sum_{t} \Big(\Big[\widehat{f}_{high}(\overline{\boldsymbol{T}}_{c,t,y}) - \widehat{f}_{high}(\boldsymbol{T}_{opt}^{high})\Big] - \Big[\widehat{f}_{low}(\overline{\boldsymbol{T}}_{c,t,y}) - \widehat{f}_{low}(\boldsymbol{T}_{opt}^{low})\Big]\Big). \tag{9}$$

Figure 4 maps each impact region's annual temperature-induced disutility in a high-risk job relative to a low-risk job, expressed as a percentage of the impact region's 2010 per capita GDP. The map reveals that the hedonic value of thermal comfort in a low-risk job is highest in regions that routinely experience a large number of extreme hot or cold days in a year; for example, it is approximately 7.7% of per capita income in Alaska and 6.9% in Sudan.

[31] Although the model developed in Section II posits a single optimum temperature, T_{opt}, for both types of workers, our estimates of high- and low-risk temperature responses (Figure 3) reveal that the temperatures at which labor supply is maximized differ slightly for the two worker types.

[32] In particular, the vector $\overline{\boldsymbol{T}}_{c,t}$ contains nonlinear transformations of daily maximum temperatures on calendar date t (e.g., January 23) taken from GMFD, averaged across the years 1950-2010 and across grid cells in c. The vector $\boldsymbol{T}_{opt}^{r}$ simply contains the nonlinear transformations of T_{opt}^{r}.

[33] Specifically, to obtain a wage rate, we multiply per capita income by the labor share of income and divide by the number of minutes worked in a year. Per capita income for 2010 is taken from the SSP3 socioeconomic scenario and downscaled to the impact region level (Appendix B.3.3). Following Karabarbounis and Neiman (2014), we use 0.6 as the labor share of income. We assume 250 work days in a year (i.e., 50 weeks, 5 days per week) with 6 work hours per day, which is roughly the average in our data (Table 1). We assign the same wage rate for high- and low-risk workers because the SSPs do not provide a breakdown of income by worker type.

[34] Chetty et al. (2011) recommend a value of 0.5, while reporting that estimates from previous studies range from 0.37 to 0.7. Using values other than 0.5 in Equation 9 will simply scale the disutility estimates proportionally.

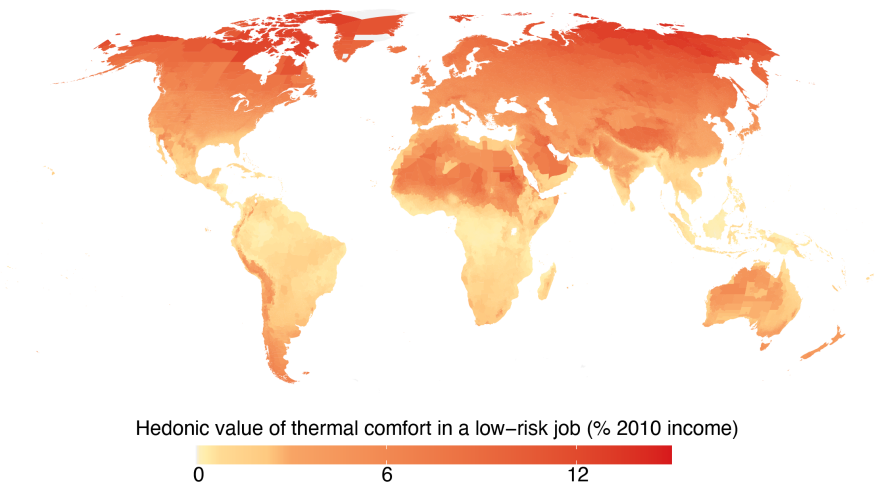

Figure 4: Hedonic value of thermal comfort in a low-risk job. Map displays the value of annual temperature-induced disutility in a high-risk job relative to a low-risk job in 24,378 impact regions. For each region, the value of disutility is calculated according to Equation 9 and then summed over days of the year and expressed as a percent of each regions's 2010 per capita income.

Table 4 summarizes the temperature disutility of high risk jobs across the world and highlights its value in key regions (Panel A) and also lists the hedonic value of other workplace amenities estimated in other studies as a basis of comparison (Panel B). Overall, it is evident that the reduction in thermal discomfort offered by low-risk jobs is a meaningful component of compensation in many parts of the world, with an average global value of 2.9% percent of annual income. Comparisons between the entries in Panels A and B reveal that thermal discomfort associated with high-risk jobs in many parts of the world is similar in magnitude to other job amenities that have been researched extensively in the workplace amenity literature. Perhaps, the most researched amenity is mortality risk; Greenberg et al. (2021) finds that U.S. army soldiers would have paid 4.1% of annual wages to avoid the increase in the occupational mortality rate between 2002 and 2007 (due to the Afghanistan and Iraq wars),[35] which is comparable to the thermal benefits of low-risk jobs in Chicago. Further, in many parts of the world, the hedonic value of thermal comfort in a low-risk job is similar to the value of a smoke-free workplace estimated in Wissmann (2022) and the value of employer-sponsored health insurance estimated in Kolstad and Kowalski (2016). However, it is generally smaller than the value of amenities related to job stability and convenient or predictable work schedules (Lanfranchi, Ohlsson, and Skalli, 2002; Mahmud et al., 2021; Mas and Pallais, 2017).

[35]This value was calculated by subtracting the predicted 4-year enlistment bonus associated with the 2007 mortality rate from the predicted 4-year enlistment bonus associated with the 2002 mortality rate (based on Figure 3, right panel, in Greenberg et al. (2021)), and then dividing this difference by mean 4-year income over the period.

Workplace Amenity	Location	Willingness-to-pay (% of income)
A. Estimates of the value of thermal comfort in a low-risk job		
Thermal comfort in a low-risk job	Global average	2.9% (2.4%)
	10^{th} percentile	0.6%
	25^{th} percentile	1.2%
	50^{th} percentile	2.9%
	75^{th} percentile	4.0%
	90^{th} percentile	5.5%
	Selected cities	
	Sao Paulo, Brazil	1.5% (1.9%)
	Delhi, India	3.3% (1.7%)
	Chicago, USA	4.8% (5.7%)
	Oslo, Norway	6.6% (7.9%)
	Baghdad, Iraq	8.3% (4.2%)

B. Estimates of the value of workplace amenities from prior studies

			Study
Mortality risk	USA army	4.1%	Greenberg, et al., 2021
Smoke-free workplace	Germany	2.4%	Wissman, 2022
Employer-sponsored health insurance	Massachusetts, USA	4.5%	Kolstad and Kowalski, 2016
Work-from-home option	USA	8%	Mas and Pallais, 2017
Predictable work schedule	USA	20%	Mas and Pallais, 2017
Day shift vs. night shift	France	16%	Lanfranchi et al., 2002
1-year contract vs. none	Bangladesh	12%	Mahmud et al., 2021
30-day termination notice vs. none	Bangladesh	27%	Mahmud et al., 2021

Table 4: Estimates of the hedonic value of workplace amenities. Table displays estimates of the value of thermal comfort in a low-risk job (standard errors in parentheses) along with estimates of the hedonic value of other workplace amenities. All values are expressed as a percent of annual income. Panel A highlights estimates of the hedonic value thermal comfort in a low-risk job from the present study, including the global average value, the value for percentiles of the global population, and the value for selected cities. Panel B presents estimates from prior studies on the hedonic value of various other workplace amenities.

VI Worker disutility impacts of climate change

The previous section demonstrated that thermal comfort is an important job amenity. At the same time, climate change is already influencing temperatures with larger changes projected in the future. This section presents estimates of workers' willingness to pay to avoid on the job thermal disutility due to climate-change-induced changes in temperature. Section VI.A reports on our efforts to estimate the ongoing structural transformations in the global economy that will alter the shares of workers in high- and low-risk sectors over the remainder of this century. Sections VI.B and VI.C outline our approach to calculating the labor disutility costs of climate change at the end of the century (accounting for changes in the shares of high- and low-risk workers) and report on the results from implementing it, respectively. Finally Section VI.D uses these ingredients to develop estimates of the labor disutility partial social cost of carbon (SCC), which is the additional global worker disutility due to the release of an additional ton of CO_2 today.

VI.A Empirical estimates of the determinants of workforce composition

The very different responses of high- and low-risk workers to temperature means that any estimates of future climate change impacts must account for the location-specific changes in the shares of these workers between today and the future. We do this in two steps. First, we use historical census data to estimate how workforce composition varies with average income per capita (a key feature of structural transformation (Matsuyama, 2017)) and long-run average temperature (a driver of workforce composition in our stylized model in Section II). We then apply these estimates to projected values of income per capita and long-run average temperature to predict workforce composition in future years for all locations around the world.

Using ADM1-level census data from 48 countries between 1980 and 2010 (Minnesota Population Center, 2019), we estimate how the share of high-risk workers varies as a function of average income per capita and long-run average temperature.[36] A large literature on structural transformation establishes that higher income per capita is associated with a lower share of high-risk workers,[37] while the theoretical framework we lay out in Section II indicates that a warmer climate can affect the share of high-risk workers (although the direction of the effect is ambiguous). Moreover, a practical reason to focus on these two explanatory variables is that credible, global projections of their future evolution are readily available and can be used to predict the future share of high-risk workers.

[36] Appendix B.3.1 contains a description of these data sources.

[37] The prior literature has focused on two mechanisms for this association— a demand-side effect due to low income elasticity for agricultural goods, pushing workers out of the agricultural sector, and a supply-side effect from differential sectoral productivity growth rates, pulling workers into high-growth, non-agricultural sectors (Alvarez-Cuadrado and Poschke, 2011; Buera and Kaboski, 2009; Dennis and İşcan, 2009; Duarte and Restuccia, 2010; Echevarria, 1997; Matsuyama, 2017).

Specifically, we estimate the following cross-sectional regression:

$$HighRiskShare_s = \gamma \overline{LogGDPpc}_s + h(\overline{\boldsymbol{T}}_s) + \eta + \epsilon_s. \tag{10}$$

where $HighRiskShare$ is observed for each ADM1 unit s (first-level administrative unit; e.g., state) in 48 countries (Minnesota Population Center, 2019) (1,073 ADM1 units). These observations are drawn from national census microdata in the most recent census year available for each country in the IPUMS database. Of the 1,073 ADM1 units in our sample, 618 have only one census year from the 1980-2010 period, so we estimate this equation cross-sectionally with the most recent census year for each country. The variable $\overline{LogGDPpc}_s$ denotes the natural logarithm of GDP per capita in ADM1 unit s averaged over the 15 years prior to the census year and is taken from Penn World Tables and Gennaioli et al. (2014),[38] while $h(\cdot)$ is a function of a daily maximum temperature vector in s averaged over the 30 years previous to the census year ($\overline{\boldsymbol{T}}_s$). In particular, the vector $\overline{\boldsymbol{T}}_s$ contains polynomials of daily maximum temperatures (up to fourth order) taken from GMFD, averaged across the 30 years and across grid cells in s.[39] The coefficient η denotes a constant, and ϵ_s denotes the stochastic error term.

Results from the estimation of Equation 10 are shown in Figure 5, Panels A and B (tabular results are reported in Table E.1 in Appendix E).[40] Panel A plots the high-risk share against $\overline{LogGDPpc}$ for all observations in the estimating sample, with the solid black line depicting the estimated relationship between these two variables, evaluated at the sample mean value of $\overline{\boldsymbol{T}}$. Consistent with the literature on structural transformation (Matsuyama, 2017), we find that locations with a higher income have a lower share of high-risk workers. A doubling of income is associated with roughly a 12 percentage point fall in the share of high-risk workers and a corresponding rise in the share of low-risk workers.

Panel B plots the high-risk share against long-run average daily maximum temperature for all observations in the estimating sample, with the solid black curve depicting the estimated relationship between these two variables, evaluated at the sample mean value of $\overline{LogGDPpc}$.[41] The estimated high-risk share of employment generally falls as long-

[38] Appendix B.3.2 describes how we combine national income data from Penn World Tables with the subnational distribution of income from Gennaioli et al. (2014). Because changes in income are unlikely to immediately be reflected in the high-risk share, we take an average over incomes in the current year and 14 previous years (equally weighted).

[39] As with the functions in Equation 6, we choose $h(\cdot)$ to be a linear function of the nonlinear elements of $\overline{\boldsymbol{T}}_s$. The duration of 30 years is chosen based on the standard definition of "climate" (Allen et al., 2018).

[40] In Appendix E, we also describe and estimate alternative specifications of Equation 10, including one that uses the full sample of census years and exploits the panel structure of the data with fixed effects for census years and countries. Results from these specifications are qualitatively similar to the ones shown here. However, specifications with country or census year fixed effects cannot be used to predict the high-risk share outside the countries and years in the sample. Because our projection of climate change impacts requires the prediction of high-risk share for all locations globally and in future years, we use predictions based on Equation 10 for this purpose.

[41] Because $\overline{\boldsymbol{T}}$ contains polynomials of daily maximum temperatures, the relationship between high risk

run daily maximum temperatures rise, although there is some evidence of nonlinearity at extremely hot temperatures. However, the economic significance of this association is considerably less than that of high-risk share and income: an increase in the long-run daily maximum temperature from 15°C to 25°C is associated with only a 7 percentage point fall in the share of high-risk workers.

We use the estimated coefficients from Equation 10, along with projected future values of income ($\overline{LogGDPpc}$) and long-run average temperature ($\overline{\boldsymbol{T}}$), to predict the share of high-risk workers in each impact region c at each year y. We denote this predicted value $\widehat{\rho}_{c,y}$.[42] Figure 5 maps the predicted shares of high-risk workers in every impact region in 2020 (Panel C) and 2099 (Panel D). At present, high-risk workers predominate in developing countries. However, by end-of-century, the proportion of high-risk workers is expected to decline in most parts of the world largely via ongoing economic development. These projected changes to workforce composition influence the below estimates of climate change's impacts; a failure to account for them would tend to overstate the costs of climate change, because it would be based on an overestimate of the share of workers in high-risk jobs where the effects of high temperatures are largest.

VI.B Methods: Calculating future climate change impacts

To estimate future labor disutility costs of climate change at high resolution over the coming century, we apply a set of probabilistic climate change projections to the labor supply response functions shown in Figure 3. In so doing, we account for future changes in workforce composition using the predicted high- and low-risk works shares illustrated in Figure 5. We then value the disutility implied by these projected labor supply changes based on Equation 4, analogous to the disutility calculations presented in Section V.

Specifically, let $\boldsymbol{T}_{c,t,y}$ represent the temperature vector for impact region c at a future date t, under a warmer climate projected for year y. In contrast, let $\boldsymbol{T}_{c,t,2015}$ represent the counterfactual temperature vector for the same impact region and date, but under a climate that is the same as that of 2015.[43] Similarly, while $\widehat{\rho}_{c,y}$ indicates the predicted share of high-risk workers in c and y under a warmer climate and future levels of income, we let $\widehat{\rho}_{c,\widetilde{y}}$ denote the counterfactual share of high-risk workers that would occur in region c in year y in the absence of climate change. This counterfactual reflects changes in workforce

employment and long-run climate depends on the full distribution of daily temperatures and cannot be plotted on a two-dimensional coordinate plane. The solid curve in Figure 5, Panel B, can be interpreted as the predicted high-risk share for a hypothetical location with the long-run temperature value on the horizontal axis, but no day-to-day variance in this temperature. See Appendix E for more detailed results.

[42] To estimate $\widehat{\rho}$ at impact region level, we downscale national income projections from the Shared Socioeconomic Pathways (SSPs) based on present-day nighttime lights (see Appendix B.3.3 for details). For high-resolution climate projections, we use the climate simulations described in Section III. We impose the restriction that $\widehat{\rho} \leq 0.95$, the highest share observed in the data used to estimate Equation 10. This ensures that predicted shares $\widehat{\rho}_{c,y}$ and $1 - \widehat{\rho}_{c,y}$ never fall outside the unit interval.

[43] These vectors are constructed in exactly the same way as is done for the temperature vectors used in estimating Equation 6, with nonlinear grid-cell level transformations of daily maximum temperature aggregated to the impact region level.

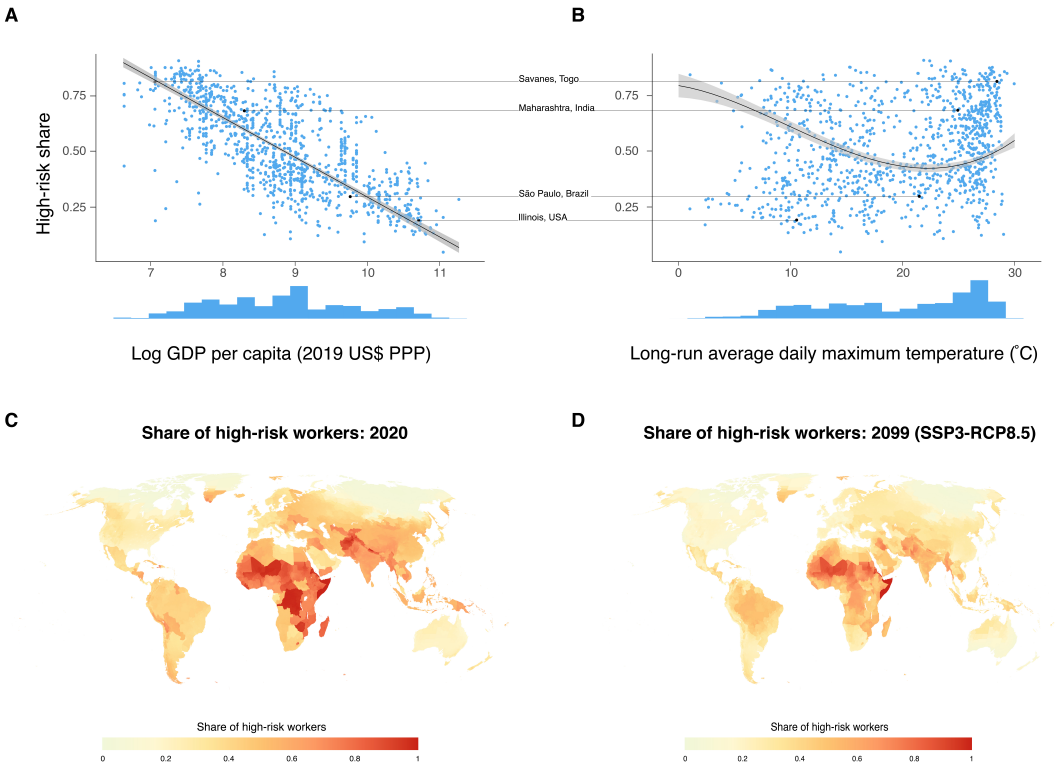

Figure 5: Workforce composition, income, and climate. The scatter of points in Panels A depicts the association between the share of high-risk workers and log GDP per capita using ADM1-level (e.g., state) data from 48 countries. The scatter of points in Panel B depicts the association between the share of high-risk workers and long-run average temperature in the same data. Selected ADM1 units in the sample are indicated in each plot. Histograms below each plot show the in-sample distribution of log GDP per capita (Panel A) and long-run average temperature (Panel B). The black line in Panel A illustrates the estimated relationship between the share of high-risk workers and log GDP per capita, evaluated at the sample mean long-run average temperature; the black curve in Panel B illustrates the estimated relationship between the share of high-risk workers and long-run average temperature, evaluated at the sample mean log GDP per capita. Both results are obtained from estimating Equation 10 and shaded areas depict 95% percent confidence intervals (see Appendix E for detailed results). Using these estimates, Panels C and D map the predicted share of high-risk workers across 24,378 impact regions in 2020 and 2099 respectively. All values shown refer to the SSP3 socioeconomic scenario and the RCP8.5 emissions scenario and represent climate model weighted mean predictions across Monte Carlo simulations conducted on 33 climate models.

composition due to economic development, but not due to climate-driven adaptation. We then calculate the labor supply impact of climate change in impact region c at future date t in year y as:

$$\textit{Labor Supply Impact Of Climate Change}_{c,t,y} = \underbrace{\left[\widehat{\rho}_{c,y}\widehat{f}_{high}(\boldsymbol{T}_{c,t,y}) + (1-\widehat{\rho}_{c,y})\widehat{f}_{low}(\boldsymbol{T}_{c,t,y})\right]}_{\substack{\text{Temperature-induced labor supply under climate change} \\ \text{(with economic development and climate-driven adaptation)}}} - \underbrace{\left[\widehat{\rho}_{c,\widetilde{y}}\widehat{f}_{high}(\boldsymbol{T}_{c,t,2015}) + (1-\widehat{\rho}_{c,\widetilde{y}})\widehat{f}_{low}(\boldsymbol{T}_{c,t,2015})\right]}_{\substack{\text{Temperature-induced labor supply without climate change} \\ \text{(with economic development)}}}, \tag{11}$$

where $\hat{f}_r(\cdot)$ represents the fitted values from Equation 6 for each of the two risk groups r. The first term in Equation 11 represents the total predicted labor supply under climate change, averaging across risk groups using predicted high-risk employment shares $\widehat{\rho}_{c,y}$. In contrast, the second term represents the total predicted labor supply under a counterfactual with no climate change, where effects in each risk group are averaged using counterfactual high-risk employment shares $\widehat{\rho}_{c,\tilde{y}}$.

The difference between these two terms measures the impacts of climate change on labor supply, accounting for climate change-induced shifts in workforce composition. The disutility costs of climate change are then calculated with the same approach outlined in Section V.B by multiplying the change in labor supply by the ratio of the impact region's projected wage rate and the Frisch elasticity of labor supply.

To highlight the importance of economic development and climate-driven adaptation, we also construct two alternative projections of disutility costs that ignore one or both of these mechanisms. The first of these is a "fixed workforce" projection in which each impact region's shares of high- and low-risk workers are held fixed through the century at their 2015 values. The second is a "no climate adaptation" projection in which each impact region's high- and low-risk shares are allowed to change due to economic development, but not due to climate-driven adaptation. These alternative calculations are detailed in Appendix F.

In all our projections, we account for uncertainty in climate projections as well as uncertainty arising from econometric estimates of the labor supply-temperature relationship (Equation 6) and risk-group shares (Equation 10). Following the procedure in Rode et al. (2021) and Carleton et al. (2022), we construct labor supply impact and disutility cost estimates under each of 33 distinct climate projections (Section III.B) using a Monte Carlo resampling of coefficient estimates from Equations 6 and Equation 10. When reporting projected values in any given year, we report summary statistics (e.g., mean, quantiles) of this entire distribution. These distributions can be used to develop certainty-equivalent estimates of climate damages.

VI.C Results: Projected impacts of climate change

Here we present projected impacts of climate change on labor supply and disutility. Specifically, Figure 6A maps changes to labor supply per worker for all impact regions at 2099, under a very high emissions scenario (RCP8.5).[44] For each impact region, the changes in daily labor supply specified in Equation 11 are averaged over all days in 2099 and over all Monte Carlo simulations from 33 climate models. Figure 6 reveals that the climate

[44]RCP8.5 is widely recognized to be an aggressive scenario for future increases in greenhouse gas emissions, while RCP6.0 is believed to be a more plausible scenario (Hausfather and Peters, 2020). However, the high spatial resolution future climate projections that we use (Appendix B.2.2) are only available for RCP8.5 and an intermediate emissions scenario, RCP4.5. We therefore present results under these 2 scenarios. Projected impacts of climate change on labor supply and disutility under RCP4.5 are mapped in Appendix F.2.

change-induced labor supply losses are distributed unevenly across locations around the world. In the warmest parts of the world with a large share of high-risk workers (e.g., much of Africa), climate change is projected to cause declines in labor supply at 2099 amounting to over 20 minutes per worker per day. In contrast, temperate regions of the world such as northern Europe are projected to experience negligible change or even slight gains in labor supply, both due to the small share of high-share risk workers and a fewer number of extreme cold days under climate change.

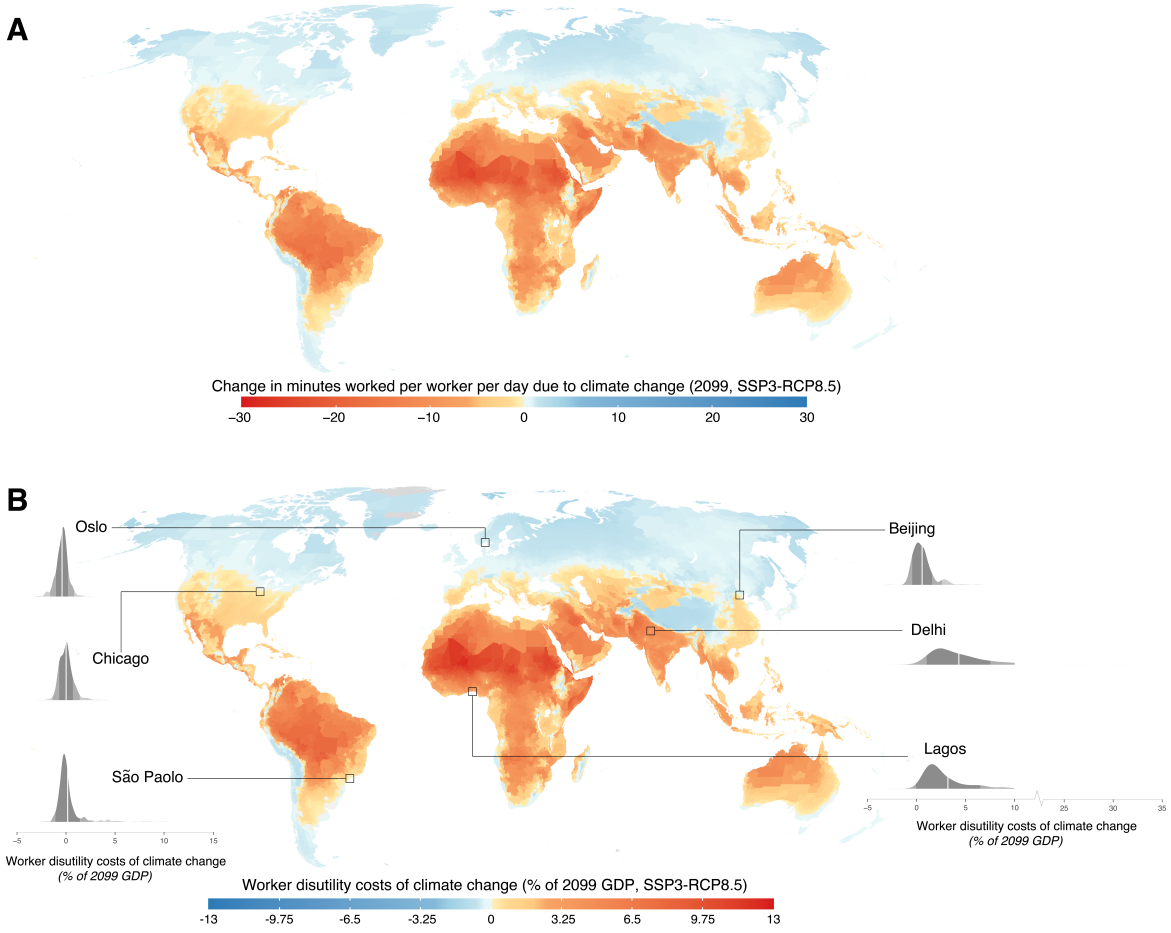

Figure 6: Projected impact of climate change on labor supply and disutility at 2099 in a very high emissions scenario. Panel A maps the labor supply impacts of climate change in the year 2099 (minutes per worker per day), across 24,378 impact regions. Panel B maps the annual worker disutility costs of climate change in the year 2099. Costs are calculated based on Equation 11 with a labor share of income = 0.6 (Karabarbounis and Neiman, 2014) and elasticity of labor supply = 0.5 (Chetty et al., 2011), and are expressed as a percentage of each impact region's 2099 GDP. Estimates account for changes to workforce composition as incomes grow and the climate warms, and the maps show the climate model weighted mean estimate across Monte Carlo simulations conducted on 33 climate models. Probability density functions in Panel B plot the full distribution of disutility costs for selected cities, accounting for climate model and econometric uncertainty. In each density plot, solid white lines indicate the mean estimate shown on the map. All values shown refer to the RCP8.5 emissions scenario and the SSP3 socioeconomic scenario.

Figure 6B maps the corresponding total annual labor disutility costs for each impact

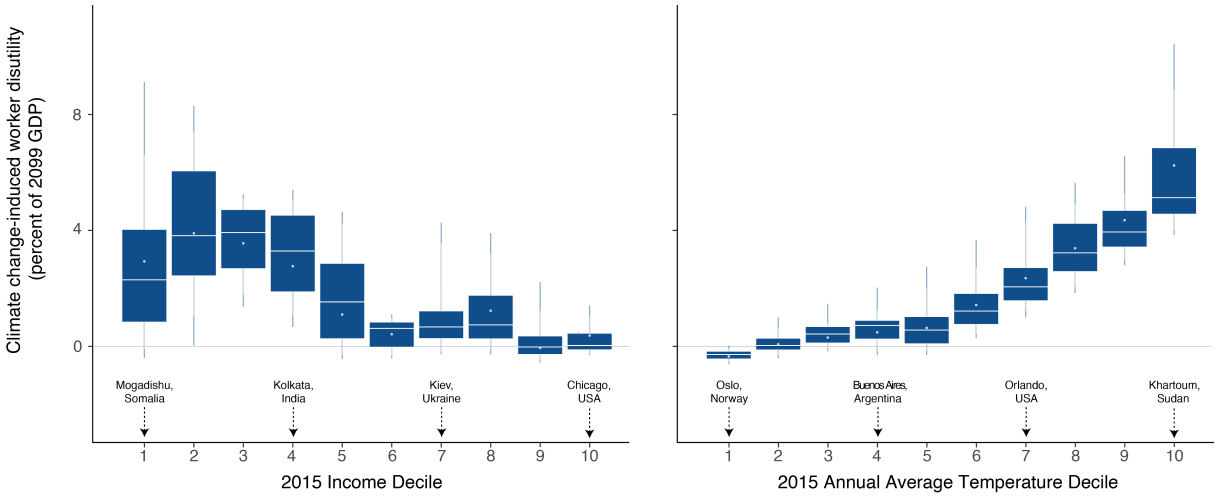

Figure 7: Climate change-induced worker disutility costs at 2099 by present-day income and annual average temperature deciles. Annual worker disutility costs of climate change in the year 2099 under the RCP8.5 emissions scenario and the SSP3 socioeconomic scenario, by decile of 2015 per capita income and annual average daily maximum temperature. Income and annual average temperature deciles are calculated across 24,378 global impact regions and are population weighted using 2015 population values; representative locations in selected deciles are indicated. Estimates account for changes to workforce composition as incomes grow and the climate warms. Costs are calculated under a labor share of income = 0.6 (Karabarbounis and Neiman, 2014) and elasticity of labor supply = 0.5 (Chetty et al., 2011), and are expressed as a percentage of the combined 2099 GDP of all regions within the decile. All box plots show statistics of the population-weighted distribution of estimated mean impacts across impact regions within a decile, where means are taken for each impact region across Monte Carlo simulations that account both for econometric and climate model uncertainty. Solid vertical lines in each box plot extend to the 5^{th} and 95^{th} percentiles of this distribution, boxes indicate the interquartile range, white horizontal lines indicate the median, and white circles indicate the mean.

region at 2099, as a percentage of the impact region's projected 2099 GDP. In the regions most affected by warming (e.g., parts of Brazil and India), the costs of increased worker disutility are projected to be as large as 12% of GDP. In contrast, in cool regions such as northern Europe, workers are projected to experience modest utility benefits. While the map displays each location's mean projected costs across econometric and climate model uncertainty, the density plots for select cities show the full distribution, with the white line equal to the mean estimate shown on the map.

The unequal disutility costs of climate change mapped in Figure 6B systematically correlate with present-day income and climate. Figure 7 reveals that today's poorest and hottest locations are projected to experience the largest disutility costs relative to their GDP at end-of-century. This pattern emerges partly because today's poorest locations tend to already experience hot climates where additional warming leads to large changes in high-risk labor supply. Furthermore, we estimate that today's poorest locations will continue to have a large share of their workforce employed in high-risk sectors, even at end-of-century. In contrast, low-risk workers are dominant in today's wealthiest locations, which also tend to have temperate climates.

Aggregating globally over all impact regions, we project that by 2099, the disutility costs of climate change under RCP8.5 will amount to nearly 1.8% of 2099 global GDP

(Figure 8A, green line). Moreover, we find that projected changes in workforce composition do not mitigate much of the overall costs of climate change. Specifically, the red line in Figure 8A plots the disutility costs of climate change under a fixed workforce projection (Appendix Equation F.2). This shows that allowing workforce composition to evolve following projected income and climate changes into the future only lowers the estimated disutility costs of climate change by 5%. This result arises due to high projected population growth in the poorest and hottest regions of the world relative to richer and cooler regions, as well as our empirical estimates that a warming climate can *increase* the share of high-risk workers in locations that are already hot (see Figure 5B).[45] Together, these imply minimal sectoral reallocation of the workforce, particularly in the poorest and hottest regions of the globe. However, we do find large returns to mitigation; under an intermediate emissions scenario (RCP4.5), projected impacts of climate change on labor disutility fall to less than 0.5% of 2099 global GDP (Figure 8B).

VI.D A social cost of carbon for labor disutility

In this subsection, we use the estimates of labor disutility under climate change from Section VI.C to compute the global social cost of labor disutility generated by emitting a marginal ton of CO_2 today. We call this object a labor disutility *partial* social cost of carbon (SCC), as it represents one component of the *total* SCC, which accounts for all climate change damages, including impacts on firm productivity, human health, and many others.

To compute the labor disutility costs imposed by a marginal ton of CO_2, we follow the approach developed in Rode et al. (2021) and Carleton et al. (2022). This involves first constructing global "damage functions" for labor disutility, which describe global aggregate disutility costs as a function of the change in global mean surface temperature (ΔGMST).[46] The procedure for estimating damage functions is detailed in Appendix H. The Finite Amplitude Impulse Response simple climate model (FAIR,117) is then used to simulate future warming trajectories that result from the marginal emission today (Smith et al., 2018). These warming trajectories, when combined with our estimated damage functions, imply a trajectory of global costs whose present discounted value represents the labor disutility component of the SCC.

[45] These estimates are reflected in the larger projected disutility costs under changing workforce composition due to economic development and climate adaptation (green line in Figure 8A), than under changing workforce composition due to economic development only (orange line in Figure 8A). Nath (2020) and Liu, Shamdasani, and Taraz (2023) also find that warming can increase the share of high-risk workers. The mechanism in the former is that a warming climate makes it harder to meet subsistence food requirements in developing countries, thereby increasing the share of workers employed in agriculture. In the latter, declining agricultural productivity under warmer temperatures reduces the demand for nonagricultural goods and services, thereby lowering nonagricultural labor demand.

[46] Global mean surface temperature is defined as the global area-weighted average of surface air temperature over the whole globe. We define ΔGMST as global mean surface temperature relative to the 2001-2010 average level, the years over which our climate change damage estimates are defined to be zero (e.g., see Figure 8).

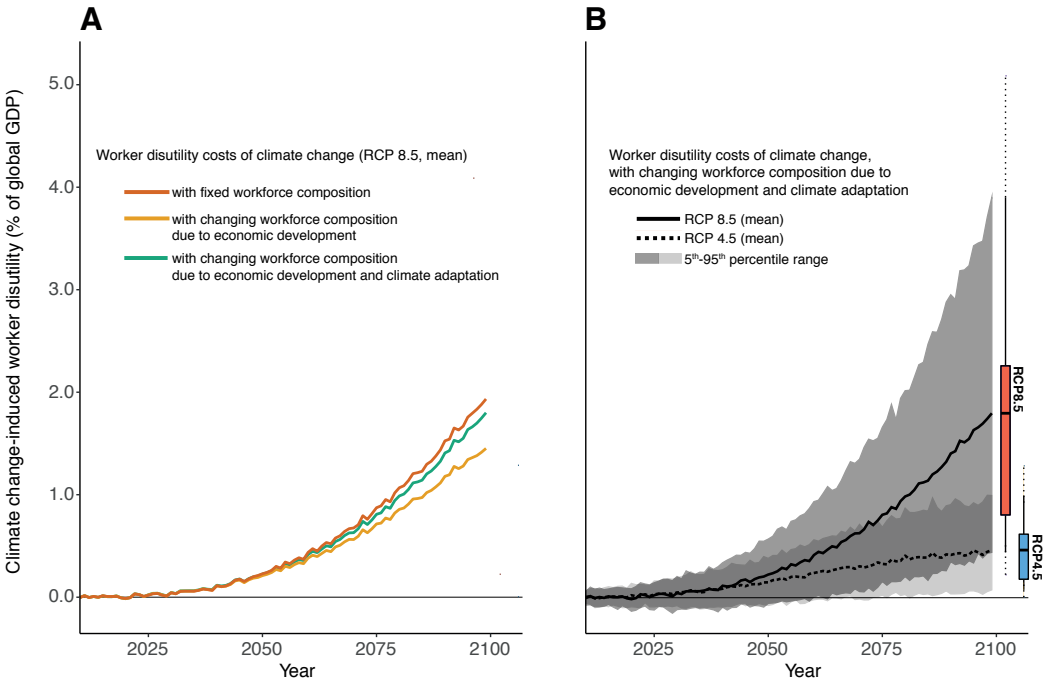

Figure 8: Time series of projected climate change-induced worker disutility costs. Costs in each year are calculated under a labor share of income = 0.6 (Karabarbounis and Neiman, 2014) and elasticity of labor supply = 0.5 (Chetty et al., 2011) and are expressed as a percentage of that year's global GDP. All estimates refer to the SSP3 socioeconomic scenario. In Panel A, lines show globally aggregated worker disutility costs of climate change under the RCP8.5 emissions scenario. The green line shows estimates that account for changes in each impact region's workforce composition as incomes grow and the climate warms (Equation 11). The orange line accounts for changes in workforce composition in association with income growth but not climate change (Appendix Equation F.3). The red line shows estimates in which each impact region's workforce composition at 2015 is held fixed into the future (Appendix Equation F.2). In Panel B, lines show globally aggregated worker disutility costs of climate change under the RCP8.5 and RCP4.5 emissions scenarios, accounting for changes to workforce composition as incomes grow and the climate warms. Lines represent a mean estimate across a set of Monte Carlo simulations accounting for both climate model and statistical uncertainty; shaded areas indicate the range between 10^{th} and 90^{th} percentiles. Boxplots show full distribution of costs in 2099 (boxes= inter-quartile range; solid whiskers= 10^{th}-90^{th} percentiles; dashed whiskers= 5^{th}-95^{th} percentiles).

While details of the calculation are described in Appendix H, Figure 9 graphically depicts its steps. An exogenous "pulse" of 1 gigaton C (equivalent to 3.66Gt CO_2) emitted in the year 2020 is shown in Panel A. The pulse alters the future trajectory of atmospheric CO_2 concentrations (Panel B), with the near-term decrease and long-term increase driven by the ocean's initial storage and subsequent release of CO_2. This results in temperature changes over multiple centuries (Panel C), which in turn cause a stream of labor disutility damages (Panel D).

The sum of the discounted stream of labor disutility damages due to the marginal pulse is the labor disutility partial SCC. Table 5 reports labor disutility partial SCC estimates under various baseline emissions scenarios and annual discount rates. Columns represent discount rates that align with those used in recent U.S. government SCC estimates (1.5%, 2%, and 2.5%) (U.S. Environmental Protection Agency, 2022) or prior estimates (2.5%,

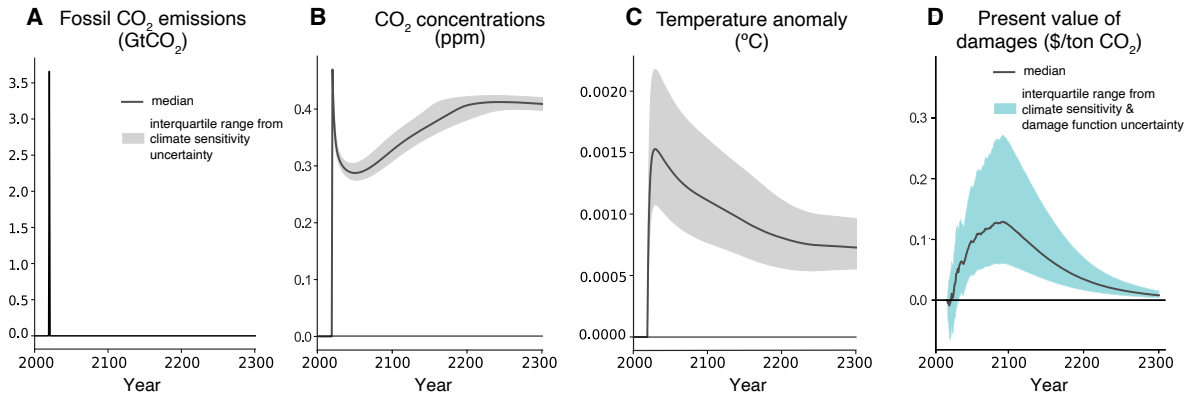

Figure 9: Effects of a marginal emission of CO_2 in 2020. Panel A depicts a 1 GtC emissions pulse (equivalent to 3.66 Gt CO2) in 2020 for a very high baseline emissions scenario (RCP8.5). Panel B displays the response of atmospheric CO_2 concentrations, relative to baseline. Panel C shows the impact of the pulse on temperature, with the levels indicating the change in global mean surface temperature relative to baseline. Panel D plots the stream change in discounted flow of labor disutility costs (2% annual discount rate) using damage functions estimated in Appendix H.1. Solid lines represent the median trajectory from sampling the joint distribution of FAIR climate model parameters (Panels B and C) and also damage function quantiles (Panel D); shading indicates interquartile ranges (Appendix H.3).

3%, and 5%) (Interagency Working Group on Social Cost of Carbon, 2010; National Academies of Sciences, Engineering, and Medicine, 2017). All values in the table represent the global sum of each impact regions marginal willingness-to-pay today (2019 USD) to avoid the additional labor disutility caused by the release of an additional metric ton of CO_2 in 2020.[47]

In Panel I of Table 5 we report central estimates of the partial SCC that use the median values of FAIR's four key parameter distributions and the mean global damage function estimate. The 1^{st}-99^{th} percentile ranges [in brackets] reflect uncertainty in climate sensitivity and in the damage function (Appendix H.3). Under a 2% discount rate, the central estimate of the labor disutility partial SCC is $10.6 for the intermediate emissions scenario and $16.7 for the very high emissions scenario. We highlight a 2% discount rate because it is the midpoint of the range of discount rates used in recent U.S. government estimates (U.S. Environmental Protection Agency, 2022).

The SCC values in Panel I of Table 5 assume that individuals are risk-neutral. In Panel II of Table 5 we report "certainty equivalent" values of the partial SCC that account for risk aversion.[48] To calculate these certainty equivalent values, we follow the method in Nath et al. (2024), adopting a standard parameterization for the shape of the utility function, i.e., a constant relative risk aversion utility function with a coefficient of relative risk aversion equal to 2. (Appendix H.3.2 details the specific procedure.) The partial

[47] Appendix H.5 displays SCC estimates under alternative baseline socioeconomic scenarios. Section VII displays SCC estimates from an empirical model that allows the effect of temperature on labor supply to differ both across and within risk groups.

[48] Recent U.S. government SCC estimates explicitly incorporate the fact that individuals are risk-averse and value reducing uncertainty (Climate Impact Lab, 2022; Howard and Sterner, 2017; Rennert et al., 2022a; U.S. Environmental Protection Agency, 2022).

SCC increases substantially when valuing the econometric and climatological uncertainty behind it. For example, under a very high emissions scenario and 2% discount rate, the certainty equivalent partial SCC is \$29.1, compared to the central estimate of \$16.7 in Panel I.

Panel III of Table 5 presents labor disutility partial SCC values from recent U.S. government estimates (U.S. Environmental Protection Agency, 2022). While these estimates are based on the empirical relationships estimated in this paper, they incorporate additional dimensions of uncertainty, making use of probabilistic socioeconomic and emissions scenarios from Rennert et al. (2022b) and a Ramsey-like discounting procedure that accounts for the relationship between economic growth and the discount rate (Newell, Pizer, and Prest, 2022).[49] Accounting for these uncertainties further increases the partial SCC.

Discount rate	$\delta = 1.5\%$	$\delta = 2\%$	$\delta = 2.5\%$	$\delta = 3\%$	$\delta = 5\%$
			I. Partial SCC estimates		
RCP 8.5	\$28.8 [\$0.2,\$215.3]	\$16.7 [-\$0.5,\$125.1]	\$10.6 [-\$0.9,\$77.7]	\$7.2 [-\$1.1,\$50.6]	\$2.4 [-\$1.4,\$12.1]
RCP 4.5	\$17.5 [-\$2.4,\$229.8]	\$10.6 [-\$2.3,\$125.5]	\$7.0 [-\$2.3,\$74.4]	\$5.0 [-\$2.2,\$46.9]	\$1.9 [-\$2.0,\$10.7]
			II. Partial SCC estimates (certainty equivalent)		
RCP 8.5	\$50.8	\$29.1	\$18.0	\$11.9	\$3.2
RCP 4.5	\$39.7	\$22.5	\$13.9	\$9.3	\$2.7
			III. Partial SCC estimates (U.S. government approach, certainty equivalent)		
Probabilistic scenarios (Rennert et al. 2022b)	\$72.7	\$38.5	\$22.0		

Table 5: Estimates of a partial social cost of carbon for labor disutility. All partial SCC values are for the year 2020, measured in PPP-adjusted 2019 USD, assuming a Frisch elasticity of labor supply of 0.5 (Chetty et al., 2011) and a labor share of income of 0.6 (Karabarbounis and Neiman, 2014). Estimates in Panels I and II are calculated using constant annual discount rates ranging from 1.5% to 5%, either a very high (RCP8.5) or intermediate (RCP4.5) baseline emissions scenario, and socioeconomic scenario SSP3 (alternative values using other SSP scenarios are shown in Appendix H.5). Point estimates displayed in Panel I rely on the median values of the four key input parameters into the climate model FAIR and a conditional mean estimate of the damage function; 1^{st}-99^{th} percentile ranges [in brackets] reflect climate sensitivity and damage function uncertainty (see Appendix H.3 for details). Panel II displays certainty equivalent values of the partial SCC, which account for risk aversion using a constant relative risk aversion utility function with a coefficient of relative risk aversion equal to 2 (see Appendix H.3.2). Estimates in Panel III follow the approach used in recent U.S. government estimates (U.S. Environmental Protection Agency, 2022), using probabilistic socioeconomic and emissions scenarios (Rennert et al., 2022b) and Ramsey discounting parameters calibrated such that the average certainty equivalent discount rate over the first ten years is equal to either 1.5%, 2%, or 2.5% (Newell, Pizer, and Prest, 2022).

[49] Under this discounting procedure, the Ramsey parameters (i.e., the pure rate of time preference and the elasticity of marginal utility of consumption) are calibrated such that the average certainty equivalent discount rate over the first ten years is equal to either 1.5%, 2%, or 2.5%.

VII Robustness to alternative labor market assumptions

This section probes the sensitivity of our hedonic value and climate change impact estimates to alternative labor market assumptions.

VII.A Inflexible daily wages

Our approach to infer changes in disutility from changes in daily hours worked (Equation 4) assumes that wage rates do not adjust on a daily basis. This assumption would be valid if, for example, labor contracts are set annually. However, if wages are flexible at daily frequency, the paper's expression for the labor disutility costs of extreme temperatures (i.e., Equation 4) that relies on changes in labor supply is incorrect, because it would confound the disutility costs with changes in labor supply due to changes in wages. We do not observe wage rates in our data, so we cannot directly test whether daily wages respond to daily temperature shocks.

This subsection graphically and mathematically demonstrates that temperature shocks that raise labor disutility and reduce productivity would have an ambiguous effect on the estimates of labor disutility when wage rates adjust at daily frequency. Consider a change in equilibrium labor supply caused by a daily temperature shift on day d. The overall labor supply change ($\frac{dL}{dT_d}$) can be divided into two components: a change that occurs from a shifting supply curve, holding the wage fixed ($\frac{\partial L|\omega}{\partial T_d}$), and a change that occurs due to a shifting wage ($\frac{\partial L_{\Delta\omega}}{\partial T_d}$).[50] The true labor disutility caused by the temperature shift should be calculated using only the first component.

Figure 10's two panels depict the cases where, in response to a daily temperature shock, the relative elasticities of the demand and supply curves cause the equilibrium wage to decrease (Panel A) and increase (Panel B), respectively. In both panels, the gridded areas correspond to the true change in worker disutility, which is based on the change in labor supply holding the wage constant ($\frac{\partial L|\omega}{\partial T_d}$). In Panel A, where the wage declines, Equation 4's approach of inferring changes in disutility from changes in labor supply will overstate the effects of temperature on disutility, because labor supply reflects the true disutility of higher temperatures (i.e., the gridded area) and the reduction in hours due to the decline in the wage (i.e., orange area). In the case where the wage rises (Panel B), Equation 4 will lead to an underestimate of the total disutility costs (i.e., gridded area) because the increase in hours due to the higher wage (i.e., orange area) obscures some of the utility loss.[51] Thus, the sign and magnitude of the potential bias in estimated disutility caused

[50] These components are depicted graphically in Appendix Figure A.1.

[51] It is also worth noting that in the case where the wage falls and the calculation overstates the disutility change, the overestimate partially consists of a different economic cost— producer surplus loss from terms A/B of the WTP expression (Equation 2) that is mislabeled as a disutility cost. This overlap is seen in Figure 10A as the orange triangle that lies within the diagonal shaded area.

by the assumption of a fixed daily wage rate depends on the extent of the labor supply and demand shifts and the relative elasticities of labor supply and demand.[52]

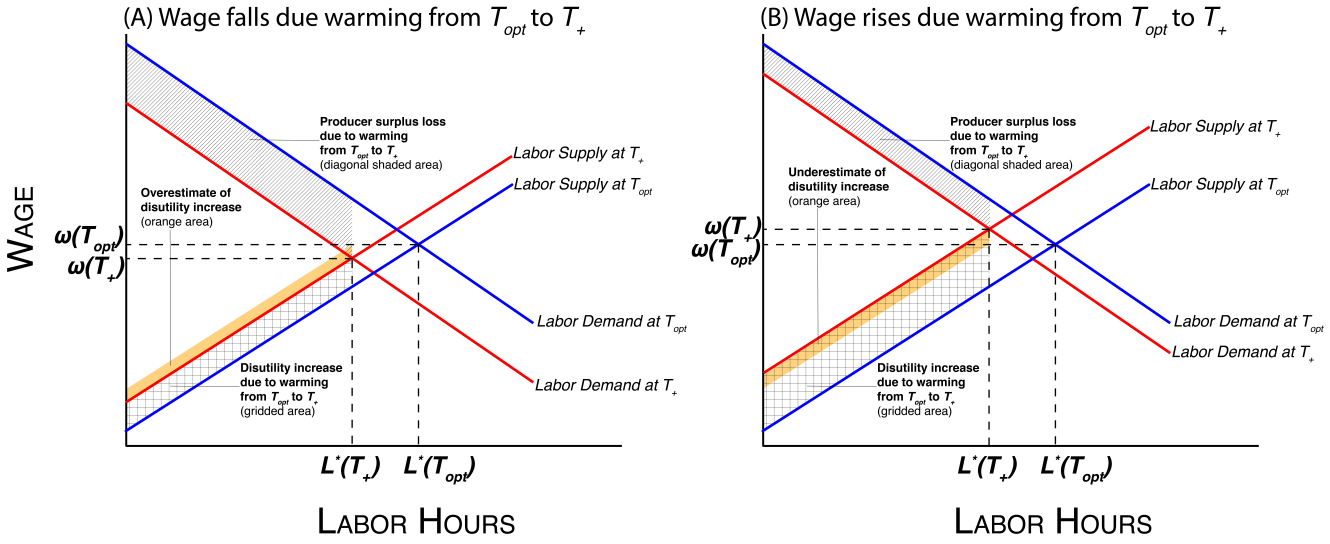

Figure 10: Effects of a temperature increase on labor supply and disutility in presence of wage change. Intersection of upward-sloping marginal disutility of labor (labor supply) and downward-sloping labor demand determines the equilibrium labor hours at a given daily temperature, either T_{opt} or $T_+ > T_{opt}$. Figure 10A illustrates a case where the temperature increase from T_{opt} to T_+ results in a decrease in the equilibrium wage. In this case, our calculation of the change in worker disutility based on the change in equilibrium labor supply overestimates the actual change in worker disutility. The gridded area denotes the actual change in disutility, while our estimate corresponds to gridded area plus the orange area. Figure 10B illustrates a case where the temperature increase from T_{opt} to T_+ results in an increase in the equilibrium wage. In this case, our calculation of the change in worker disutility based on the change in equilibrium labor supply underestimates the actual change in worker disutility. The gridded area denotes the actual change in disutility, while our estimate corresponds to the gridded area that is not shaded in orange.

The potential bias in the calculation of labor disutility due to temperature shocks when using the observed change in labor supply (as in Equation 4) can be expressed formally. Equation 12 divides the true temperature-induced change in disutility into the estimated change in disutility when using observed labor supply changes, and the bias due to the change in labor supply from the wage change (i.e., the orange area in Figure 10):

$$\underbrace{\frac{\omega\left(\frac{\partial L|\omega}{\partial T_d}\right)}{\epsilon}}_{\text{True temperature-induced disutility}} = \underbrace{\frac{\omega\left(\frac{dL}{dT_d}\right)}{\epsilon}}_{\substack{\text{Temperature-induced disutility} \\ \text{calculated from observed} \\ \text{labor supply changes}}} - \underbrace{\frac{\omega\left(\frac{\partial L_{\Delta\omega}}{\partial T_d}\right)}{\epsilon}}_{\substack{\text{Bias due to} \\ \text{temperature-induced} \\ \text{wage change}}} . \tag{12}$$

With some manipulation, we can use the Frisch elasticity of labor supply ϵ to write the

[52]It is possible that the temperature-induced shifts in daily labor demand and labor supply curves perfectly offset, such that the wage rate remains unchanged. In this special case, the estimated disutility would not be biased.

bias term as:

$$\frac{\omega\left(\frac{\partial L_{\Delta\omega}}{\partial T_d}\right)}{\epsilon} = \frac{L\omega\left(\frac{\epsilon(\partial\omega/\omega)}{\partial T_d}\right)}{\epsilon}. \tag{13}$$

We use Equation 13 and two assumptions to characterize the potential bias in the paper's estimates of labor disutility from daily temperature shocks. The first assumption is that the wage rate fluctuates in response to daily temperature conditions for a fraction of workers r. The second one is that for these workers, we assume that the wage response to daily temperature is related in a fixed proportion, x, to the labor supply response. Specifically, we assume $\frac{d\omega/\omega}{dT_d} = \frac{x(dL/L)}{dT_d}$.[53] This assumption is consistent with estimates of the relationship between temperature and worker productivity (Seppanen, Fisk, and Faulkner, 2004; Stevens, 2019), which find larger effects for more extreme temperatures, just as we find for temperature and labor supply.

With these two assumptions, the true disutility caused by a shift in the daily temperature for workers with a flexible wage is equal to the disutility calculated from the observed change in labor supply multiplied by a scaling factor $(1-\epsilon x)$. For the remaining $1-r$ fraction of workers, $x = 0$, and no adjustment is necessary. Thus, to obtain the true temperature-induced disutility for all workers, the disutility calculated from the observed labor supply change is multiplied by a scaling factor $(1-\epsilon x r)$. The construction of the corresponding hedonic value of thermal comfort in a low-risk job and the impacts of future climate change on labor disutility requires multiplying the formulas described in Equations 9 and 11, respectively, by this scaling factor.

Table 6 explores the sensitivity of the paper's estimates of the hedonic value of thermal comfort on the job (Row 1) and the estimated impacts of climate change on measures of climate damages (Rows 2 - 5) to allowing the wage rate to fluctuate with daily temperature for some workers. The scaling factor, $(1-\epsilon x r)$, is constructed using $\epsilon = 0.5$ again, $r = 0.35$, and a range of values for x based on our data and other prior surveys and studies. Appendix A.4 describes in detail our data, the prior surveys, and the previous literatures that govern the choices for x and r. The baseline estimates that assume inflexible daily wages and were reported above are repeated in Column 1, while Columns 2 - 5 consider the alternative scenarios that allow for daily wage adjustments.

Across the range of parameter values, daily flexibility in the wage rate has a relatively modest impact on the paper's measures of labor disutility. For example, the baseline point estimate for the global average value of thermal comfort in a low-risk job is 2.9% and ranges between 1.4% and 3.2% with the alternative assumptions. Additionally, the 5^{th} to 95^{th} percentile ranges all have considerable overlap. It is also apparent in Rows 2 - 5 that relaxing the assumption of daily inflexibility in the wage rate does not qualitatively alter the paper's conclusions about the labor disutility costs of climate change.

[53] Note that x will be positive in the case of a wage decrease (as illustrated in Figure 10A) and negative in the case of a wage increase (as illustrated in Figure 10B).

VII.B Other assumptions

Here we explore the implications of allowing for heterogeneous labor supply-temperature responses within risk groups. It is possible that workers of the same risk group may respond differently to temperature, based on income and climate. However, as described in Section IV, an important data limitation in this context is that some of the time use and labor force surveys are only nationally representative, and not representative at subnational levels.

Nevertheless, we estimate an augmented version of Equation 6 that includes interactions of the nonlinear temperature response functions for each risk group with location-specific measures of income per capita and climate (Carleton et al., 2022; Rode et al., 2021) at the level that the surveys are representative. Under this model, which is presented in Appendix G, we fail to find statistically significant differences in the labor supply-temperature response of low-risk workers by income or climate. We also do not find statistically significant evidence that the labor supply-temperature response of high-risk workers differs by climate, though do find evidence that high-risk labor supply is less sensitive to daily temperatures in richer locations. This could be explained by occupational safety rules that require breaks, access to water, or other compensatory responses to extreme temperatures in richer locations.

Table 6 explores the consequences of allowing for income to be protective for high-risk workers. Column 6, Row 1 finds that the estimate of the hedonic value of thermal comfort would fall from 2.9% to 1.8% of annual income globally. It is noteworthy that the 5^{th} to 95^{th} percentile ranges for these estimates overlap. Similarly, the end-of-century disutility costs of climate change under RCP8.5 decrease from 1.8% to 0.7% of 2099 global GDP when the model allows for income-driven adaptation for high-risk workers (Column 6, Row 2). These estimates also have wide 5^{th} to 95^{th} percentile ranges with considerable overlap (0.2% to 5.1% and -0.3% to 2.5%, respectively).[54] Estimates of the partial social cost of carbon for labor disutility reduce by roughly half, again with wide and substantially overlapping uncertainty ranges (Column 6, Rows 4 and 5).

A separate assumption in our stylized model is that workers are homogeneous in their preferences for thermal comfort in the workplace. However, if workers differ in their preferences, the employment composition of the high- and low-risk sectors will be endogenously determined by preference-based selection of workers into each sector. The result is that estimates of the population average hedonic value of thermal comfort in a low-risk job would be biased.[55] The bias would arise because the temperature responses of high- and low-risk labor supply are estimated on the set of workers who selected into each sector, and not the full population of workers. To correct for this potential bias, we estimate high-

[54]Correspondingly, the end-of-century disutility costs of climate change under RCP4.5 reduce from 0.5% to 0.2% of 2099 global GDP, with 5^{th} to 95^{th} percentile ranges 0.0% to 1.3% and -0.1% to 0.7%, respectively (Column 6, Row 3).

[55]In Appendix A.5, we develop a version of the stylized model with heterogeneous worker preferences and illustrate how this biases our hedonic value estimates.

and low-risk labor supply-temperature responses using the Heckman (1979) two-stage estimator, and calculate the hedonic value using these estimates, following Equation 9.[56] Because we do not identify a potentially valid exclusion restriction, our application of the Heckman approach is only identified through functional form assumptions. Appendix A.5 describes the estimation procedure in detail and shows that the hedonic value estimate remains very similar to the one from our main specification.

VIII Conclusion

Using a new theoretical framework and novel data representing one-third of the world's population, this paper finds that worker thermal comfort is an important non-wage workplace amenity and projects that it will become a substantial share of the costs of climate change. Specifically, the empirical results suggest that the value of a weather-protected job's thermal comfort is about 2.9% of annual income on average but it varies widely across the globe depending on the local climate. Additionally, we project that climate change will increase worker thermal discomfort by 1.8% of global GDP at the end of the century under a very high emissions scenario and 0.5% under an intermediate scenario. This cost has not previously been accounted for in analyses of climate damages and is distinct from the effects of climate change on labor productivity.

Several caveats and limitation are worth noting. First, we believe that we have collected the most comprehensive data set ever compiled on daily or weekly worker labor supply and weather, but, at the same time, these data are incomplete because they are missing two-thirds of the world's population. This is a particular concern in sub-Saharan Africa and other places where exposure to extremely hot temperatures and high-risk jobs are both common. Another data limitation is that the paper does not shed light on other ways in which climate change may affect worker utility. For example, it is unable to directly measure the impacts of humidity and storms.

Second, the analysis assumes that daily weather realizations provide a setting where wages are fixed and, as we show, this is useful for inferring the disutility costs of extreme temperatures. In many respects this is the other side of the coin, compared to the workhorse hedonic model that assumes that labor is supplied inelastically (generally over longer time horizons). We attempt to quantify the bias that arises if daily wages respond to daily temperature and find that it is likely small. Nevertheless, richer data would allow for a further investigation of the relative roles of labor supply and demand in the particular contexts where this can occur.

Third, it is possible that we have understated the degree to which adaptation will reduce the costs of climate change. The finding that there are not differences in the labor

[56] If workers endogenously select into sectors based on preferences both today and under future climate change, correcting the selection bias is not appropriate for calculating the impacts of climate change on worker disutility. We therefore only apply the selection correction when calculating the hedonic value of thermal comfort.

		Sensitivity to assumptions					
		Baseline model	Short-term wage flexibility				Within risk group heterogeneity
	Estimate	(1)	(2)	(3)	(4)	(5)	(6)
			$x = 0.5$ $r = 0.35$	$x = 1.5$ $r = 0.35$	$x = 3$ $r = 0.35$	$x = -2/3$ $r = 0.35$	
(1)	Global average value of thermal comfort in a low-risk job (% annual income)	2.9% [-1.0%,6.8%]	2.6% [-0.9%,6.2%]	2.1% [-0.8%,5.0%]	1.4% [-0.5%,3.2%]	3.2% [-1.2%,7.6%]	1.8% [0.3%,3.3%]
(2)	Labor disutility cost of climate change at 2099 (RCP8.5, % 2099 global GDP)	1.8% [0.2%,5.1%]	1.6% [0.2%,4.7%]	1.3% [0.1%,3.8%]	0.9% [0.1%,2.4%]	2.0% [0.2%,5.7%]	0.7% [-0.3%,2.5%]
(3)	Labor disutility cost of climate change at 2099 (RCP4.5, % 2099 global GDP)	0.5% [0.0%,1.3%]	0.5% [0.0%,1.2%]	0.4% [0.0%,1.0%]	0.2% [0.0%,0.6%]	0.6% [0.0%,1.5%]	0.2% [-0.1%,0.7%]
(4)	Partial social cost of carbon for labor disutility (RCP8.5, $\delta = 2\%$)	\$16.7 [\$1.7,\$73.9]	\$15.2 [\$1.6,\$67.4]	\$12.3 [\$1.3,\$54.5]	\$7.9 [\$0.8,\$35.1]	\$18.6 [\$1.9,\$82.5]	\$7.8 [-\$1.8,\$38.0]
(5)	Partial social cost of carbon for labor disutility (RCP4.5, $\delta = 2\%$)	\$10.6 [\$0.0,\$67.6]	\$9.7 [\$0.0,\$61.7]	\$7.8 [\$0.0,\$49.9]	\$5.0 [\$0.0,\$32.1]	\$11.8 [\$0.0,\$75.5]	\$5.0 [-\$3.2,\$35.6]

Table 6: Sensitivity of estimates to assumptions. Column 1 reproduces our baseline estimates for the global average hedonic value of thermal comfort in a low risk job (Table 4, Panel A), the labor disutility costs of climate change at 2099 (Figure 8), and partial social cost of carbon for labor disutility (Table 5, Panel I). Columns 2-5 present estimates where we relax the assumption that wages do not respond to daily temperature fluctutations; estimates depend on the how responsive the wage is to daily temperature relative to how responsive labor supply is to daily temperature (x), and the fraction of workers whose wages can fluctuate in response to daily temperature (r). Appendix A.4 describes the choices of values for x and r. Column 6 presents estimates where labor supply-temperature responses can vary within each risk group (Appendix G). Brackets display 5^{th}-95^{th} percentile ranges.

supply responsiveness of high-risk workers across climate zones suggests that these workers' adaptation opportunities are limited currently. However, climate change is likely to cause innovation that protects people against the heat (e.g., personal cooling devices) and such climate-biased innovation will work to reduce the costs of worker thermal comfort. Relatedly, there may exist forms of adaptation like migration from areas where thermal comfort is a challenge to more temperate locations that are outside the paper's analysis.

There are two broader implications of this research. The paper's conceptual approach demonstrates that labor supply can be used to value other workplace disamenities, including air pollution, noise pollution, and power outages. Further this paper adds to growing literature that finds that the non-market effects of climate change are likely to account for an important, if not predominant, share of its costs. For example, Carleton and Greenstone (2022) demonstrate that the mortality costs of climate change are much larger than had been understood and Rennert et al. (2022a) show that they dominate current estimates of damages. Other areas where the economic impacts of climate climate are largely unquantified include biodiversity, morbidity, migration, and conflict. An important area for future research is to develop new theoretical and empirical approaches to quantify willingness-to-pay for these and other non-market impacts of climate change, just as this paper has tried to do with on-the-job thermal comfort.

References

Adhvaryu, Achyuta, Namrata Kala, and Anant Nyshadham. 2020. "The Light and the Heat: Productivity Co-Benefits of Energy-Saving Technology." *Review of Economics and Statistics* 102 (4):779–792.

Akerlof, George A, William T Dickens, George L Perry, Robert J Gordon, and N Gregory Mankiw. 1996. "The macroeconomics of low inflation." *Brookings papers on economic activity* 1996 (1):1–76.

Allen, M, OP Dube, W Solecki, F Aragón-Durand, W Cramer, S Humphreys, M Kainuma et al. 2018. "Special Report: Global Warming of 1.5 C." *Intergovernmental Panel on Climate Change (IPCC)* .

Alvarez-Cuadrado, Francisco and Markus Poschke. 2011. "Structural change out of agriculture: Labor push versus labor pull." *American Economic Journal: Macroeconomics* 3 (3):127–58.

Arrow, Kenneth J. 2007. "Global climate change: A challenge to policy." *The Economists' Voice* 4 (3).

Auffhammer, Maximilian and Anin Aroonruengsawat. 2011. "Simulating the impacts of climate change, prices and population on California's residential electricity consumption." *Climatic change* 109 (1):191–210.

Barattieri, Alessandro, Susanto Basu, and Peter Gottschalk. 2014. "Some evidence on the importance of sticky wages." *American Economic Journal: Macroeconomics* 6 (1):70–101.

Barrage, Lint and William D Nordhaus. 2023. "Policies, Projections, and the Social Cost of Carbon: Results from the DICE-2023 Model." Tech. rep., National Bureau of Economic Research.

Bell, CR and AJ Watts. 1971. "Thermal limits for industrial workers." *British journal of industrial medicine* 28 (3):259–264.

Bright, E. A., P. R. Coleman, A. N. Rose, and M. L. Urban. 2012. "LandScan 2011." Digital dataset: web.ornl.gov/sci/landscan/index.shtml.

Buera, Francisco J and Joseph P Kaboski. 2009. "Can traditional theories of structural change fit the data?" *Journal of the European Economic Association* 7 (2-3):469–477.

Burke, Marshall, Solomon M Hsiang, and Edward Miguel. 2015. "Global non-linear effect of temperature on economic production." *Nature* .

Cachon, Gerard P, Santiago Gallino, and Marcelo Olivares. 2012. "Severe weather and automobile assembly productivity." *Columbia Business School Research Paper* (12/37).

Carleton, Tamma and Michael Greenstone. 2022. "A guide to updating the US Governments social cost of carbon." *Review of Environmental Economics and Policy* 16 (2):196–218.

Carleton, Tamma, Amir Jina, Michael Delgado, Michael Greenstone, Trevor Houser, Solomon Hsiang, Andrew Hultgren, Robert E Kopp, Kelly E McCusker, Ishan Nath et al. 2022. "Valuing the global mortality consequences of climate change accounting for adaptation costs and benefits." *The Quarterly Journal of Economics* 137 (4):2037–2105.

Center for Population and Policy Studies, Gadjah Mada University (Indonesia), RAND Corporation, SurveyMETER. 2007-2008. "Indonesia Family Life Survey Wave 4." Tech. rep., RAND Corporation.

Chetty, Raj, Adam Guren, Day Manoli, and Andrea Weber. 2011. "Are micro and macro labor supply elasticities consistent? A review of evidence on the intensive and extensive margins." *American Economic Review* 101 (3):471–75.

Climate Impact Lab. 2022. "Data-driven Spatial Climate Impact Model User Manual, Version 092022EPA." Tech. rep., Climate Impact Lab.

Dasgupta, Partha. 2007. "The Stern Review's economics of climate change." *National institute economic review* 199 (1):4–7.

———. 2008. "Discounting climate change." *Journal of risk and uncertainty* 37 (2):141–169.

Davis, Lucas W and Paul J Gertler. 2015. "Contribution of air conditioning adoption to future energy use under global warming." *Proceedings of the National Academy of Sciences* 112 (19):5962–5967.

Dellink, Rob, Jean Chateau, Elisa Lanzi, and Bertrand Magné. 2015. "Long-term economic growth projections in the Shared Socioeconomic Pathways." *Global Environmental Change* .

Dennis, Benjamin N and Talan B İşcan. 2009. "Engel versus Baumol: Accounting for structural change

using two centuries of US data." *Explorations in Economic history* 46 (2):186–202.

Depsky, Nicholas, Ian Bolliger, Daniel Allen, Jun Ho Choi, Michael Delgado, Michael Greenstone, Ali Hamidi, Trevor Houser, Robert E Kopp, and Solomon Hsiang. 2023. "DSCIM-Coastal v1. 1: an open-source modeling platform for global impacts of sea level rise." *Geoscientific Model Development* 16 (14):4331–4366.

Deryugina, Tatyana and Solomon M Hsiang. 2014. "Does the environment still matter? Daily temperature and income in the United States." Tech. rep., National Bureau of Economic Research.

Dickens, William T, Lorenz Goette, Erica L Groshen, Steinar Holden, Julian Messina, Mark E Schweitzer, Jarkko Turunen, and Melanie E Ward. 2007. "How wages change: micro evidence from the International Wage Flexibility Project." *Journal of Economic Perspectives* 21 (2):195–214.

Duarte, Margarida and Diego Restuccia. 2010. "The role of the structural transformation in aggregate productivity." *The Quarterly Journal of Economics* 125 (1):129–173.

Echevarria, Cristina. 1997. "Changes in sectoral composition associated with economic growth." *International economic review* :431–452.

Garg, Teevrat, Matthew Gibson, and Fanglin Sun. 2019. "Extreme Temperatures and Time-Use in China." *IZA Discussion Paper No. 12372* .

Gennaioli, Nicola, Rafael La Porta, Florencio Lopez De Silanes, and Andrei Shleifer. 2014. "Growth in regions." *Journal of Economic Growth* 19 (3):259–309. URL https://ideas.repec.org/a/kap/jecgro/v19y2014i3p259-309.html.

Glazer, James L. 2005. "Management of heatstroke and heat exhaustion." *Am Fam Physician* 71 (11):2133–2140.

Graff Zivin, Joshua and Matthew Neidell. 2014. "Temperature and the allocation of time: Implications for climate change." *Journal of Labor Economics* 32 (1):1–26.

Greenberg, Kyle, Michael Greenstone, Stephen P Ryan, and Michael Yankovich. 2021. "The heterogeneous value of a statistical life: Evidence from US Army reenlistment decisions." Tech. rep., National Bureau of Economic Research.

Grigsby, John, Erik Hurst, and Ahu Yildirmaz. 2021. "Aggregate nominal wage adjustments: New evidence from administrative payroll data." *American Economic Review* 111 (2):428–471.

Guiteras, Raymond P and B Kelsey Jack. 2018. "Productivity in piece-rate labor markets: Evidence from rural Malawi." *Journal of Development Economics* 131:42–61.

Hancock, Peter A, Jennifer M Ross, and James L Szalma. 2007. "A meta-analysis of performance response under thermal stressors." *Human Factors: The Journal of the Human Factors and Ergonomics Society* 49 (5):851–877.

Hart, Robert A. 2016. "The rise and fall of piecework." *IZA World of Labor* .

Hausfather, Zeke and Glen P Peters. 2020. "Emissions–the business as usualstory is misleading." *Nature* 577 (7792):618–620.

Heal, Geoffrey and Jisung Park. 2013. "Feeling the heat: Temperature, physiology & the wealth of nations." Tech. rep., National Bureau of Economic Research.

Heckman, James J. 1979. "Sample selection bias as a specification error." *Econometrica: Journal of the econometric society* :153–161.

Heutel, Garth, Nolan H Miller, and David Molitor. 2021. "Adaptation and the mortality effects of temperature across US climate regions." *The review of economics and statistics* 103 (4):740–753.

Howard, Peter H and Thomas Sterner. 2017. "Few and not so far between: a meta-analysis of climate damage estimates." *Environmental and Resource Economics* 68 (1):197–225.

Hsiang, Solomon. 2016. "Climate Econometrics." *Annual Review of Resource Economics* 8 (1):43–75.

Hsiang, Solomon, Robert Kopp, Amir Jina, James Rising, Michael Delgado, Shashank Mohan, DJ Rasmussen, Robert Muir-Wood, Paul Wilson, Michael Oppenheimer et al. 2017. "Estimating economic damage from climate change in the United States." *Science* 356 (6345):1362–1369.

Hsiang, Solomon and Robert E Kopp. 2018. "An Economist's Guide to Climate Change Science." *Journal*

of Economic Perspectives 32 (4):3–32.

Hsiang, Solomon M. 2010. "Temperatures and cyclones strongly associated with economic production in the Caribbean and Central America." *Proceedings of the National Academy of sciences* 107 (35):15367–15372.

Hsiang, Solomon M, Kyle C Meng, and Mark A Cane. 2011. "Civil conflicts are associated with the global climate." *Nature* 476 (7361):438–441.

Hultgren, Andrew, Tamma Carleton, Michael Delgado, Diana R Gergel, Michael Greenstone, Trevor Houser, Solomon Hsiang, Amir Jina, Robert E Kopp, Steven B Malevich et al. 2022. "Estimating global impacts to agriculture from climate change accounting for adaptation." *Available at SSRN* .

Huntington, Ellsworth. 1922. *Civilization and climate*. Yale University Press.

IIASA Energy Program. 2016. "SSP Database, Version 1.1 [Data set]." Tech. rep., National Bureau of Economic Research. URL https://tntcat.iiasa.ac.at/SspDb.Accessed25December,2016.

Interagency Working Group on Social Cost of Carbon. 2010. "Social Cost of Carbon for Regulatory Impact Analysis - Under Executive Order 12866." Tech. rep., United States Government.

IPCC. 2021. *Summary for Policymakers*. Cambridge, United Kingdom and New York, NY, USA: Cambridge University Press, 332.

Kahn, Shulamit. 1997. "Evidence of nominal wage stickiness from microdata." *The American Economic Review* 87 (5):993–1008.

Karabarbounis, Loukas and Brent Neiman. 2014. "The global decline of the labor share." *The Quarterly journal of economics* 129 (1):61–103.

Kaur, Supreet. 2019. "Nominal wage rigidity in village labor markets." *American Economic Review* 109 (10):3585–3616.

Kolstad, Jonathan T and Amanda E Kowalski. 2016. "Mandate-based health reform and the labor market: Evidence from the Massachusetts reform." *Journal of health economics* 47:81–106.

Lanfranchi, Joseph, Henry Ohlsson, and Ali Skalli. 2002. "Compensating wage differentials and shift work preferences." *Economics Letters* 74 (3):393–398.

Lavetti, Kurt. 2023. "Compensating Wage Differentials in Labor Markets: Empirical Challenges and Applications." *Journal of Economic Perspectives* 37 (3):189–212. URL https://www.aeaweb.org/articles?id=10.1257/jep.37.3.189.

Liu, Maggie, Yogita Shamdasani, and Vis Taraz. 2023. "Climate change and labor reallocation: Evidence from six decades of the Indian Census." *American Economic Journal: Economic Policy* 15 (2):395–423.

Mahmud, Minhaj, Italo A Gutierrez, Krishna B Kumar, and Shanthi Nataraj. 2021. "What aspects of formality do Workers value? Evidence from a choice experiment in Bangladesh." *The World Bank Economic Review* 35 (2):303–327.

Mas, Alexandre and Amanda Pallais. 2017. "Valuing alternative work arrangements." *American Economic Review* 107 (12):3722–3759.

Matsuyama, Kiminori. 2017. *Structural Change*. London: Palgrave Macmillan UK, 1–6. URL https://doi.org/10.1057/978-1-349-95121-5_1775-2.

Meinshausen, M., S. C. B. Raper, and T. M. L. Wigley. 2011. "Emulating coupled atmosphere-ocean and carbon cycle models with a simpler model, MAGICC6 – Part 1: Model description and calibration." *Atmos. Chem. Phys.* 11 (4):1417–1456. URL http://www.atmos-chem-phys.net/11/1417/2011/.

Millar, Richard J, Zebedee R Nicholls, Pierre Friedlingstein, and Myles R Allen. 2017. "A modified impulse-response representation of the global near-surface air temperature and atmospheric concentration response to carbon dioxide emissions." *Atmospheric Chemistry and Physics* 17 (11):7213–7228.

Minnesota Population Center. 2019. *Integrated Public Use Microdata Series, International: Version 7.2 [dataset]*. Minneapolis, MN: IPUMS. URL https://doi.org/10.18128/D020.V7.2.

Mitchell, Timothy D. 2003. "Pattern Scaling: An Examination of the Accuracy of the Technique for Describing Future Climates." *Climatic Change* 60 (3):217–242. URL http://link.springer.com/article/10.1023/A%3A1026035305597.

Moore, Frances C and David B Lobell. 2014. "Adaptation potential of European agriculture in response to climate change." *Nature Climate Change* 4 (7):610–614.

Nath, Ishan, Tamma Carleton, Michael Greenstone, Trevor Houser, Solomon Hsiang, Andrew Hultgren, Amir Jina, Robert E. Kopp, Kelly McCusker, James Rising, and Ashwin Rode. 2024. "The welfare economics of a data-driven social cost of carbon." *Working paper* .

Nath, Ishan B. 2020. "The Food Problem and the Aggregate Productivity Consequences of Climate Change." Working Paper 27297, National Bureau of Economic Research. URL http://www.nber.org/papers/w27297.

National Academies of Sciences, Engineering, and Medicine. 2017. *Valuing Climate Damages: Updating Estimation of the Social Cost of Carbon Dioxide*. Washington, DC: The National Academies Press.

National Sample Survey Organisation. 2005. "National Sample Survey 61st Round." Tech. rep., Ministry of Statistics and Programme Implementation, Government of India.

Newell, Richard G, William A Pizer, and Brian C Prest. 2022. "A discounting rule for the social cost of carbon." *Journal of the Association of Environmental and Resource Economists* 9 (5):1017–1046.

Nordhaus, William D. 1992. "An optimal transition path for controlling greenhouse gases." *Science* 258 (5086):1315–1319.

O'Neill, Brian C, Elmar Kriegler, Keywan Riahi, Kristie L Ebi, Stephane Hallegatte, Timothy R Carter, Ritu Mathur, and Detlef P van Vuuren. 2014. "A new scenario framework for climate change research: the concept of shared socioeconomic pathways." *Climatic Change* 122 (3):387–400.

Parsons, Ken. 2014. *Human thermal environments: the effects of hot, moderate, and cold environments on human health, comfort, and performance*. Crc Press.

Pilcher, June J, Eric Nadler, and Caroline Busch. 2002. "Effects of hot and cold temperature exposure on performance: a meta-analytic review." *Ergonomics* 45 (10):682–698.

Ramsey, Jerry D. 1995. "Task performance in heat: a review." *Ergonomics* 38 (1):154–165.

Rasmussen, D. J., Malte Meinshausen, and Robert E. Kopp. 2016. "Probability-weighted ensembles of U.S. county-level climate projections for climate risk analysis." *Journal of Applied Meteorology and Climatology* 55 (10):2301–2322. URL http://journals.ametsoc.org/doi/abs/10.1175/JAMC-D-15-0302.1.

Rennert, Kevin, Frank Errickson, Brian C Prest, Lisa Rennels, Richard G Newell, William Pizer, Cora Kingdon, Jordan Wingenroth, Roger Cooke, Bryan Parthum et al. 2022a. "Comprehensive evidence implies a higher social cost of CO2." *Nature* 610 (7933):687–692.

Rennert, Kevin, Brian C Prest, William A Pizer, Richard G Newell, David Anthoff, Cora Kingdon, Lisa Rennels, Roger Cooke, Adrian E Raftery, Hana Ševčíková et al. 2022b. "The social cost of carbon: advances in long-term probabilistic projections of population, GDP, emissions, and discount rates." *Brookings Papers on Economic Activity* 2021 (2):223–305.

Riahi, Keywan, Shilpa Rao, Volker Krey, Cheolhung Cho, Vadim Chirkov, Guenther Fischer, Georg Kindermann, Nebojsa Nakicenovic, and Peter Rafaj. 2011. "RCP 8.5—A scenario of comparatively high greenhouse gas emissions." *Climatic Change* 109 (1-2):33–57.

Riahi, Keywan, Detlef P Van Vuuren, Elmar Kriegler, Jae Edmonds, Brian C O'neill, Shinichiro Fujimori, Nico Bauer, Katherine Calvin, Rob Dellink, Oliver Fricko et al. 2017. "The shared socioeconomic pathways and their energy, land use, and greenhouse gas emissions implications: an overview." *Global Environmental Change* 42:153–168.

Rode, Ashwin, Tamma Carleton, Michael Delgado, Michael Greenstone, Trevor Houser, Solomon Hsiang, Andrew Hultgren, Amir Jina, Robert E Kopp, Kelly E McCusker et al. 2021. "Estimating a social cost of carbon for global energy consumption." *Nature* 598 (7880):308–314.

Rosen, Sherwin. 1974. "Hedonic prices and implicit markets: product differentiation in pure competition." *Journal of political economy* 82 (1):34–55.

———. 1986. "The theory of equalizing differences." *Handbook of labor economics* 1:641–692.

Sahu, Subhashis, Moumita Sett, and Tord Kjellstrom. 2013. "Heat exposure, cardiovascular stress and work productivity in rice harvesters in India: implications for a climate change future." *Industrial*

health 51 (4):424–431.

Samir, KC and Wolfgang Lutz. 2014. "The human core of the shared socioeconomic pathways: Population scenarios by age, sex and level of education for all countries to 2100." *Global Environmental Change* .

Seppanen, Olli, William J Fisk, and David Faulkner. 2004. "Control of temperature for health and productivity in offices." .

Seppanen, Olli, William J Fisk, and QH Lei. 2006. "Effect of temperature on task performance in office environment." *Lawrence Berkeley National Laboratory* .

Sheffield, Justin, Gopi Goteti, and Eric F Wood. 2006. "Development of a 50-year high-resolution global dataset of meteorological forcings for land surface modeling." *Journal of Climate* 19 (13):3088–3111.

Smith, Adam. 1776. *An Inquiry into the Nature and Causes of the Wealth of Nations*. McMaster University Archive for the History of Economic Thought. URL https://EconPapers.repec.org/RePEc:hay:hetboo:smith1776.

Smith, Christopher J, Piers M Forster, Myles Allen, Nicholas Leach, Richard J Millar, Giovanni A Passerello, and Leighton A Regayre. 2018. "FAIR v1. 3: a simple emissions-based impulse response and carbon cycle model." *Geoscientific Model Development* 11 (6):2273–2297.

Somanathan, Eswaran, Rohini Somanathan, Anant Sudarshan, Meenu Tewari et al. 2018. "The impact of temperature on productivity and labor supply: Evidence from Indian manufacturing." *Becker Friedman Institute Working Paper* :No. 2018–69.

Stevens, Andrew. 2019. "Temperature, wages, and agricultural labor productivity." Tech. rep., UC Berkeley Working Paper, Accessible on UC Berkeley website.

Taylor, Karl E, Ronald J Stouffer, and Gerald A Meehl. 2012. "An overview of CMIP5 and the experiment design." *Bulletin of the American Meteorological Society* 93 (4):485.

Tebaldi, Claudia and Reto Knutti. 2007. "The use of the multi-model ensemble in probabilistic climate projections." *Philosophical Transactions of the Royal Society of London A: Mathematical, Physical and Engineering Sciences* 365 (1857):2053–2075. URL http://rsta.royalsocietypublishing.org/content/365/1857/2053.

Thomson, Allison M., Katherine V. Calvin, Steven J. Smith, G. Page Kyle, April Volke, Pralit Patel, Sabrina Delgado-Arias, Ben Bond-Lamberty, Marshall A. Wise, Leon E. Clarke, and James A. Edmonds. 2011. "RCP4.5: a pathway for stabilization of radiative forcing by 2100." *Climatic Change* 109 (1):77. URL https://doi.org/10.1007/s10584-011-0151-4.

Thrasher, Bridget, Edwin P Maurer, C McKellar, and PB Duffy. 2012. "Technical Note: Bias correcting climate model simulated daily temperature extremes with quantile mapping." *Hydrology and Earth System Sciences* 16 (9):3309–3314.

U.S. Environmental Protection Agency. 2022. "Report on the Social Cost of Greenhouse Gases: Estimates Incorporating Recent Scientific Advances." Tech. rep., U.S. Environmental Protection Agency.

Vaile, Joanna, Shona Halson, Nicholas Gill, and Brian Dawson. 2008. "Effect of cold water immersion on repeat cycling performance and thermoregulation in the heat." *Journal of sports sciences* 26 (5):431–440.

Van Vuuren, Detlef P, Jae Edmonds, Mikiko Kainuma, Keywan Riahi, Allison Thomson, Kathy Hibbard, George C Hurtt, Tom Kram, Volker Krey, Jean-Francois Lamarque et al. 2011. "The representative concentration pathways: An overview." *Climatic Change* 109 (1-2):5.

Weitzman, Martin L. 2007. "A review of the Stern Review on the economics of climate change." *Journal of economic literature* 45 (3):703–724.

———. 2009. "On modeling and interpreting the economics of catastrophic climate change." *The Review of Economics and Statistics* 91 (1):1–19.

Wissmann, Daniel. 2022. "Finally a smoking gun? Compensating differentials and the introduction of smoking bans." *American Economic Journal: Applied Economics* 14 (1):75–106.

Wood, Andrew W, Lai R Leung, V Sridhar, and DP Lettenmaier. 2004. "Hydrologic implications of dynamical and statistical approaches to downscaling climate model outputs." *Climatic change* 62 (1-3):189–216.

Wyon, David P. 2001. *Indoor Air Quality Handbook*, chap. Thermal Effects on Performance. McGraw-Hill.

Zhang, Peng, Olivier Deschenes, Kyle Meng, and Junjie Zhang. 2018. "Temperature effects on productivity and factor reallocation: Evidence from a half million Chinese manufacturing plants." *Journal of Environmental Economics and Management* 88:1–17.

Appendix for Online Publication

Contents

A A stylized model of labor demand and supply under extreme temperatures: Derivations and sensitivity to assumptions

In this appendix, we provide mathematical details for the worker and firm decision problems and the equilibrium conditions of the model described in Section II. We then show the steps for deriving the components of the total willingness-to-pay (WTP) for a change in climate. Finally, we illustrate the implications for our disutility calculation in the case where wages can adjust in response to daily temperature shocks, and in the case where workers differ in their preferences for thermal comfort in the workplace.

A.1 Worker and firm decisions

A.1.1 Worker sectoral choice

We denote the indirect utility functions of a high- and low-risk worker as $V^h(\boldsymbol{T}, p, \kappa; \omega^h, \omega^l)$ and $V^l(\boldsymbol{T}, p, \kappa; \omega^h, \omega^l)$, respectively. These functions represent the maximum utility a worker can achieve in each sector, given daily temperature realizations ($\boldsymbol{T}$), prices (p), asset income (κ), and wages (ω^h, ω^l). Because the daily temperatures are not yet realized at the time of the worker's sectoral choice, and the price p and amount of asset income κ will depend on their realized values, a worker chooses the sector $s \in \{l, h\}$ that yields the higher expected utility given wages ω^h and ω^l, conditional on the climate $\boldsymbol{\tau}$:

$$\max_{s \in \{l,h\}} \Big\{ \mathbb{E}_{\boldsymbol{T}} \Big[V^s \Big(\boldsymbol{T}(\boldsymbol{\tau}), p(\boldsymbol{T}(\boldsymbol{\tau})), \kappa(\boldsymbol{T}(\boldsymbol{\tau})); \omega^h, \omega^l \Big) \;\Big|\; \boldsymbol{\tau} \Big] \Big\}. \tag{A.1}$$

A.1.2 Firm sectoral choice and wage determination

Prior to the realization of daily temperatures, a firm j must choose which sector to operate in and the wage rate to offer in that sector. Firm j's expected profit maximization problem (conditional on the climate $\boldsymbol{\tau}$) thus nests a wage offer decision within a sectoral choice decision, where the wage offer decision is subject to a participation constraint that the worker does not choose the other sector:

$$\begin{aligned}
&\max_{s \in \{l,h\}} \Big\{ \max_{\omega^h} \mathbb{E}_{\boldsymbol{T}} \Big[p(\boldsymbol{T}) a f^1 (\sum_{d=1}^{365} L_d^h(T_d), \boldsymbol{T}) - \omega^h \sum_{d=1}^{365} L_d^h(T_d) \;\Big|\; \boldsymbol{\tau} \Big], \max_{\omega^l} \mathbb{E}_{\boldsymbol{T}} \Big[a f^2 (\sum_{d=1}^{365} L_d^l(T_d), \widetilde{\boldsymbol{T}}) - \omega^l \sum_{d=1}^{365} L_d^l(T_d) \;\Big|\; \boldsymbol{\tau} \Big] - \beta_j \Big\} \\
&\textit{such that } \mathbb{E}_{\boldsymbol{T}} \Big[V^h \Big(\boldsymbol{T}, p(\boldsymbol{T}), \kappa(\boldsymbol{T}); \omega^h, \omega^l \Big) \;\Big|\; \boldsymbol{\tau} \Big] \geq \mathbb{E}_{\boldsymbol{T}} \Big[V^l \Big(\boldsymbol{T}, p(\boldsymbol{T}), \kappa(\boldsymbol{T}); \omega^h, \omega^l \Big) \;\Big|\; \boldsymbol{\tau} \Big] \; if \; s = h, \\
&\qquad\qquad \mathbb{E}_{\boldsymbol{T}} \Big[V^l \Big(\boldsymbol{T}, p(\boldsymbol{T}), \kappa(\boldsymbol{T}); \omega^h, \omega^l \Big) \;\Big|\; \boldsymbol{\tau} \Big] \geq \mathbb{E}_{\boldsymbol{T}} \Big[V^h \Big(\boldsymbol{T}, p(\boldsymbol{T}), \kappa(\boldsymbol{T}); \omega^h, \omega^l \Big) \;\Big|\; \boldsymbol{\tau} \Big] \; if \; s = l.
\end{aligned} \tag{A.2}$$

When deciding the wage within a sector, the firm takes into account its expected effect on the worker's labor supply, which a worker chooses after the realization of daily temperature.

A.1.3 Worker labor supply and consumption

The worker's daily labor supply decision is described in the main text Equation 1. At the end of the year, after all daily temperatures, goods prices, and annual wage and asset income are realized, workers choose how much to consume of the 2 goods, C_1 and C_2. The consumption decision of a worker in sector $s \in \{h, l\}$ is thus:

$$\begin{aligned} &\max_{C_1^s, C_2^s} U(C_1^s, C_2^s), \\ &\text{such that } pC_1^s + C_2^s = \omega^s \sum_{d=1}^{365} L_d^s + \kappa, \end{aligned} \tag{A.3}$$

A.2 Equilibrium conditions

Our model of labor supply and demand under extreme temperatures has several important conditions that hold in equilibrium. The first two of these conditions relate to equilibrium wages and employment shares across sectors, determined prior to the realization of daily temperature. The next four conditions relate to equilibrium goods consumption, labor supply, and asset income after daily temperatures are realized.

First, prior to the realization of daily temperature, expected worker utility is equalized across the two sectors to guarantee employment in both sectors with homogeneous workers. This equalization necessarily arises from the participation constraints for high- and low-risk workers in Equation A.2:

$$\mathbb{E}_{\boldsymbol{T}}\left[V^h\left(\boldsymbol{T}, p^*(\boldsymbol{T}), \kappa^*(\boldsymbol{T}); \omega^{h*}(\boldsymbol{\tau}), \omega^{l*}(\boldsymbol{\tau})\right) \;\middle|\; \boldsymbol{\tau}\right] = \mathbb{E}_{\boldsymbol{T}}\left[V^l\left(T, p^*(\boldsymbol{T}), \kappa^*(\boldsymbol{T}); \omega^{h*}(\boldsymbol{\tau}), \omega^{l*}(\boldsymbol{\tau})\right) \;\middle|\; \boldsymbol{\tau}\right], \tag{A.4}$$

where $p^*(\boldsymbol{T})$ and $\kappa^*(\boldsymbol{T})$ respectively denote the equilibrium good 1 price and asset income (with an expectation taken over the daily temperature realizations), and $\omega^{h*}(\boldsymbol{\tau})$ and $\omega^{l*}(\boldsymbol{\tau})$ are the equilibrium wages in the high-risk and low-risk sectors (determined prior to the daily temperature realizations, based on the climate $\boldsymbol{\tau}$). It is apparent that there is a compensating differential of higher wages for workers at high-risk firms (Rosen, 1974, 1986).[57]

[57] Equation A.4 can be equivalently expressed as $\mathbb{E}_{\boldsymbol{T}}\left[U(C_1^{h*}(\boldsymbol{T}), C_2^{h*}(\boldsymbol{T})) - \sum_{d=1}^{365} D(L_d^{h*}(T_d), T_d) \;\middle|\; \boldsymbol{\tau}\right] = \mathbb{E}_{\boldsymbol{T}}\left[U(C_1^{l*}(\boldsymbol{T}), C_2^{l*}(\boldsymbol{T})) - \sum_{d=1}^{365} D(L_d^{l*}(T_d), \widetilde{T}_d) \;\middle|\; \boldsymbol{\tau}\right]$, where $C_1^{s*}(\boldsymbol{T})$, $C_2^{s*}(\boldsymbol{T})$, and $L_d^{s*}(T_d)$ denote equilibrium good 1 and good 2 consumption and daily labor supply of a worker in sector $s \in \{h, l\}$ (with an expectation taken over the daily temperature realizations).

Second, it is also possible to derive an expression that governs the equilibrium shares of employment in the low- and high-risk sectors. These shares are determined by the distribution across firms of the β_j costs of protection from extreme temperatures. Firms with a sufficiently low β_j will choose the low-risk sector as their expected profits are greater there than in the high-risk sector. Let $\Delta^*(\boldsymbol{\tau})$ denote the equilibrium cross-sector differential in expected revenues less labor costs:

$$\Delta^*(\boldsymbol{\tau}) = \mathbb{E}_{\boldsymbol{T}}\left[af^2(\sum_{d=1}^{365} L_d^{l*}(T_d), \widetilde{\boldsymbol{T}}) - \omega^{l*}(\boldsymbol{\tau})\sum_{d=1}^{365} L_d^{l*}(T_d) \;\middle|\; \boldsymbol{\tau}\right] - \mathbb{E}_{\boldsymbol{T}}\left[p^*(\boldsymbol{T})af^1(\sum_{d=1}^{365} L_d^{h*}(T_d), \boldsymbol{T}) - \omega^{h*}(\boldsymbol{\tau})\sum_{d=1}^{365} L_d^{h*}(T_d) \;\middle|\; \boldsymbol{\tau}\right], \tag{A.5}$$

where $L_d^{l*}(T_d)$ and $L_d^{h*}(T_d)$ denote the equilibrium daily labor supply of a low- and high-risk worker respectively (with an expectation taken over the daily temperature realizations). From Equation A.2, it is evident that in equilibrium, only firms with $\beta_j < \Delta^*(\boldsymbol{\tau})$ will choose to operate in the low-risk sector. Thus the equilibrium shares of employment in the low- and high-risk sectors are respectively $G(\Delta^*(\boldsymbol{\tau}))$ and $1-G(\Delta^*(\boldsymbol{\tau}))$. Equations A.4 and A.5 reveal that the climate $\boldsymbol{\tau}$ influences both the equilbrium wages and composition of the economy across sectors by affecting expected disutility and output in the two sectors.

Third, combining the worker's first-order conditions from the consumption decision in Equation A.3 reveals that the marginal rate of substitution between C_1 and C_2 is set equal to the relative equilibrium price of C_1 (p^*):

$$\frac{U_1(C_1^{h*}(\boldsymbol{T}), C_2^{h*}(\boldsymbol{T}))}{U_2(C_1^{h*}(\boldsymbol{T}), C_2^{h*}(\boldsymbol{T}))} = \frac{U_1(C_1^{l*}(\boldsymbol{T}), C_2^{l*}(\boldsymbol{T}))}{U_2(C_1^{l*}(\boldsymbol{T}), C_2^{l*}(\boldsymbol{T}))} = p^*(\boldsymbol{T}). \tag{A.6}$$

Fourth, this equilibrium relative price clears the markets for the 2 goods, such that total consumption is equal to total production of each good:

$$G(\Delta^*(\boldsymbol{\tau}))C_1^{l*}(\boldsymbol{T}) + [1 - G(\Delta^*(\boldsymbol{\tau}))]C_1^{h*}(\boldsymbol{T}) = [1 - G(\Delta^*(\boldsymbol{\tau}))]af^1(\textstyle\sum_{d=1}^{365} L_d^h(T_d), \boldsymbol{T});$$

$$G(\Delta^*(\boldsymbol{\tau}))C_2^{l*}(\boldsymbol{T}) + [1 - G(\Delta^*(\boldsymbol{\tau}))]C_2^{h*}(\boldsymbol{T}) = G(\Delta^*(\boldsymbol{\tau}))af^2(\textstyle\sum_{d=1}^{365} L_d^l(T_d), \widetilde{\boldsymbol{T}}) - \int_0^{\Delta^*(\boldsymbol{\tau})} \beta g(\beta)\, d\beta. \tag{A.7}$$

The integral $\int_0^{\Delta^*(\boldsymbol{\tau})} \beta g(\beta)\, d\beta$ represents the lost output of low-risk firms due to the costs of protection from extreme temperature.

Fifth, the marginal disutility of labor and the pre-determined wage are equalized within each sector after each daily temperature realization:

$$\begin{aligned} \frac{D_L(L_d^{h*}(T_d), T_d)}{\mathbb{E}\left[U_2(C_1^{h*}(\boldsymbol{T}), C_2^{h*}(\boldsymbol{T})) \;\middle|\; \boldsymbol{\tau}\right]} &= \omega^{h*}(\boldsymbol{\tau}); \\ \frac{D_L(L_d^{l*}(T_d), \widetilde{T}_d)}{\mathbb{E}\left[U_2(C_1^{l*}(\boldsymbol{T}), C_2^{l*}(\boldsymbol{T})) \;\middle|\; \boldsymbol{\tau}\right]} &= \omega^{l*}(\boldsymbol{\tau}). \end{aligned} \tag{A.8}$$

Sixth, firms in each sector realize zero profits after payments to shareholders (i.e., workers, who own the firms):

$$\begin{aligned}\kappa^*(\boldsymbol{T}) = [1 - G(\Delta^*(\boldsymbol{\tau}))][p^*(\boldsymbol{T}) a f^1(\sum_{d=1}^{365} L_d^{h*}(T_d), \boldsymbol{T}) - \omega^{h*}(\boldsymbol{\tau}) \sum_{d=1}^{365} L_d^{h*}(T_d)] \\ + G(\Delta^*(\boldsymbol{\tau}))[a f^2(\sum_{d=1}^{365} L_d^{l*}(T_d), \widetilde{\boldsymbol{T}}) - \omega^{l*}(\boldsymbol{\tau}) \sum_{d=1}^{365} L^{l*}(T_d)] - \int_0^{\Delta^*(\boldsymbol{\tau})} \beta g(\beta)\, d\beta.\end{aligned} \tag{A.9}$$

A.3 Total willingness-to-pay

Equation 2 in the main text provides an expression for the total willingness-to-pay (WTP) for a change in $\boldsymbol{\tau}$, which comprises the WTP for (1) changes in output of high- and low-risk goods and (2) the disutility effects to workers. Here we provide details of how these components of total WTP are derived.

Our starting point is the indirect utility functions of high- and low-risk workers, V^h and V^l respectively. For an individual worker (high- or low-risk), the WTP for a change in $\boldsymbol{\tau}$ is obtained by totally differentiating the negative of indirect utility with respect to $\boldsymbol{\tau}$, dividing by the marginal utility of income (i.e., marginal utility of the numeraire good, C_2) to convert utils to dollars, and taking the expectation over daily temperatures $\boldsymbol{T}$. The total WTP, summed across all high- and low-risk workers, is thus:

$$Total\ WTP = (1 - G(\Delta^*(\boldsymbol{\tau})))\mathbb{E}_{\boldsymbol{T}}\Big[- \frac{\partial V^h / \partial \boldsymbol{\tau}}{U_2(C_1^{h*}, C_2^{h*})} \ \Big|\ \boldsymbol{\tau}\Big] + G(\Delta^*(\boldsymbol{\tau}))\mathbb{E}_{\boldsymbol{T}}\Big[- \frac{\partial V^l / \partial \boldsymbol{\tau}}{U_2(C_1^{l*}, C_2^{l*})} \ \Big|\ \boldsymbol{\tau}\Big]. \tag{A.10}$$

Applying the budget constraints of high- and low-risk workers (from Equation A.3) and the envelope theorem, we can rewrite Equation A.10 as:

$$\begin{aligned}Total\ WTP = &\underbrace{(1 - G(\Delta^*(\boldsymbol{\tau})))\mathbb{E}_{\boldsymbol{T}}\Big[\sum_{d=1}^{365}\Big(\frac{D_T(L_d^{h*}, T_d)}{U_2(C_1^{h*}, C_2^{h*})}\frac{\partial T_d}{\partial \boldsymbol{\tau}}\Big) + \frac{\partial p^*}{\partial \boldsymbol{T}}\frac{\partial \boldsymbol{T}}{\partial \boldsymbol{\tau}} C_1^{h*} - \frac{\partial \omega^{h*}}{\partial \boldsymbol{\tau}} \sum_{d=1}^{365} L_d^{h*} \ \Big|\ \boldsymbol{\tau}\Big]}_{\text{Temperature-induced disutility and price and wage changes for high-risk workers}} \\ &+ \underbrace{G(\Delta^*(\boldsymbol{\tau}))\mathbb{E}_{\boldsymbol{T}}\Big[\sum_{d=1}^{365}\Big((1-\gamma)\frac{D_T(L_d^{l*}, \widetilde{T}_d)}{U_2(C_1^{l*}, C_2^{l*})}\frac{\partial T_d}{\partial \boldsymbol{\tau}}\Big) + \frac{\partial p^*}{\partial \boldsymbol{T}}\frac{\partial \boldsymbol{T}}{\partial \tau} C_1^{l*} - \frac{\partial \omega^{l*}}{\partial \boldsymbol{\tau}} \sum_{d=1}^{365} L_d^{l*} \ \Big|\ \boldsymbol{\tau}\Big]}_{\text{Temperature-induced disutility and price and wage changes for low-risk workers}} \\ &- \underbrace{\mathbb{E}_T\Big[\frac{\partial \kappa}{\partial \boldsymbol{T}}\frac{\partial \boldsymbol{T}}{\partial \boldsymbol{\tau}} \ \Big|\ \boldsymbol{\tau}\Big]}_{\text{Effect of temperature on firm profits}}.\end{aligned} \tag{A.11}$$

Equation A.11 decomposes the total WTP into WTP for temperature-induced worker

disutility, price and wage changes faced by workers, and changes in firm profits.[58] Expanding the final term in Equation A.11 (i.e., the derivative of firm profits with respect to temperature) and applying the envelope theorem leads to:

$$
\begin{aligned}
Total\ WTP = & \underbrace{(1-G(\Delta^*(\boldsymbol{\tau})))\mathbb{E}_{\boldsymbol{T}}\Big[\sum_{d=1}^{365}\Big(\frac{D_T(L_d^{h*},T_d)}{U_2(C_1^{h*},C_2^{h*})}\frac{\partial T_d}{\partial \boldsymbol{\tau}}\Big)+\frac{\partial p^*}{\partial \boldsymbol{T}}\frac{\partial \boldsymbol{T}}{\partial \boldsymbol{\tau}}C_1^{h*}-\frac{\partial \omega^{h*}}{\partial \boldsymbol{\tau}}\sum_{d=1}^{365}L_d^{h*}\ \Big|\ \boldsymbol{\tau}\Big]}_{\text{Temperature-induced disutility and price and wage changes for high-risk workers}} \\
& + \underbrace{G(\Delta^*(\boldsymbol{\tau}))\mathbb{E}_{\boldsymbol{T}}\Big[\sum_{d=1}^{365}\Big((1-\gamma)\frac{D_T(L_d^{l*},\widetilde{T}_d)}{U_2(C_1^{l*},C_2^{l*})}\frac{\partial T_d}{\partial \boldsymbol{\tau}}\Big)+\frac{\partial p^*}{\partial \boldsymbol{T}}\frac{\partial \boldsymbol{T}}{\partial \tau}C_1^{l*}-\frac{\partial \omega^{l*}}{\partial \boldsymbol{\tau}}\sum_{d=1}^{365}L_d^{l*}\ \Big|\ \boldsymbol{\tau}\Big]}_{\text{Temperature-induced disutility and price and wage changes for low-risk workers}} \\
& + \underbrace{(1-G(\Delta^*(\boldsymbol{\tau})))\mathbb{E}_{\boldsymbol{T}}\Big[\Big(-p^*af_T^1(\sum_{d=1}^{365}L_d^{h*},\boldsymbol{T})-\frac{\partial p^*}{\partial \boldsymbol{T}}af^1(\sum_{d=1}^{365}L^{h*},\boldsymbol{T})\Big)\frac{\partial \boldsymbol{T}}{\partial \tau}-\sum_{d=1}^{365}\Big(p^*af_L^1(\sum_{d=1}^{365}L_d^{h*},\boldsymbol{T})-\omega^{h*}\Big)\frac{\partial L_d^{h*}}{\partial T_d}\frac{\partial T_d}{\partial \tau}+\frac{\partial \omega^{h*}}{\partial \boldsymbol{\tau}}\sum_{d=1}^{365}L_d^{h*}\ \Big|\ \boldsymbol{\tau}\Big]}_{\text{Effect of temperature on firm profits (high-risk sector)}} \\
& + \underbrace{G(\Delta^*(\boldsymbol{\tau}))\mathbb{E}_{\boldsymbol{T}}\Big[\Big(-(1-\gamma)af_T^2(\sum_{d=1}^{365}L_d^{l*},\widetilde{\boldsymbol{T}})\frac{\partial \boldsymbol{T}}{\partial \boldsymbol{\tau}}-\sum_{d=1}^{365}\Big(af_L^2(\sum_{d=1}^{365}L_d^{l*},\widetilde{\boldsymbol{T}})-\omega^{l*}\Big)\frac{\partial L_d^{l*}}{\partial T_d}\frac{\partial T_d}{\partial \boldsymbol{\tau}}\Big)+\frac{\partial \omega^{l*}}{\partial \boldsymbol{\tau}}\sum_{d=1}^{365}L_d^{l*}\ \Big|\ \boldsymbol{\tau}\Big]+\frac{\partial}{\partial \boldsymbol{\tau}}\int_0^{\Delta^*(\boldsymbol{\tau})}\beta g(\beta)\,d\beta}_{\text{Effect of temperature on firm profits (low-risk sector)}} \\
& - \underbrace{\Delta^*(\boldsymbol{\tau})g(\Delta^*(\boldsymbol{\tau}))\frac{\partial \Delta^*(\boldsymbol{\tau})}{\partial \boldsymbol{\tau}}}_{\substack{\text{Effect of temperature on firm profits} \\ \text{(net effects of sectoral shifts)}}} .
\end{aligned}
\tag{A.12}
$$

A change in $\boldsymbol{\tau}$ affects firm profits in the high- and low-risk sectors through multiple channels. These include a change in expected output in both high- and low-risk sectors,[59] a change in the total costs of protection for firms in the low-risk sector (i.e, $\frac{\partial}{\partial \boldsymbol{\tau}}\int_0^{\Delta^*(\boldsymbol{\tau})}\beta g(\beta)\,d\beta$), and price and wage changes.[60] Furthermore, a change in $\boldsymbol{\tau}$ also affects total profits by altering the share of employment in high- and low-risk sectors (i.e., $\frac{\partial G(\Delta^*(\boldsymbol{\tau}))}{\partial \boldsymbol{\tau}}$). This effect is captured in the last line of Equation A.12.

At this point, we observe in Equation A.12 that the WTP for climate-induced price and wage changes is zero on net, as the sets of terms containing $\frac{\partial p^*}{\partial \boldsymbol{T}}\frac{\partial \boldsymbol{T}}{\partial \boldsymbol{\tau}}$, $\frac{\partial \omega^{h*}}{\partial \boldsymbol{\tau}}$, and $\frac{\partial \omega^{l*}}{\partial \boldsymbol{\tau}}$ each sum to zero.[61] Price and wage changes amount to transfers between workers and firms and thus have no net effect on total WTP. Furthermore, applying the Leibniz integral rule reveals that the change in the total costs of protection for firms in the low-risk sector

[58] As specified by the zero profit condition (Equation A.9), changes in firm profits are equivalent to changes in the asset income of workers, κ.

[59] The change in output includes a direct effect of temperture in each sectors (i.e., $af_T^1(\sum_{d=1}^{365}L_d^{h*},\boldsymbol{T})$ and $af_T^2(\sum_{d=1}^{365}L_d^{l*},\widetilde{\boldsymbol{T}})$), and an effect driven by changes in labor supply in each sector (i.e., $\sum_{d=1}^{365}(p^*af_L^1(\sum_{d=1}^{365}L_d^{h*},\boldsymbol{T})-\omega^{h*})\frac{\partial L_d^{h*}}{\partial T_d}$ and $\sum_{d=1}^{365}(af_L^2(\sum_{d=1}^{365}L_d^{l*},\widetilde{\boldsymbol{T}})-\omega^{l*})\frac{\partial L_d^{l*}}{\partial T_d}$). This latter effect is not eliminated by an envelope condition due to the timing of when firms set wages and also due to worker participation constraints in the firms' profit maximization problem (Equation A.2 in main text). In setting wages before the daily temperature is realized, firms take into account how the wage will influence the worker's labor supply decision after the daily temperature is realized. Thus, even if not facing constraints for worker participation, firms would not equate their expected marginal revenue product of labor with the wage, and would instead equate expected marginal revenue product with the wage multiplied by $1+\frac{1}{\epsilon}$, where ϵ denotes the wage elasticity of labor supply. However, even this first-order condition will not hold with equality since firms must set wages that satisfy worker participation constraints.

[60] All these effects are captured in the third and fourth lines of Equation A.12.

[61] The sets of terms containing $\frac{\partial \omega^{h*}}{\partial \boldsymbol{\tau}}$ and $\frac{\partial \omega^{l*}}{\partial \boldsymbol{\tau}}$ each directly sum to zero, while the market clearing condition for the high-risk good (stated in Equation A.7) ensures that the set of terms containing $\frac{\partial p^*}{\partial \boldsymbol{T}}\frac{\partial \boldsymbol{T}}{\partial \boldsymbol{\tau}}$ sums to zero.

(i.e., $\frac{\partial}{\partial \boldsymbol{\tau}} \int_0^{\Delta^*(\boldsymbol{\tau})} \beta g(\beta)\, d\beta$) exactly offsets the change in total profits due to the altered sectoral composition (i.e., the last line of Equation A.12). Thus cancelling out all terms in Equation A.12 that sum to zero leads to:

$$
\begin{aligned}
Total\ WTP = & \underbrace{(1-G(\Delta^*(\boldsymbol{\tau})))\mathbb{E}_{\boldsymbol{T}}\Big[-p^* a f_T^1(\sum_{d=1}^{365} L_d^{h*}, \boldsymbol{T})\frac{\partial \boldsymbol{T}}{\partial \boldsymbol{\tau}} - \sum_{d=1}^{365}\Big(p^* a f_L^1(\sum_{d=1}^{365} L_d^{h*}, \boldsymbol{T}) - \omega^{h*}\Big)\frac{\partial L_d^{h*}}{\partial T_d}\frac{\partial T_d}{\partial \boldsymbol{\tau}} \;\Big|\; \boldsymbol{\tau}\Big]}_{\text{(A) Output loss for high-risk sector (good 1)}} \\
& + \underbrace{G(\Delta^*(\boldsymbol{\tau}))\mathbb{E}_{\boldsymbol{T}}\Big[-(1-\gamma) a f_T^2(\sum_{d=1}^{365} L_d^{l*}, \widetilde{\boldsymbol{T}})\frac{\partial \boldsymbol{T}}{\partial \boldsymbol{\tau}} - \sum_{d=1}^{365}\Big(a f_L^2(\sum_{d=1}^{365} L_d^{l*}, \boldsymbol{T}) - \omega^{l*}\Big)\frac{\partial L_d^{l*}}{\partial T_d}\frac{\partial T_d}{\partial \boldsymbol{\tau}} \;\Big|\; \boldsymbol{\tau}\Big]}_{\text{(B) Output loss for low-risk sector (good 2)}} \\
& + \underbrace{(1-G(\Delta^*(\boldsymbol{\tau})))\mathbb{E}_{\boldsymbol{T}}\Big[\sum_{d=1}^{365}\frac{D_T(L_d^{h*}, T_d)}{U_2(C_1^{h*}, C_2^{h*})}\frac{\partial T_d}{\partial \boldsymbol{\tau}} \;\Big|\; \boldsymbol{\tau}\Big]}_{\text{(C) Disutility effects for high-risk workers}} + \underbrace{G(\Delta^*(\boldsymbol{\tau}))\mathbb{E}_{\boldsymbol{T}}\Big[(1-\gamma)\sum_{d=1}^{365}\frac{D_T(L_d^{l*}, \widetilde{T}_d)}{U_2(C_1^{l*}, C_2^{l*})}\frac{\partial T_d}{\partial \boldsymbol{\tau}} \;\Big|\; \boldsymbol{\tau}\Big]}_{\text{(D) Disutility effects for low-risk workers}}.
\end{aligned}
\tag{A.13}
$$

which is identical to Equation 2 in the main text.

A.4 Implications of flexible daily wages for disutility calculation

In the main text Section VII.A, we illustrate how our approach to inferring a change in disutility from a change in daily labor supply (i.e., Equation 4 in main text) is affected by relaxing the assumption that wage rates do not fluctuate on a day-to-day basis in response to changing work conditions. Figure A.1 graphically depicts the implications for our disutility calculation, demonstrating that the amount by which the change in disutility is under- or over-estimated depends on the extent of the wage increase or decrease, respectively. In this situation, the overall labor supply change in the event of a temperature increase from T_{opt} to $T_+ > T_{opt}$ (i.e., $L^*(T_+) - L^*(T_{opt})$ in Figure A.1) can be divided into two components: a change that occurs from a shifting supply curve, holding the wage fixed (i.e., $L|\omega - L^*(T_{opt})$), and a change that occurs due to a shifting wage (i.e., $L^*(T_+) - L|\omega$). The true labor disutility caused by the temperature shift (corresponding to the gridded area in Figure A.1) should be calculated using only the first component. Calculating the disutility based on the overall observed change in labor supply (i.e., $L^*(T_+) - L^*(T_{opt})$) introduces a bias (orange area in Figure A.1) whose direction and magnitude depend on the second component, i.e., the change in labor supply due to the wage shift.

Equations 12 and 13 in the main text formalize a procedure for correcting this bias, which involves multiplying the disutility calculated from the observed labor supply change by a scaling factor. The value of the scaling factor depends on the Frisch elasticity of labor supply and two other parameters— i.e., the fraction of workers for whom the wage rate can fluctuate in response to daily temperature conditions (r), and the percentage change in wage due to a marginal change in daily temperature as a proportion of the percentage

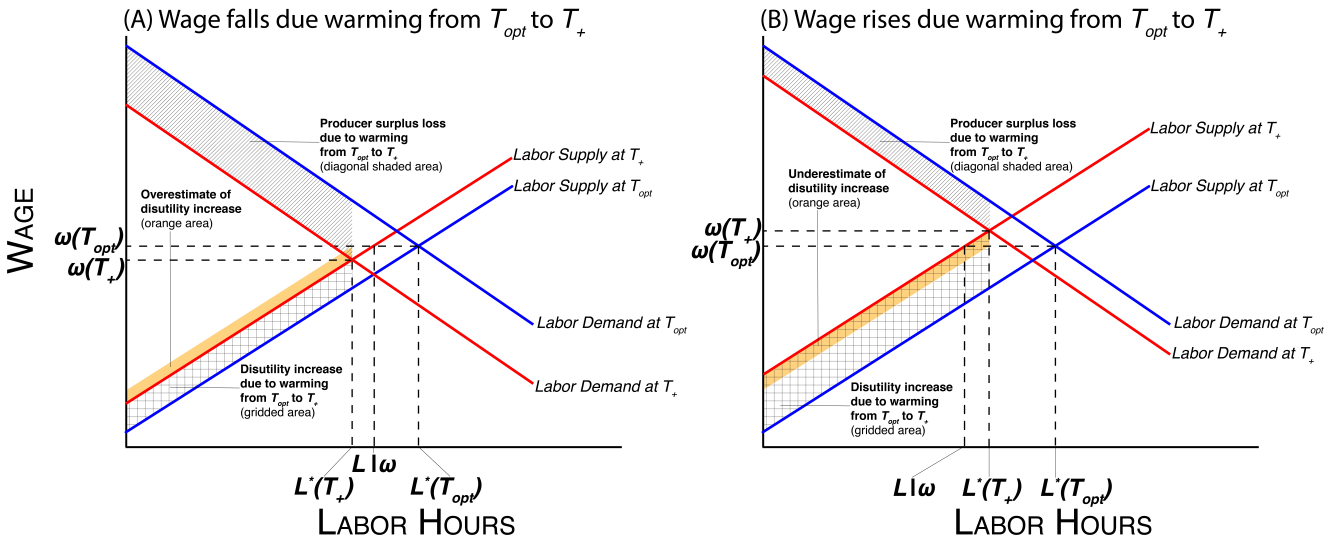

Figure A.1: Effects of a temperature increase on labor supply and disutility in presence of wage change. Intersection of upward-sloping marginal disutility of labor (labor supply) and downward-sloping labor demand determines the equilibrium labor hours at a given daily temperature, either T_{opt} or $T_+ > T_{opt}$. Figure A.1A illustrates a case where the temperature increase from T_{opt} to T_+ results in a decrease in the equilibrium wage. In this case, our calculation of the change in worker disutility based on the change in equilibrium labor supply (i.e., $L^*(T_+) - L^*(T_{opt})$) overestimates the actual change in worker disutility, which should be calculated based on the labor supply change that occurs from a shifting supply curve, holding the wage fixed (i.e., $L|\omega - L^*(T_{opt})$). The gridded area denotes the actual change in disutility, while the estimate based on the change in equilibrium labor supply corresponds to gridded area plus the orange area. Figure A.1B illustrates a case where the temperature increase from T_{opt} to T_+ results in an increase in the equilibrium wage. In this case, calculating the change in worker disutility based on the change in equilibrium labor supply underestimates the actual change in worker disutility. The gridded area denotes the actual change in disutility, while the estimate based on the change in equilibrium labor supply corresponds to the gridded area that is not shaded in orange.

change in labor supply due to a marginal change in daily temperature, which we assume to be a constant x.

In order to implement the scaling, it is necessary to calibrate plausible values of r and x. To characterize r, we note that there are certain types of workers for whom wage rates implicitly adjust at high frequency in response to productivity shocks. These include self-employed workers and piece rate workers. Approximately 20% of the workers in our data are self-employed. While it is not possible to identify piece rate workers in our data and globally comprehensive data do not exist, survey evidence suggests that piece rate compensation is rare in advanced industrial economies (Hart, 2016). Although it is more common in developing economies, survey evidence suggests that even in these countries, the vast majority of workers are not piece rate workers (Guiteras and Jack, 2018). Countries with the largest documented share of piece rate workers include India and Indonesia, where under 15% of the workforce is compensated by piece rate.[62] Based on these values, we conservatively set r to 35% (i.e., assuming 15% of workers are compensated by piece rate, plus 20% of workers recorded as self-employed in our data).

One way to obtain values for x is to look to prior studies on how extreme temperature conditions affect productivity per worker hour. In a perfectly competitive labor market free of wage rigidities, such changes in productivity will be directly reflected in the wage rate. Although these type of studies are limited to specific workplace or laboratory settings, they provide a range of values for x that can be used to adjust for potential bias in our calculated disutility. For instance, in his study on blueberry picking on 2 California farms, Stevens (2019) finds a roughly 5% decrease in productivity at the most extreme temperatures relative to moderate temperatures, while metastudies of laboratory experiments find up to a 15% decrease at the most extreme temperatures (Seppanen, Fisk, and Faulkner, 2004). Productivity decreases of roughly 30% are found by Sahu, Sett, and Kjellstrom (2013) in their study on rice harvesters in India. When combined with our estimates equivalent to a reduction of roughly 10% of a day's labor supply at 40°C for weather-exposed workers, these three estimates of productivity effects imply x values of 0.5, 1.5, and 3, respectively.[63]

While prior studies provide a basis for considering positive values of x (i.e., a due

[62]India's National Sample Survey (National Sample Survey Organisation, 2005) and the Indonesia Family Life Survey (Center for Population and Policy Studies, Gadjah Mada University (Indonesia), RAND Corporation, SurveyMETER, 2007-2008) reveal that roughly 12% of workers in each country are compensated by piece rate. In both countries, piece rate compensation is prevalent both in industries we classify as high-risk and low-risk, with slightly higher rates (up to 15%) in high-risk industries.

[63]We estimate that for high-risk workers, a 40°C day causes roughly a 30 minute decline in labor supply relative to a 27°C (Table 2, Column 3). This represents roughly 10% of a day's labor supply, based on 300 average minutes worked in a day in our data (Table 1). Because the highest temperatures considered in the productivity studies do not exceed 40°C, we use our estimated labor supply reduction at 40°C to calibrate values of x, even though we estimate larger reductions from days higher than 40°C. Moreover, it should be noted that the productivity studies do not consider effects that persist beyond a single day, while we estimate the effect of daily temperature on labor supply over a week. Our construction of values for x assumes that the productivity effects beyond the day of exposure are zero.

to a decrease in the wage rate in the numerator and a decrease in labor supply in the denominator), Figure A.1B illustrates that moving to a more extreme temperature may *increase* the wage rate while reducing labor supply, resulting in a negative value for x. In this case, our calculated disutility is biased downwards and the adjustment by a factor of $(1 - \epsilon xr)$ would increase it. Estimating the response of labor supply to temperature separately for self-employed and non-self-employed workers in our data suggests that negative values of x are not implausible. In particular, the point estimates in Table A.1 reveal that extreme hot days cause a smaller decline in labor supply for self-employed workers than for non-self-employed workers.[64] If wages of non-self-employed workers are assumed to not vary in response to daily temperature fluctuations, then the smaller labor supply reduction of self-employed workers indicates that their implied wage rate must have increased, as illustrated in Figure A.1B.[65] For instance, relative to a 27°C day, a 45°C day causes roughly an hour reduction in labor supply for a high-risk non-self-employed worker, but only a 45 minute reduction for a high-risk self-employed worker (Table A.1, Columns 3-4). The 15 minutes of additional labor supply represent a 5% increase in daily labor supply, which corresponds to a 10% increase in the wage rate when assuming a Frisch elasticity of 0.5. With the 45 minute labor supply reduction for a self-employed worker representing a 15% reduction in labor supply, this implies $x = -2/3$. We therefore consider a value of $x = -2/3$, in addition to the values of 0.5, 1.5, and 3 derived from the productivity studies.

A.5 Heterogeneous worker preferences for thermal comfort

The stylized model presented in the main text and previous sections of this appendix assumes that workers are identical in their preferences for thermal comfort in the workplace. Here we derive an expression for the WTP to avoid the disutility effects of daily temperature when this assumption is relaxed. We also develop estimates of the hedonic value of thermal comfort in a low-risk job that account for the endogenous, preference-based selection of workers into high- and low-risk sectors.

A.5.1 Stylized model with heterogeneous worker preferences

Let z_i denote a multiplier on the labor disutility function D that is specific to worker i. The probability density function $h(\cdot)$ and cumulative distribution function $H(\cdot)$ specify the distribution of z_i values across firms. For a given day of the year $d = \underline{d}$, the daily labor supply of worker i if working in the high-risk sector is thus:

[64] This pattern is reversed on cold days, which would justify positive x values as derived from the productivity studies.

[65] The downward effect on the wage of the demand curve shifting inwards is more than offset by the upward effect of supply curve shifting inwards.

	Weekly minutes worked per worker			
	Low-risk workers		High-risk workers	
Daily maximum temperature	(1)	(2)	(3)	(4)
	Non-self employed	Self-employed	Non-self employed	Self-employed
45°	-16.9	10.7	-61.1	-45.5
	(13.2)	(14.2)	(23.3)	(42.7)
40°	-9.0	7.4	-30.1	-21.3
	(6.9)	(7.4)	(12.4)	(22.3)
35°	-2.2	4.3	-4.2	-1.5
	(2.3)	(2.4)	(4.7)	(8.6)
27°	–	–	–	–
	–	–	–	–
10°	0.0	-8.7	-11.9	-14.0
	(5.3)	(5.7)	(11.6)	(23.3)
5°	0.0	-11.3	-15.3	-18.1
	(6.8)	(7.4)	(15)	(30.1)
0°	0.0	-13.9	-18.8	-22.2
	(8.4)	(9.1)	(18.4)	(36.9)
-5°	-0.1	-16.5	-22.3	-26.3
	(9.9)	(10.8)	(21.8)	(43.8)
-10°	-0.1	-19.0	-25.8	-30.5
	(11.5)	(12.5)	(25.2)	(50.6)
Adj R-squared	0.59	0.59	0.59	0.59
N	3,442,813	732,454	1,876,287	547,560

Table A.1: Labor supply response to temperature: Self-employed vs. non-self-employed workers. This table shows estimates for labor supply-temperature responses that differ self-employed and non-self-employed workers within each risk group. All regression estimates are from a restricted cubic spline in daily maximum temperature; observations within each country are weighted by the sample weights specified in that country's survey, while across countries, observations are differentially weighted according to the country's total population of workers in the particular risk group. Point estimates indicate the effect on weekly labor supply of a single day at each daily maximum temperature value shown, relative to a day with a maximum temperature of 27°C (81°F). Standard errors (in parentheses) are clustered at the ADM1 (e.g., state) × month-of-sample level. Regressions employ the fixed effects specified in main text Equation 6, but separated by risk group × self-employment status.

$$\max_{L_{\underline{d}}^{h,i}} \mathbb{E}_{\boldsymbol{T}_{d>\underline{d}}}\Big[U(C_1^{h,i}, C_2^{h,i}) \;\Big|\; \boldsymbol{\tau}\Big] - z_i D(L_{\underline{d}}^{h,i}, T_{\underline{d}}),$$

$$\text{such that } p(\boldsymbol{T}(\boldsymbol{\tau}))C_1^{h,i}(\boldsymbol{T}(\boldsymbol{\tau})) + C_2^{h,i}(\boldsymbol{T}(\boldsymbol{\tau})) = \omega^h\Big[\sum_{d=1}^{\underline{d}} L_d^{h,i} + \sum_{d=\underline{d}+1}^{365} L_d^{h,i}(T_d(\boldsymbol{\tau}))\Big] + \kappa(\boldsymbol{T}(\boldsymbol{\tau})), \tag{A.14}$$

This expression is similar to main text Equation 1, except that the choices are now specific to worker i. Worker i's labor supply is chosen similarly if working in the low-risk sector, except that the worker experiences daily temperatures $\widetilde{T}_d$ instead of T_d.

Let $V^{h,i}(\boldsymbol{T}, p, \kappa; \omega^h, \omega^l)$ and $V^{l,i}(\boldsymbol{T}, p, \kappa; \omega^h, \omega^l)$ respectively denote worker i's indirect utility in the high- and low-risk sectors. At the beginning of the year, worker i chooses the sector $s \in \{l, h\}$ that yields the higher expected utility given wages ω^h and ω^l, conditional on the climate $\boldsymbol{\tau}$:

$$\max_{s\in\{l,h\}} \Big\{\mathbb{E}_{\boldsymbol{T}}\Big[V^{s,i}\Big(\boldsymbol{T}(\boldsymbol{\tau}), p(\boldsymbol{T}(\boldsymbol{\tau})), \kappa(\boldsymbol{T}(\boldsymbol{\tau})); \omega^h, \omega^l\Big) \;\Big|\; \boldsymbol{\tau}\Big]\Big\}. \tag{A.15}$$

In equilibrium, only workers with a sufficiently low z_i, will choose to work in the high-risk sector, with wages ω^{h*} and ω^{l*} providing a compensating differential to ensure that the share of workers in each sector is equal to the share of firms in each sector.[66]

The WTP to avoid the disutility effects of daily temperature on workers is similar to that in main text, except it now differs not only across high- and low-risk sectors but also across individual workers in each sector. As in the main text, we derive an expression for the wage change necessary to keep worker's utility constant, given a change in labor disutility caused by a marginal change in daily temperature, holding all else equal. For a high-risk worker i on day d, we denote this compensatory wage change $\frac{\partial \omega^{h*}}{\partial T_d}\frac{\partial T_d}{\partial \boldsymbol{\tau}}\big|_{V_0^{h,i}}$, where $V_0^{h,i}$ represents worker i's initial, pre-temperature change utility level. The compensatory wage change is obtained by taking the total derivative of worker i's indirect utility with respect to $\boldsymbol{\tau}$, while holding constant all other prices and income, and setting this derivative equal to zero. This results in the following expression:

$$\frac{D_T(L_d^{h,i*}, T_d)}{U_2(C_1^{h,i*}, C_2^{h,i*})}\frac{\partial T_d}{\partial \boldsymbol{\tau}} = L_d^{h,i*}\Big[\frac{\partial \omega^{h*}}{\partial T_d}\frac{\partial T_d}{\partial \boldsymbol{\tau}}\Big|_{V_0^{h,i}}\Big]. \tag{A.16}$$

Using the Frisch elasticity of labor supply (ϵ), we can rearrange Equation A.16 to obtain an expression of the disutility cost to high-risk worker i in terms of changes in

[66] Specifically, in equilibrium there exists a $\bar{z}^*(\boldsymbol{\tau})$ such that the shares of workers in the low- and high-risk sectors ($1 - H(\bar{z}^*(\boldsymbol{\tau}))$ and $H(\bar{z}^*(\boldsymbol{\tau}))$,respectively) are equal to the shares of firm's in the low- and high-risk sectors ($G(\Delta^*(\boldsymbol{\tau}))$ and $1 - G(\Delta^*(\boldsymbol{\tau}))$, respectively).

worker i's daily labor supply:

$$\frac{D_T(L_d^{h,i*}, T_d)}{U_2(C_1^{h,i*}, C_2^{h,i*})} \frac{\partial T_d}{\partial \boldsymbol{\tau}} = \frac{\omega^{h*}\left(\frac{\partial L_d^{h,i*}}{\partial T_d}\frac{\partial T_d}{\partial \boldsymbol{\tau}}\right)}{\epsilon}. \tag{A.17}$$

A similar expression can be derived for a low-risk worker i:

$$(1-\gamma)\frac{D_T(L_d^{l,i*}, \widetilde{T}_d)}{U_2(C_1^{l,i*}, C_2^{l,i*})} \frac{\partial T_d}{\partial \boldsymbol{\tau}} = \frac{\omega^{l*}\left(\frac{\partial L_d^{l,i*}}{\partial T_d}\frac{\partial T_d}{\partial \boldsymbol{\tau}}\right)}{\epsilon}. \tag{A.18}$$

Developing estimates of the value of labor disutility (i.e., the left-hand side of Equations A.17 and A.18) would require worker-specific estimates of the labor supply response to daily temperature (i.e. $\frac{\partial L_d^{h,i*}}{\partial T_d}$, $\frac{\partial L_d^{l,i*}}{\partial T_d}$). These are impossible to construct given our data. In the main text Section V.A, we only estimate an average response for the workers who have selected into the high-risk sector or low-risk sector. This introduces a selection bias in our estimates of the hedonic value of thermal comfort in a low-risk job (main text Equation 9), because the labor-supply temperature responses ($\widehat{f}_{high}$ and $\widehat{f}_{low}$) used to calculate the hedonic value are estimated not on the overall population of workers but on the set of workers who selected into each sector based on preferences.

A.5.2 Correcting for selection bias in hedonic value estimates

To correct for the selection bias in the estimates of labor supply temperature responses of high- and low-risk workers, we apply the two-stage estimator developed in Heckman (1979). Let $HighRisk_{i,j,t}$ denote an indicator variable that takes on a value of 1 if worker i (observed in subnational location j on date t) works in the high-risk sector. The worker's sectoral choice is determined by the latent variable $HighRisk^*_{i,j,t}$, which we model as follows:

$$HighRisk^*_{i,j,t} = \lambda_1 \boldsymbol{X}_i + \alpha_{1j} + \psi_{1k,y} + \delta_{1k,w} + \phi_{1d} + \epsilon_{1i,j,t}, \tag{A.19}$$

where the explanatory variables consist of a vector of individual-level covariates ($\boldsymbol{X}_i$) along with fixed effects for subnational location (α_{1j}), country k × year y ($\psi_{1k,y}$), country k × week-of-year w ($\delta_{1k,w}$), and day-of-week d (ϕ_{1d}). Worker i chooses the high-risk sector only when $HighRisk^*_{i,j,t}$ takes on a positive value:

$$HighRisk_{i,j,t} = \begin{cases} 1 \; if \; HighRisk^*_{i,j,t} > 0 \\ 0 \; if \; HighRisk^*_{i,j,t} \leq 0. \end{cases} \tag{A.20}$$

We assume that the daily temperature and precipitation realization only affects a worker's labor supply decision and not sectoral choice— an assumption that is consistent with the the timing of decisions in our stylized model. Let $Labor^{high*}_{i,j,t}$ denote a latent

variable of worker i's labor supply in the high-risk sector, which we model as follows:

$$Labor_{i,j,t}^{high*} = f_{high}(\boldsymbol{T}_{j,t}) + g_{high}(\boldsymbol{P}_{j,t}) + \lambda_2 \boldsymbol{X}_i + \alpha_{2j} + \psi_{2k,y} + \delta_{2k,w} + \phi_{2d} + \epsilon_{2i,j,t}. \quad \text{(A.21)}$$

The observed labor supply of worker i in the high-risk sector, which we denote $Labor_{i,j,t}^{high}$, is equal to $Labor_{i,j,t}^{high*}$ only if worker i chose the high-risk sector, and zero otherwise:

$$Labor_{i,j,t}^{high} = \begin{cases} Labor_{i,j,t}^{high*} \; if \; HighRisk_{i,j,t} = 1 \\ 0 \; if \; HighRisk_{i,j,t} = 0. \end{cases}$$

Assuming the error terms (ϵ_1, ϵ_2) have a joint normal distribution, we can apply the Heckman two-stage procedure to correct for the potential bias in the estimates of f_{high}, and similarly f_{low}. However, the set of variables that determine sectoral choice is entirely contained in the set of variables that determine labor supply, so identification in our application of the Heckman procedure depends crucially on its parametric assumptions, in particular the normality of the error terms.[67]

Table A.2 displays estimates of f_{high} and f_{low} and Table A.3 displays estimates of the hedonic value, when using the Heckman two-stage procedure. The estimates are qualitatively similar to those based on our main specification, suggesting that our results are not driven by endogenous selection of workers into sectors.

[67]The first stage of the two-stage procedure involves estimating a probit model of Equation A.19 and using these estimates to calculate the inverse Mills ratio. The second step involves estimating Equation A.21 with $Labor_{i,high,j,t}$ as the dependent variable while including the inverse Mills ratio as an additional regressor. Because the inverse Mills ratio is a function of the other regressors in the second stage, identification is possible only because of its nonlinear functional form, arising from the assumption of normally distributed errors.

	Weekly minutes worked per worker			
	(1)	(2)	(3)	(4)
Daily maximum temperature	Low-risk workers	High-risk workers	Low-risk workers	High-risk workers
45°	-11.0	-58.6	-16.7	-60.6
	(11.8)	(22.4)	(13.2)	(23.5)
40°	-5.7	-28.7	-8.9	-29.4
	(6.2)	(12.1)	(6.9)	(12.4)
35°	-1.2	-3.8	-2.3	-3.6
	(2.1)	(4.9)	(2.3)	(4.7)
27°	–	–	–	–
	–	–	–	–
10°	-0.9	-12.3	0.1	-13.7
	(4.9)	(12.0)	(5.3)	(11.8)
5°	-1.1	-16.0	0.2	-17.7
	(6.3)	(15.6)	(6.8)	(15.2)
0°	-1.3	-19.6	0.2	-21.8
	(7.7)	(19.1)	(8.4)	(18.7)
-5°	-1.6	-23.2	0.2	-25.8
	(9.2)	(22.7)	(9.9)	(22.2)
-10°	-1.8	-26.9	0.3	-29.8
	(10.6)	(26.2)	(11.5)	(25.6)
Heckman 2-stage	No	No	Yes	Yes
Adj R-squared	0.56	0.56	0.56	0.56
N	4,175,377	2,423,958	4,175,377	2,423,958

Table A.2: Labor supply response to temperature: Accounting for selection into high- and low-risk sectors Columns 1 and 2 show estimates for labor supply-temperature responses that differ for low- and high-risk workers respectively, as specified in main text Equation 6 (reproducing Columns 2 and 3 from main text Table 2). Columns 3 and 4 show estimates that correct for endogenous selection of workers into high- and low-risk sectors using the Heckman two-stage estimator as specified in Equations A.19-A.5.2. In all regressions, observations within each country are weighted by the sample weights specified in that country's survey, while across countries, observations are differentially weighted according to the country's total population of workers in the particular risk group. All estimates are from a restricted cubic spline in daily maximum temperature. Point estimates indicate the effect on weekly labor supply of a single day at each daily maximum temperature value shown, relative to a day with a maximum temperature of 27°C (81°F). Standard errors (in parentheses) are clustered at the ADM1 (e.g., state) × month-of-sample level.

	Baseline model	Heterogeneous thermal comfort preferences
	(1)	(2)
Global average value of thermal comfort in a low-risk job (% annual income)	2.9% [-1.0%,6.8%]	3.2% [-0.7%,7.1%]

Table A.3: Sensitivity of hedonic value estimate to heterogeneous worker preferences for thermal comfort. Column 1 reproduces our baseline estimates for the global average hedonic value of thermal comfort in a low risk job (Table 4, Panel A). Column 2 presents an estimate that accounts for preference-based selection of workers into high- and low-risk sectors through a Heckman (1979) selection correction (Appendix A.5). Brackets display 5^{th}-95^{th} percentile ranges.

B Data sources

B.1 Work hours data

In this section, we describe the multiple time use surveys and labor force surveys from which we obtain worker-level observations of time spent working. These surveys together cover observations from Brazil, France, India, Mexico, Spain, UK, and USA.

B.1.1 Brazil: *Pesquisa Mensal de Emprego*

The *Pesquisa Mensal de Emprego* (PME) is a monthly employment survey conducted in six major metropilitan areas (Belo Horizonte, Porto Alegre, Recife, Rio de Janiero, Salvador, and Sao Paulo), each of which covers multiple municipalities. The survey is used by the government to track the status of the labor force in Brazil, including monthly unemployment rates and earnings. Data collection for the PME began in 1994 but the survey was significantly altered in 2002 into its current format so only post-2002 data is used for this study.

Data on weekly work hours of individual workers are collected for four weeks per month, meaning there are a total of 48 weeks of responses per year.[68] We assign temperature exposure at the municipality level. Respondents are asked about how many hours they worked in the previous week where a week is defined as Saturday-Sunday. A two stage sampling process is used to select respondents at the city level. A city is divided into sub-regions and then these regions are randomly sampled with probability weighted by the population in that region. Once sub-regions are selected, households from within that sub-region are sampled randomly based on current lists of local residents.

The dataset is structured as a rotating panel such that each respondent is interviewed 8 times across the course of the survey. A respondent enters the survey on a particular week of the month and is surveyed again on that same week of the month for four consecutive months and then again for those same months one year later. For instance, someone may enter the survey on the third week in February 2002 and would then be surveyed again on the third week in March, April, May 2002 and the third week in February, March, April, May 2003. We restrict our sample to all respondents aged 15-65 who reported working more than zero hours in a particular week.

The survey asks respondents about their primary source of employment. There are multiple detailed occupational categories. For purposes of our analysis, we classify agriculture, mining, construction and manufacturing as high risk and all others as low risk.

[68] As there are 52 weeks in a year this means that 4 weeks are not surveyed annually. The rationale for removing those four weeks is to create comparable employment statistics for each month. The weeks that are chosen to represent a month are those with the maximum number of days overlapping that month. The weeks that are dropped are the remainder.

B.1.2 France, Spain, and UK: Multinational Time-Use Survey

Time use data from France, Spain, and the UK were drawn from the Multinational Time Use Study (MTUS). The MTUS consists of data from time diary surveys conducted by 23 individual national governments and harmonized into a single dataset by the Centre for Time Use Research at the University of Oxford. To collect these time diaries, researchers asked participants to record the days activities in 5-30 minute intervals.[69] As part of the harmonization process, responses were classified into 69 standardized activity categories.[70] The number of hours worked was computed by summing the time reported under all activity codes within the category paidwork (activity codes 7-14).

Although the surveys that were harmonized for inclusion in the MTUS span 23 countries and range over several decades, we only include observations from surveys that report the respondent's subnational location, occupation, and exact date of the time diary. This leaves us with observations from 3 countries: France (1998-1999), Spain (2002-2003), and the UK (various years from 1974-2001).[71] The analysis is restricted to those individuals 15-65 years of age who report having worked in their diary or who self-identify as employed.[72] Observations falling on national holidays, or observations which were identified as "bad cases" by the Centre for Time Use Research, are also excluded from the analysis. Temperatures are assigned to individuals based on subnational regions (the highest tier administrative unit in each of the three countries) as more granular location identifiers are not available. High-risk workers are defined to be those employed in either of two categories: Farming, forestry, and fishing; or Construction, assembly and repair, moving goods, transport, and extraction. Low-risk workers are anyone not in these categories.

B.1.3 India: India Time-Use Survey

The India Time-Use Survey was conducted from July 1998 through June 1999 across the six states of Gujarat, Haryana, Madhya Pradesh, Meghalaya, Orissa, and Tamil Nadu. Indias Ministry of Statistics and Programme Implementation (MOSPI) conducted the survey in conjunction with state-level agencies. The survey used a 3-stage stratified design at the levels of district (i.e. second administrative unit), village/urban block, and household. Six sub-strata in both rural and urban sectors were used to ensure sample representation across a range of land-holding classes (rural) and per capita expenditure levels (urban). Enumeration occurred over four sub-rounds of 3-months duration to address seasonality

[69] For the UK 1995 survey, respondents were asked to recall their activities from the previous day. For all other surveys included in this study, respondents recorded their activities on the day of the survey.

[70] For details on the harmonization process, see the MTUS Users Guide and Documentation Version 9 (2016) from the Centre for Time Use Research at http://www.timeuse.org/MTUS-User-Guide.

[71] US data from the American Time Use Survey (ATUS) are also part of the MTUS and contain the necessary information. However, for this analysis, we obtain the US data directly from the ATUS

[72] In France and Spain, individuals are observed only once. In the UK, depending on the survey year individuals may have been observed once (1995), twice (2000-01), or over seven consecutive days (1974-75, 1983-84, and 1987).

in time-use patterns.

Time-use records were collected on a one-day recall basis. Enumerators would spend multiple days in a location, inform respondents for which date data would be collected, and then meet the respondent the following day to itemize the number of minutes the respondent spent in each activity for each hour of the day. MOSPIs data team ensured that the total time spent across all categories in a day summed to 24 hours.[73] Our analysis is restricted to respondents aged 15-65 who either performed some work in the survey period, or who claimed a primary status as a worker or someone seeking and available for work. We calculate total time worked as the sum of minutes engaged in any activity falling under the three top-level categories of primary production, secondary production, or trade, business, and services. Temperatures are assigned to individuals at the district level. Risk status is assigned based on the National Classification of Occupations 3-digit industry code reported for each respondent. Individuals engaged in agriculture, agricultural services, mining, manufacturing, or construction were all defined as high-risk, with the remainder defined as low-risk.

B.1.4 Mexico: National Survey of Occupation and Employment

Work hours data are available from Mexicos National Survey of Occupation and Employment or *La Encuesta Nacional de Ocupacion y Empleo* (ENOE). This survey has been conducted on a quarterly basis by the Mexican statistical agency, INEGI, since 2005. While prior labor force surveys focused on metropolitan areas, ENOE covers rural and urban areas throughout Mexico.

The survey is nationally representative with a stratified, two-stage clustered design. INEGI creates primary sampling units (PSUs) of groups of roughly 100 households split into types: urban, semi-urban, and rural. Stratification of PSUs is based on sociodemographic and physical characteristics of the houses, and their physical location. After sampling the PSUs, clusters of households are sampled for interview. The timing of the survey occurs throughout the year, with the only restriction being that a specific household must be surveyed at some point during the quarter. Once in the survey, households are interviewed in 4 subsequent quarters.

We obtain weekly hours worked for individuals within sampled households. While the survey provides a measure of time use for each day of the week prior to the survey date, we aggregate these days to the weekly level to reduce the potential for recall bias as the survey may have taken place more than a week after the date in question. Our analysis

[73] As time-use patterns vary by type of day, the survey collected records on "normal", "weekly variant", and abnormal days to account for variation in behavior across typical workdays, rest days, and infrequent days associated with festivals or some disruption to ones typical schedule. Accordingly, slightly under a third of respondents were interviewed on multiple days, to generate a view of their activity behavior across different day types. Most of these repeat respondents were interviewed twice, usually on a "normal" day and "weekly variant" day. Less than two percent of the full sample were interviewed more than twice.

includes individuals aged 15-65 employed at the time of the survey. Temperatures are assigned according the municipality of the respondent's location.[74] Workers employed in agriculture-related industries, mining, construction, and manufacturing are defined as high risk, with all others defined as low risk.

B.1.5 USA: American Time-Use Survey

The American Time-Use Survey (ATUS) has been conducted by the US Census Bureau since 2003 as a follow-up survey administered to a subset of respondents surveyed in the Current Population Survey. For each selected household, a randomly-selected member age 15 or above is selected for participation. Respondents are notified in advance by mail that they have been selected for participation and provide time-use data for a 24 hour period through computer-assisted telephone interviewing.

The survey employs a three-stage, stratified sampling design. The first stage stratifies by state and aims for representation which is proportional to state population. Second-stage stratification is at the household level, with Hispanic and non-Hispanic black households, and households with children all oversampled. The third stage involves random selection of any civilian household member aged 15 or older. We restrict attention to individuals 65 or younger who claim to be in the workforce. Temperatures are assigned at the county level. However, the ATUS only identifies county location for individual residing in Metropolitan Statistical Areas.[75] We thus exclude observations from outside these areas.

Total work is calculated as the sum of all time spent engaged in sub-activities listed under Category 5, Work and Work-Related Activities. Relevant sub-categories include time spent in work itself, income-generating activities, socializing as a part of work, job searching, and other miscellaneous work-related activities. Respondents are categorized as low-risk or high-risk based on their main jobs major industry. Following Graff Zivin and Neidell (2014), workers engaged in agriculture/forestry/fishing/hunting, mining, construction, manufacturing, and transportation/utilities are coded as high-risk. All remaining workers are coded as low-risk.

B.2 Climate data

This section describes the climate data that we use in this analysis as well as the methods employed to make these data consistent with the spatial and temporal resolution of the work hours data. Broadly speaking, we use two classes of climate data, the first being historical data to estimate labor supply-temperature responses, and the other being future

[74] There are more than 2400 municipalities in Mexico.

[75] According to the US Census Bureau, over 80 percent of the US population resided in Metropolitan Statistical Areas in 2010.

climate data which are used to project the damages of climate change into the future under various emissions scenarios. We begin by describing the historical data, followed by the future projection data, and finally we detail the method we use to spatially and temporally aggregate these outputs to match the resolution of the work hours data.

B.2.1 Historical climate data

Data on historical climate exposure is used to estimate the labor supply-temperature response as well as the heterogeneity in the share of high-risk workers by average climatology. For these purposes, we use the Global Meteorological Forcing Dataset, v1 (GMFD) (Sheffield, Goteti, and Wood, 2006). These data provide surface temperature and precipitation information using a combination of both observations and reanalysis. The reanalysis process uses a weather forecasting model to assimilate observational weather data in order to establish a gridded dataset of meteorological variables. The particular reanalysis used is the NCEP/NCAR reanalysis, which is downscaled and bias-corrected using a number of station-based observational datasets to remove biases in monthly temperature and precipitation while retaining daily variability from the NCEP/NCAR reanalysis product (Sheffield, Goteti, and Wood, 2006).[76] Data are available on a $0.25° \times 0.25°$ resolution grid from 1948-2010. The temporal frequency is up to 3-hourly, but the daily data are used for this analysis. We obtain daily average temperatures and daily total precipitation for all grid cells globally. A primary reason for using GMFD in our regression analysis is that GMFD is used to bias-correct the climate model projections (described below).[77]

B.2.2 Climate projection data

Data on the future evolution of the climate is obtained from a multi-model ensemble of Global Climate Model (GCM) output. However, two important limitations arise when integrating GCM outputs into the current analysis. First, the relatively coarse resolution ($\sim 1°$ of longitude and latitude) of GCMs limits their ability to capture small-scale climate patterns, which renders them unsuitable for climate impact assessment at high spatial resolution. Second, the GCM climate variables exhibit large local bias when compared with observational data.

To address both of these limitations, we use a high-resolution ($0.25°$ X $0.25°$) set of global, bias-corrected climate projections produced by NASA Earth Exchange (NEX): the Global Daily Downscaled Projections (GDDP) (Thrasher et al., 2012).[78] The NEX-

[76] These observational datasets are generally available at finer spatial resolutions, but coarser temporal resolutions (e.g., monthly) than the reanalysis product. Therefore, while the observational datasets are used to downscale the reanalysis in space, they are employed for bias correction on a monthly temporal scale, with submonthly temporal variation provided by the reanalysis (Sheffield, Goteti, and Wood, 2006).

[77] Because GMFD only contains climate data up to 2010, we are necessarily limited to using labor supply data only up to 2010 in this analysis.

[78] Climate projections used were from the NEX-GDDP dataset, prepared by the Climate Analytics

GDDP dataset comprises 21 climate projections, which are downscaled from the output of GCM runs in the Coupled Model Intercomparison Project Phase 5 (CMIP5) archive (Taylor, Stouffer, and Meehl, 2012). The statistical downscaling algorithm used to generate the NEX-GDDP dataset is the Bias-Correction Spatial Disaggregation (BCSD) method (Thrasher et al., 2012; Wood et al., 2004), which was developed to address the aforementioned two limitations. This algorithm first compares the GCM outputs with observational data on daily maximum temperature, daily minimum temperature, and daily precipitation during the period 1950-2005. NEX-GDDP uses a climate dataset from GMFD for this purpose (Sheffield, Goteti, and Wood, 2006). A daily, quantile-specific relation between GCM historical period outputs and historical observations is derived from this comparison. This relation is then used to adjust the GCM outputs in historical and in future time periods so that the systemic bias of the GCM is removed. To disaggregate the bias-corrected GCM outputs to higher resolution, this algorithm interpolates the daily changes relative to climatology in GCM outputs into the spatial resolution of GMFD, and merges the fine-resolution changes with the climatology of the GMFD data.[79]

For each GCM, three different datasets are generated. The first uses historical emissions to simulate the response of the climate to historical forcing from 1850 to 2005. The second and third use projected emissions from Representative Concentration Pathways 4.5 and 8.5 (RCP4.5 and RCP8.5) to simulate emissions under those two emissions scenarios up to 2100. RCP 4.5 represents a "stabilization" scenario in which total radiative forcing is stabilized around 2100 (Riahi et al., 2011; Van Vuuren et al., 2011); RCP8.5 simulates climate change under intensive growth in fossil fuel emissions from 2006 to the end of the 21^{st} century. We use daily average temperature in the RCP4.5 and RCP8.5 scenarios from these datasets, where the daily average temperature is approximated as the mean of daily maximum and daily minimum temperatures.

The CMIP5 ensemble of GCMs described above is an "ensemble of opportunity", not a systematic sample of possible futures. Thus, it does not produce a probability distribution of future climate change. Moreover, relative to "simple climate models" designed for probabilistic sampling of the global mean surface temperature (GMST) response to radiative forcing, the CMIP5 ensemble systematically fails to sample tail outcomes (Rasmussen, Meinshausen, and Kopp, 2016; Tebaldi and Knutti, 2007). To provide an ensemble of climate projections with a probability distribution of GMST responses consistent with that estimated by a probabilistic simple climate model, we use the surrogate model mixed ensemble (SMME) method (Rasmussen, Meinshausen, and Kopp, 2016) to assign probabilistic weights to climate projections produced by GCMs and to improve representation of the tails of the distribution missing from the ensemble of GCMs. Generally speaking,

Group and NASA Ames Research Center using the NASA Earth Exchange, and distributed by the NASA Center for Climate Simulation (NCCS).

[79]Details are available in Appendix A of the NEX-GDDP documentation: https://gdo-dcp.ucllnl.org/downscaled_cmip_projections/techmemo/downscaled_climate.pdf

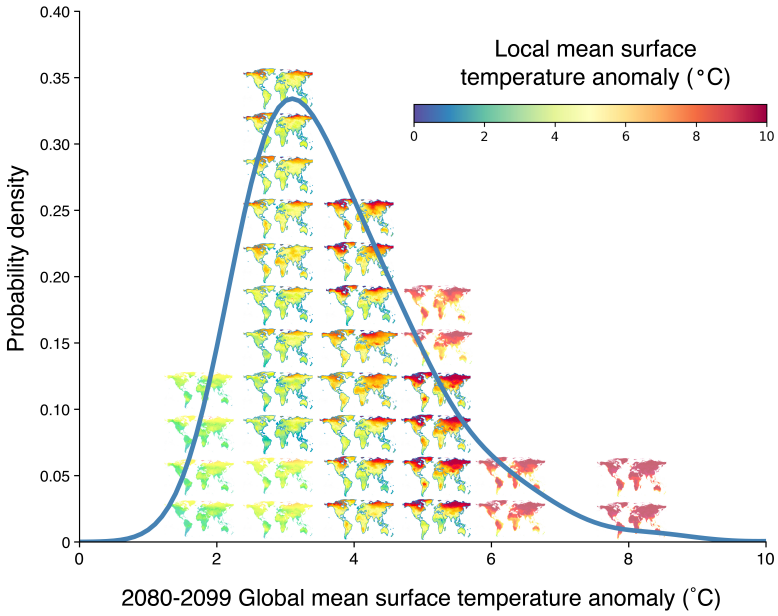

Figure B.1: Future climate projections used in generating the projected impact of climate change on labor disutility. Graph shows the 21 climate models (outlined maps) and 12 model surrogates (maps without outlines) that are weighted in climate change projections so that the weighted distribution of the 2080 to 2099 global mean surface temperature anomaly (ΔGMST) exhibited by the 33 total models matches the probability distribution of estimated ΔGMST responses (blue-gray curve) under RCP8.5. For this construction, the anomaly is relative to values in 1986-2005.

the SMME uses (1) a weighting scheme based on a probabilistic projection of global mean surface temperature from a simple climate model (in this case, MAGICC6) (Meinshausen, Raper, and Wigley, 2011) and (2) a form of linear pattern scaling (Mitchell, 2003) that preserves high-frequency variability to construct model surrogates to fill the tails of probability distribution that are not captured by the GCM ensembles. This method, details of which are provided in Rode et al. (2021), provides us with an additional 12 model surrogates.

The 21 models and 12 model surrogates are treated identically in our calculations and we describe them collectively as the surrogate/model mixed ensemble (SMME). Figure 2B shows the resulting weighted climate model distribution across the 33 models for the 2080 to 2099 global mean surface temperature anomaly (relative to 1986-2005) under RCP8.5.

B.2.3 Aggregation of gridded climate data to administrative boundaries

Although we have access to gridded daily climate data, the location of individual workers in the work hours data is recorded at the level of an administrative unit (e.g., county)– a coarser spatial resolution than the grid cell. Moreover, in some of our work hours data sources, work hours are recorded at a coarser temporal resolution than daily (e.g., weekly). Thus it is necessary to link the gridded daily historical climate data to work hours data by aggregating grid-cell-by-day information to the spatial and temporal scale reported in each

work hours data source (see Table 1). Similarly, to generate future climate change impact projections for workers in each of our 24,378 custom impact regions (Section III.B), it is necessary aggregate grid cell climate projections to impact region scale. In both cases, nonlinear transformations of temperature or precipitation are computed at the grid-cell-by-day level before averaging values across space using population weights and, in cases where work hours data are at weekly scale, summing over days within a week.

To see how this calculation is operationalized, consider, for example, a second-order polynomial specification for temperature.[80] In this case, we begin with data on maximum temperatures for each day d at each grid cell z in administrative unit j indicated in the work hours data source (e.g., county). Let such grid-cell-level daily maximum temperatures be denoted by T_{zjd}. These grid-cell-level values must then be aggregated to the level of administrative unit j. To do this, we first raise grid-cell-level temperature to the power k, computing $(T_{zjd})^k$ for $k \in \{1, 2\}$. Let $\boldsymbol{T}_{zjd}$ denote the grid cell-by-day temperature vector $[(T_{zjd})^1, (T_{zjd})^2]$. We then take a spatial average over administrative unit j for each element in $\boldsymbol{T}_{zjd}$, weighting the average by grid-cell-level population.[81] The vector of administrative unit-by-day temperature variables is thus:

$$\boldsymbol{T}_{jd} = \sum_{z \in j} w_{zj} \boldsymbol{T}_{zjd} = \left[\sum_{z \in j} w_{zj} (T_{zjd})^1, \sum_{z \in j} w_{zj} (T_{zjd})^2 \right], \tag{B.1}$$

where w_{zj} is the share of j's population that falls into grid cell z, and where superscripts indicate exponents. In future projections, all daily gridded climate projection data from each of the 33 members of the SMME are analogously aggregated to the impact region level.

When linking historical climate data to data sources where work hours are recorded at weekly scale, we further sum over all days d within a week w:

$$\boldsymbol{T}_{jw} = \sum_{d \in w} \sum_{z \in j} w_{zj} \boldsymbol{T}_{zjd} = \left[\sum_{d \in w} \sum_{z \in j} w_{zj} (T_{zjd})^1, \sum_{d \in w} \sum_{z \in j} w_{zj} (T_{zjd})^2 \right]. \tag{B.2}$$

This order of operations, in which nonlinear transformations are computed *before* aggregating across space and time, recovers nonlinearities in the response of daily labor supply to daily temperature.

[80] For ease of illustration, we demonstrate the calculation here using a second-order polynomial specification for temperature, which is estimated in Appendix D. The calculation can be similarly carried out for any nonlinear transformation, including the restricted cubic spline specification for temperature used in our main estimating equation 6.

[81] Because we do not know the specific grid cell at which an individual worker is located within administrative unit j, this spatial averaging assigns each worker within j the temperature exposure of the average person in j. Population weights are time-invariant and calculated from the 2010 Gridded Population of the World dataset. Data are available here: https://sedac.ciesin.columbia.edu/data/collection/gpw-v4. We account for fractional grid cells that fall partially within administrative units.

Apart from constructing the temperature and precipitation vectors as described above, we also implement a series adjustments so that data at both daily and weekly temporal resolutions can be pooled in a single regression. These adjustments, which are necessary for our estimates to have a consistent interpretation across different timescales, include rescaling and incorporating within-week lags and leads of temperature and precipitation vector terms for daily observations. Details are provided in Appendix C.

B.3 Socioeconomic data and downscaling methodologies

This section provides details of the socioeconomic data used throughout our analysis, which includes historical subnational incomes and workforce compositions, future projections of incomes, and future projections of population counts. Additionally, because we require certain variables at high spatial resolution both for econometric estimation and for future projections, we detail the downscaling procedures we use to disaggregate available socioeconomic data, which is generally provided at relatively low resolution.

B.3.1 Workforce composition data

We obtain data on workforce composition in every ADM1 unit (first-level administrative unit, e.g., state) in 48 countries using census microdata from IPUMS (Minnesota Population Center, 2019). This information is contained in the "Industry, general recode" variable, which defines industry categories in a way that is comparable across censuses from different countries.[82] Industry categories are reported for each person-level observation. We aggregate across all persons to obtain the number of workers in each industry in each ADM1 unit $\times$ year.[83] For each ADM1 unit $\times$ year, the share of high-risk workers is calculated by dividing the number of workers in the Agriculture, fishing, and forestry; Mining and extraction; Manufacturing; and Construction categories by the total number of workers across all categories.[84] The share of low-risk workers is calculated as one minus the share of high-risk workers.

B.3.2 Historical income data

Equation 10 estimates how the share of high-risk workers varies as a function of income and long-run average temperature in each location. In order to obtain income data for

[82]The categories are: Agriculture, fishing, and forestry; Mining and extraction; Manufacturing; Electricity, gas, water and waste management; Construction; Wholesale and retail trade; Hotels and restaurants; Transportation, storage, and communications; Financial services and insurance; Public administration and defense; Services, not specified; Business services and real estate; Education; Health and social work; Other services; Private household services; and Other industry, not elsewhere classified.

[83]Person weights provided in the data are used when aggregating across persons.

[84]To obtain the total number of workers we aggregate across persons in all industry categories, excluding persons where the industry category is missing, or is reported as "Not in universe", "Response suppressed", or "Unknown".

each subnational region in our workforce compositon data, we draw subnational incomes from two main sources, using a combination of subnational GDP datasets as well as globally-comprehensive national GDP data:

- **Penn World Tables (PWT) national GDP**.[85] This dataset provides national level incomes from 1950 to 2014 for most of the countries in the world. We use Penn World Tables version 9.0 to obtain national level income for countries in the workforce composition data.
- **Gennaioli et al. (2014) subnational GDP**. This dataset provides national and sub-national income data for 1,503 administrative regions from 83 countries. We use this dataset to obtain subnational level income data for all countries in the workforce composition data. Data are provided by the authors at the first administrative subdivision for each country (i.e., ADM1).

Using these data, we construct a consistent multi-country panel of subnational incomes at ADM1 level, which we use for estimation of Equation 10. To do so, we use Gennaioli et al. (2014) to downscale the PWT national-level incomes. We prefer this approach to using the subnational data directly, as there are known inconsistencies in measurement of subnational GDP across countries. Thus, we make the assumption that the within-country distributions of GDP recorded in Gennaioli et al. (2014) are accurate, but the exact levels may not be. We rely on the PWT data as a consistent measure of GDP levels for all countries; thus, our subnational GDP estimates sum to national GDP from PWT for all countries in the sample. For administrative region s in country k in year t we calculate a weight, ν_{skt} that will apportion national income to subnational regions as follows:

$$\begin{aligned} \nu_{sct} =& \frac{GDPpc_{skt}^{Gennaioli}}{\sum_{s \in k} GDPpc_{skt}^{Gennaioli}} \\ GDPpc_{skt} =& \nu_{sct} \times GDPpc_{kt}^{PWT} \end{aligned}$$

where $GDPpc^{PWT}$ corresponds to per capita GDP drawn from the PWT dataset. Using these estimates of administrative-level GDP per capita, we construct the time-invariant income covariate $LogGDPpc_s$ used for estimation of Equation 10 as follows. First, we take the log of our GDP per capita estimate for year t and region s. Second, for each year t, we compute a average over 15 years of lagged values to obtain $\overline{LogGDPpc}_{st}$. Finally, we fix the year t to match the year for which workforce composition exists for region s, thereby obtaining the variable $\overline{LogGDPpc}_s$ used in Equation 10.

[85] Penn World Tables (PWT) database: https://www.rug.nl/ggdc/productivity/pwt/.

The data collected by Gennaioli et al. (2014) are drawn from disparate sources, often using census data, which are typically not annual, leading to an unbalanced panel. To construct annual values of income per capita using the Gennaioli et al. (2014) data, we linearly interpolate between years, before constructing the moving average values across all years.

B.3.3 Income projections

Future projections of national incomes are derived from the Organization for Economic Co-operation and Development (OECD) Env-Growth model (Dellink et al., 2015) and the International Institute for Applied Systems Analysis (IIASA) GDP model (Samir and Lutz, 2014), as part of the "socioeconomic conditions" (population, demographics, education, income, and urbanization projections) of the Shared Socioeconomic Pathways (SSPs). The SSPs propose a set of plausible scenarios of socioeconomic development over the 21^{st} century in the absence of climate impacts for use by the Integrated Assessment Modeling (IAM) and Impacts, Adaptation, and Vulnerability (IAV) scientific communities.

While there are many models within the SSP database, only the IIASA GDP model and OECD Env-Growth model provide GDP per capita projections for a wide range of countries. The IIASA GDP model describes incomes that are lower than the OECD Env-Growth model, so we produce results for both of these models to capture uncertainty within each socioeconomic scenario (we compute results for three socioeconomic scenarios: SSP2, SSP3, and SSP4). To construct annual estimates, we linearly interpolate between the logged time series data in the SSP database, which are provided in 5-year increments. For each 5-year period, we calculate the average annual growth rate, and apply this growth rate to produce each year's estimate of GDP per capita.[86]

Although the SSP scenarios provide national-level income projections, our high-resolution analysis requires estimates of location-specific GDP within country borders. To generate values of income for each of our 24,378 impact regions over time, we allocate national GDP per capita values from the SSPs across impact regions within a country through a downscaling procedure that relies on nightlights imagery from the NOAA Defense Meteorological Satellite Program (DMSP). This approach proceeds in two steps. First, we use available subnational income data from Gennaioli et al. (2014) in combination with higher-resolution income data from the U.S., China, Brazil, and India, to empirically estimate the relationship between GDP per capita and nightlight intensity.[87] Second, we

[86]OECD estimates of income are provided for 184 countries and IIASA's GDP projections cover 171 countries. For the remaining countries, we apply the average GDP per capita from the available countries for the baseline period, and allow this income to grow at the globally averaged growth rate.

[87]Due to cross-country inconsistencies in subnational income data, the income data for the US are primarily used to estimate the relationship between GDP per capita and nightlights intensity; other countries' data provide validation only.

use this estimated relationship to allocate national-level GDP data across impact regions within each country, based on relative intensity of night lights in the present. While this approach models heterogeneity in income levels across impact regions, each region grows in the future at the same rate as the national country projection from the SSPs. We detail these two steps below.

Estimation of the GDP-nightlights relationship While there exists a growing literature linking economic output to nightlights intensity, we take an unconventional regression approach to recovering this relationship because our goal is to apportion national income within a country, as opposed to predicting the level of income at any given location. In particular, we are interested in the ratio $\frac{GDPpc_{ck}}{\sum_{c \in k} GCPpc_{ck}}$ for impact region c in country k, which will allow us to predict income at the impact region level, given projections of national GDP per capita from the SSPs, $\sum_{c \in k} GDPpc_{ck} = GDPpc_k^{SSP}$. Thus, we estimate a regression relating *relative* GDP per capita to *relative* nightlights intensity, where each administrative region's values are calculated as relative to the country mean. The dependent variable for administrative region j in country k and year t is thus $\frac{GDPpc_{ikt}}{\sum_{j \in k} GDPpc_{ikt}}$.[88] To construct a measure of location-specific relative nightlight intensity, we calculate a z-score of nightlights (ZNL) for each administrative region j within a country k using:

$$ZNL_{jkt} = \frac{NL_{jkt} - \overline{NL}_{kt}}{\sigma(NL_{kt})}$$

where $\overline{NL}_{kt}$ is the country average nightlights intensity, $\sigma(NL_{kt})$ is the standard deviation of nightlights intensity across all administrative regions within country k, and the stable nightlights data product from 1992-2012 is used to construct time-varying measures of average nightlights intensity across an administrative region, NL_{jkt}.

The regression we estimate is as follows:

$$\frac{GDPpc_{jkt}}{\sum_{i \in c} GDPpc_{jkt}} = \alpha + \beta ZNL_{jkt} + \epsilon_{jkt} \tag{B.3}$$

where β represents the impact of a one standard deviation increase in a region's nightlights intensity, relative to its country average, on that region's relative GDP per capita.

Allocation of national GDP to impact regions using relative nightlight intensity We use the estimated coefficients from Equation B.3 to compute income at the impact region level. To do so, we construct values $ZNL_{ckt} = \frac{NL_{ckt} - \overline{NL}_{kt}}{\sigma(NL_{kt})}$ for each impact region c using the average of stable nightlights from DMSP across the years 2008-2012. We then estimate $GDPpc_{ckt}$ as follows:

$$\widehat{GDPpc}_{ckt} = \left[\hat{\alpha} + \hat{\beta} ZNL_{ckt}\right] \times GDPpc_{kt}^{SSP}$$

[88] The income data available from Gennaioli et al. (2014) are at the first administrative level (i.e., ADM1).

where $GDPpc_{kt}^{SSP}$ comes from one of the SSP projected income scenarios. The result of this approach is that the subnational downscaled incomes will sum to the national income from the SSPs, as these ratios sum to one, by construction.

B.3.4 Population projections and downscaling methodology

Future projections of national populations are derived from the International Institute for Applied Systems Analysis (IIASA) (Samir and Lutz, 2014) population projections as part of the Shared Socioeconomic Pathways (SSPs).[89] The IIASA SSP population projections provide estimates of population by age cohort, gender, and level of education for 193 countries from 2010 to 2100 in five-year increments. Each projection corresponds to one of the five SSPs, as defined in O'Neill et al. (2014).

To assemble population projections for each of our 24,378 impact regions, we downscale the country-level projections from the SSPs using 2011 high-resolution LandScan estimates of populations (Bright et al., 2012). Populations for impact regions in countries or areas not given in the SSP database are held constant at the values estimated by LandScan in 2011. Thus, for any given impact region c in year t, population for scenario v (pop_{ctv}) is estimated as:

$$\widehat{pop}_{ctv} = \begin{cases} pop_{ctv}^{SSP} \left(\frac{pop_{c,2011}^{LandScan}}{\sum_{c \in k} pop_{c,2011}^{LandScan}} \right), & \text{if } c \in K \\ pop_{c,2011}^{LandScan}, & \text{if } c \notin K \end{cases} \tag{B.4}$$

where pop_{ktv}^{SSP} is the SSP population given for country k and year t for scenario v, $pop_{c,2011}^{LandScan}$ is the LandScan estimate for impact region r, and K is the set of 193 countries available in the SSP Database. Note that while this approach distributes country-level projections of population heterogeneously to impact regions within a country, it fixes the relative population distribution within each country at the observed distribution today.

[89] The population data are accessed from the SSP database (IIASA Energy Program, 2016).

C Combining labor supply data at daily and weekly resolutions

The labor supply data used in our analysis are measured at the daily level in certain countries (USA, UK, France, Spain, India) and at the weekly level in others (Mexico, Brazil). In order to conduct a global analysis that encompasses data from all these countries, it is necessary to harmonize data measured at different temporal resolutions. In this appendix, we demonstrate that estimates of the labor-temperature response derived from daily data differ fundamentally from those derived from weekly data (Proposition C.1). While daily estimates reflect the effect of a daily temperature shock on that day's labor supply, weekly estimates reflect the net effect of all within-week repercussions to labor supply as a result of a daily temperature shock. In Propositions C.2, C.3, and C.4, we outline the adjustments necessary to make daily and weekly estimates comparable. These include incorporating within-week lags and leads of temperature for daily observations, and also appropriately rescaling outcome, climate, and person-level control variables in the regression.

In the propositions that follow, we consider an outcome $Y_{i,d,w}$ (e.g., labor supply) observed for person i on date d falling in a Sunday-Saturday week w. The weekly outcome for person i in week w is thus obtained by summing over all 7 days in the week: $Y_{i,w} \equiv \sum_{d \in w} Y_{i,d,w}$.[90] Let $\boldsymbol{T}_{i,d,w}$ denote the K-element temperature vector experienced by person i on date d in week w, and let $\boldsymbol{T}_{i,w}$ denote the temperature vector for week w. Each element of the vector $\boldsymbol{T}_{i,w}$ is obtained by summing the corresponding element in the daily vector over all days in the week. Formally $\boldsymbol{T}_{i,w} = (\sum_{d \in w} T^1_{i,d,w}, \ldots, \sum_{d \in w} T^K_{i,d,w})$, where $T^k_{i,d,w}$ denotes the k^{th} element of $\boldsymbol{T}_{i,d,w}$ $\forall\ k \in \{1, \ldots, K\}$.

Suppose there exist N_{daily} person-day observations, and $N_{weekly} = N_{daily}/7$ observations if aggregated to the weekly level. For notational parsimony, we define $\boldsymbol{Y}_{daily}$ as the $N_{daily} \times 1$ vector of daily observations and $\boldsymbol{Y}_{weekly}$ as the $N_{weekly} \times 1$ vector of weekly observations. Similarly, let $\boldsymbol{T}_{daily}$ denote the $N_{daily} \times K$ matrix of temperature vectors for all person-day observations and $\boldsymbol{T}_{weekly}$ denote the $N_{weekly} \times K$ matrix of temperature vectors for all person-week observations.

We refer to the least squares regression of $\boldsymbol{Y}_{daily}$ on $\boldsymbol{T}_{daily}$ as the "daily regression", with $\widehat{\boldsymbol{\beta}}_{daily}$ denoting the $K \times 1$ vector of estimated coefficients on $\boldsymbol{T}_{daily}$. In contrast, the least squares regression of $\boldsymbol{Y}_{weekly}$ on $\boldsymbol{T}_{weekly}$ is referred to as the "weekly regression", with $\widehat{\boldsymbol{\beta}}_{weekly}$ denoting the $K \times 1$ vector of estimated coefficients on $\boldsymbol{T}_{weekly}$.

Proposition C.1. *Coefficient estimates on the temperature vector from the daily regression do not equal those from the weekly regression (i.e., $\widehat{\boldsymbol{\beta}}_{daily} \neq \widehat{\boldsymbol{\beta}}_{weekly}$).*

[90] For exposition, we define a week to span Sunday to Saturday. However, it can be defined to start on any day-of-week and end 7 days later.

Proof. Let $\mathbf{1}_{1\times 7}$ denote a seven-element row vector of ones and let $\boldsymbol{I}_{N_{weekly}\times N_{weekly}}$ denote the $N_{weekly} \times N_{weekly}$ identity matrix. Define $\Psi \equiv \mathbf{1}_{1\times 7} \otimes \boldsymbol{I}_{N_{weekly}\times N_{weekly}}$. Note that $\boldsymbol{T}_{weekly} = \Psi \boldsymbol{T}_{daily}$ and $\boldsymbol{Y}_{weekly} = \Psi \boldsymbol{Y}_{daily}$.

Thus by the formula for the least squares estimate,

$$\widehat{\boldsymbol{\beta}}_{daily} = (\boldsymbol{T}'_{daily}\boldsymbol{T}_{daily})^{-1}(\boldsymbol{T}'_{daily}\boldsymbol{Y}_{daily}), \tag{C.1}$$

and

$$\widehat{\boldsymbol{\beta}}_{weekly} = (\boldsymbol{T}'_{daily}\Psi'\Psi\boldsymbol{T}_{daily})^{-1}(\boldsymbol{T}'_{daily}\Psi'\Psi\boldsymbol{Y}_{daily}). \tag{C.2}$$

From (C.2), it can be seen that estimating the weekly regression is equivalent to estimating the daily regression using $\Psi'\Psi$ as a weighting matrix. Noting that

$$\begin{aligned}
\Psi'\Psi =& (\mathbf{1}_{1\times 7} \otimes \boldsymbol{I}_{N_{weekly}\times N_{weekly}})'(\mathbf{1}_{1\times 7} \otimes \boldsymbol{I}_{N_{weekly}\times N_{weekly}}) \\
=& (\mathbf{1}_{7\times 1} \otimes \boldsymbol{I}_{N_{weekly}\times N_{weekly}})(\mathbf{1}_{1\times 7} \otimes \boldsymbol{I}_{N_{weekly}\times N_{weekly}}) \\
=& (\mathbf{1}_{7\times 7} \otimes \boldsymbol{I}_{N_{weekly}\times N_{weekly}}),
\end{aligned}$$

it is evident that $\Psi'\Psi$ contains ones along the diagonal but has non-zero off-diagonal elements. Thus estimating $\widehat{\boldsymbol{\beta}}_{weekly}$, from the weekly regression, does not yield the same coefficient estimates as estimating $\widehat{\boldsymbol{\beta}}_{daily}$, from the daily regression.

□

Although the coefficient estimates from the daily regression do not match those from the weekly regression, in Proposition C.2, we show that weekly regression coefficient estimates can be recovered by estimating a regression with daily data that controls for within-week lag and lead temperatures.

To implement this regression, we define for each $k \in \{1, \ldots, K\}$, 7 within-week lag and lead temperature variables, $T^k_{i,d^0,w}, \ldots, T^k_{i,d^6,w}$:

$$\begin{aligned}
\text{for } l = 0 \; T^k_{i,d^l,w} &= T^k_{i,d,w} \\
\text{for } l = \{1, \ldots, 6\} \; T^k_{i,d^l,w} &= \begin{cases} T^k_{i,d+l,w} \text{ if } d + l \in w \\ T^k_{i,d-(7-l),w} \text{ if } d + l \notin w. \end{cases}
\end{aligned} \tag{C.3}$$

Aside from the variable $T^k_{i,d^0,w}$ that caputures the contemporaneous temperature experienced by person i on date d, these variables are constructed to encompass lags and leads of temperature *within* the Sunday-Saturday week w. For instance, the variable $T^k_{i,d^1,w}$ either takes on the value of T^k experienced the next day $(d+1)$, or the value experienced 6 days prior $(d-6)$, whichever of the two falls in the same week w as date d. As a concrete

example, suppose date d is the Friday in week w. In that case, the following date ($d+1$, Saturday) also falls in week w, while the 6^{th} lag date falls on the Saturday of the previous week, $w-1$. Therefore $T^k_{i,d^1,w} = T^k_{i,d+1,w}$ in the case of a Friday observation. Alternatively, suppose date d is the Saturday in week w. In that case, the following date is the Sunday in week $w+1$, while the 6^{th} lag date is the Sunday of week w. Therefore $T^k_{i,d^1,w} = T^k_{i,d-6,w}$ in the case of a Saturday observation. All variables $T^k_{i,d^1,w}, \ldots, T^k_{i,d^6,w}$ are similarly defined depending on the day-of-week of date d, according to (C.3).

Let $\widetilde{\boldsymbol{T}}^k_l$ denote the $N_{daily} \times 1$ vector of $T^k_{i,d^l,w}$ for all person-day observations, and define the $N_{daily} \times 7$ matrix $\widetilde{\boldsymbol{T}}^k \equiv [\widetilde{\boldsymbol{T}}^k_0, \ldots, \widetilde{\boldsymbol{T}}^k_6]$. For notational parsimony, we define the $N_{daily} \times 7K$ matrix:

$$\widetilde{\boldsymbol{T}} \equiv [\widetilde{\boldsymbol{T}}^1, \ldots, \widetilde{\boldsymbol{T}}^K].$$

We refer to the least squares regression of $\boldsymbol{Y}_{daily}$ on $\widetilde{\boldsymbol{T}}$ as the "daily regression with within-week lags and leads", with $\widehat{\widetilde{\boldsymbol{\beta}}}$ representing the $7K \times 1$ vector of estimated coefficients on $\widetilde{\boldsymbol{T}}$.

Proposition C.2. *The coefficient estimates on the temperature vector from the weekly regression (i.e., $\widehat{\boldsymbol{\beta}}_{weekly}$) can be exactly recovered by estimating the daily regression with within-week lags and leads and summing across each set of within-week lag and lead coefficient estimates. Specifically, the k^{th} element of $\widehat{\boldsymbol{\beta}}_{weekly}$ is equal to the sum over the k^{th} set of 7 elements in $\widehat{\widetilde{\boldsymbol{\beta}}}$. In matrix notation:*

$$\Phi\widehat{\widetilde{\boldsymbol{\beta}}} = \widehat{\boldsymbol{\beta}}_{weekly}, \tag{C.4}$$

where $\Phi \equiv \mathbf{1}_{1\times 7} \otimes \boldsymbol{I}_{K\times K}$.

Proof. We will prove the claim by contradiction. Suppose $\Phi\widehat{\widetilde{\boldsymbol{\beta}}} \neq \widehat{\boldsymbol{\beta}}_{weekly}$, which implies the following sequence of expressions:

$$\begin{aligned}
\Phi\widehat{\widetilde{\boldsymbol{\beta}}} &\neq \widehat{\boldsymbol{\beta}}_{weekly} && \Rightarrow \\
\Phi(\widetilde{\boldsymbol{T}}'\widetilde{\boldsymbol{T}})^{-1}(\widetilde{\boldsymbol{T}}'\boldsymbol{Y}_{daily}) &\neq (\boldsymbol{T}'_{weekly}\boldsymbol{T}_{weekly})^{-1}(\boldsymbol{T}'_{weekly}\boldsymbol{Y}_{weekly}) && \Rightarrow \\
\Phi(\widetilde{\boldsymbol{T}}'\widetilde{\boldsymbol{T}})^{-1}(\widetilde{\boldsymbol{T}}'\boldsymbol{Y}_{daily}) &\neq 7(\Phi\widetilde{\boldsymbol{T}}'\widetilde{\boldsymbol{T}}\Phi')^{-1}(\Phi\widetilde{\boldsymbol{T}}'\boldsymbol{Y}_{daily}) && \Rightarrow \\
\Phi(\widetilde{\boldsymbol{T}}'\widetilde{\boldsymbol{T}})^{-1} &\neq 7(\Phi\widetilde{\boldsymbol{T}}'\widetilde{\boldsymbol{T}}\Phi')^{-1}\Phi && \Rightarrow \\
\Phi\Phi' &\neq 7(\Phi\widetilde{\boldsymbol{T}}'\widetilde{\boldsymbol{T}}\Phi')^{-1}\Phi(\widetilde{\boldsymbol{T}}'\widetilde{\boldsymbol{T}})\Phi' && \Rightarrow \\
\Phi\Phi' &\neq 7\boldsymbol{I}_{K\times K} && ,
\end{aligned}$$

where the second line uses the formula for the least squares estimate, and the third line is obtained by noting that $\boldsymbol{T}'_{weekly}\boldsymbol{T}_{weekly} = \frac{1}{7}(\Phi\widetilde{\boldsymbol{T}}'\widetilde{\boldsymbol{T}}\Phi')$ and $\boldsymbol{T}'_{weekly}\boldsymbol{Y}_{weekly} = \Phi\widetilde{\boldsymbol{T}}'\boldsymbol{Y}_{daily}$.

Noting that

$$\begin{aligned}\Phi\Phi' =&(\mathbf{1}_{1\times 7}\otimes \boldsymbol{I}_{K\times K})(\mathbf{1}_{1\times 7}\otimes \boldsymbol{I}_{K\times K})'\\ =&(\mathbf{1}_{1\times 7}\otimes \boldsymbol{I}_{K\times K})(\mathbf{1}_{7\times 1}\otimes \boldsymbol{I}_{K\times K})\\ =&(7\otimes \boldsymbol{I}_{K\times K})\\ =&7\boldsymbol{I}_{K\times K},\end{aligned}$$

we reach a contradiction. Therefore $\Phi\widehat{\widetilde{\boldsymbol{\beta}}} = \widehat{\boldsymbol{\beta}}_{weekly}$.

□

Having established that the coefficients from the weekly regression can be recovered through the daily regression with within-week lags and leads, we now consider a situation resembling our data structure, where labor supply for a part of the sample is reported at the daily level while labor supply for the rest of the sample is only reported as a weekly aggregate. Proposition C.3 demonstrates how the coefficient estimates from the weekly regression can be recovered in this situation by appropriately rescaling observations to account for the different temporal resolutions, in addition to including within-week lags and leads in the regression. Before stating and proving the proposition, we first explain the basic constructs needed for a "mixed daily/weekly" regression that combines daily and weekly observations.

Suppose that daily labor supply is reported for $N_{\underline{daily}}$ of the N_{daily} person-days in the sample. For the remaining $N_{daily} - N_{\underline{daily}}$ person-days, labor supply is only reported as an aggregate over the 7 days of the Sunday-Saturday week, resulting in $N_{\underline{weekly}} \equiv (N_{daily} - N_{\underline{daily}})/7$ person-week observations. The econometrician thus has $\underline{N} \equiv N_{\underline{daily}} + N_{\underline{weekly}}$ observations to use in the mixed daily/weekly regression, which are a mix of person-days and person-weeks.

Define $\boldsymbol{Y}_{\underline{daily}}$ as the $N_{\underline{daily}} \times 1$ vector of daily labor supply observations, and $\boldsymbol{Y}_{\underline{weekly}}$ as the $N_{\underline{weekly}} \times 1$ vector of weeky labor supply observations. From these vectors, we construct the $\underline{N} \times 1$ vector $\underline{\boldsymbol{Y}}$, containing the labor supply values for all $\underline{N}$ observations:

$$\underline{\boldsymbol{Y}} = \begin{bmatrix} \sqrt{7}\boldsymbol{Y}_{\underline{daily}} \\ \boldsymbol{Y}_{\underline{weekly}} \end{bmatrix}.$$

Note that the outcome variable (i.e., labor supply) for daily observations is rescaled through multiplying by $\sqrt{7}$, a step that is necessary to recover the same coefficient estimates as the weekly regression.

For daily observations, $7K$ temperature regressors are defined as in (C.3) based on within-week lag and lead temperatures. Let $\boldsymbol{T}^k_{l,\underline{daily}}$ denote the $N_{\underline{daily}} \times 1$ vector of $T^k_{i,d^l,w}$

for all daily observations, and define the $N_{\underline{daily}} \times 7$ matrix $\boldsymbol{T}^k_{\underline{daily}} \equiv [\boldsymbol{T}^k_{0,\underline{daily}}, \ldots, \boldsymbol{T}^k_{6,\underline{daily}}]$. For notational parsimony, we then define the $N_{\underline{daily}} \times 7K$ matrix:

$$\boldsymbol{T}_{\underline{daily}} \equiv [\boldsymbol{T}^1_{\underline{daily}}, \ldots, \boldsymbol{T}^K_{\underline{daily}}].$$

In order to implement the mixed daily/weekly regression, it is necessary to also define values of the $7K$ temperature regressors for the weekly observations. For person i and week w of the weekly observations, we define these values, $T^k_{i,0,w}, \ldots, T^k_{i,6,w}$ for each $k \in \{1, \ldots, K\}$, as simply the sum of the k^{th} element in the daily temperature vector over all days of the week. Formally:

$$\text{for } l = \{0, \ldots, 6\} \; T^k_{i,l,w} = \sum_{d \in w} T^k_{i,d,w}.$$

Let $\boldsymbol{T}^k_{l,\underline{weekly}}$ denote the $N_{\underline{weekly}} \times 1$ vector of $T^k_{i,l,w}$ for all weekly observations, and define the $N_{\underline{weekly}} \times 7$ matrix $\boldsymbol{T}^k_{\underline{weekly}} \equiv [\boldsymbol{T}^k_{0,\underline{weekly}}, \ldots, \boldsymbol{T}^k_{6,\underline{weekly}}]$.[91] For notational parsimony, we then define the $N_{\underline{weekly}} \times 7K$ matrix:

$$\boldsymbol{T}_{\underline{weekly}} \equiv [\boldsymbol{T}^1_{\underline{weekly}}, \ldots, \boldsymbol{T}^K_{\underline{weekly}}].$$

From the matrices $\boldsymbol{T}_{\underline{daily}}$ and $\boldsymbol{T}_{\underline{weekly}}$, we construct the $\underline{N} \times 7K$ matrix $\underline{\boldsymbol{T}}$, containing the temperature regressors for all $\underline{N}$ observations:

$$\underline{\boldsymbol{T}} = \begin{bmatrix} \sqrt{7}\boldsymbol{T}_{\underline{daily}} \\ \boldsymbol{T}_{\underline{weekly}} \end{bmatrix}.$$

As with the outcome variable, note that the temperature regressors for daily observations are rescaled through multiplying by $\sqrt{7}$, a step that is necessary to recover the same coefficient estimates as the weekly regression. Let $\underline{\widehat{\boldsymbol{\beta}}}$ represent the $7K \times 1$ vector of estimated coefficients on $\underline{\boldsymbol{T}}$ from the least squares regression of $\underline{\boldsymbol{Y}}$ on $\underline{\boldsymbol{T}}$ (i.e., mixed daily/weekly regression).

Proposition C.3. *The coefficient estimates on the temperature vector from the weekly regression (i.e., $\widehat{\boldsymbol{\beta}}_{weekly}$) can be exactly recovered by estimating the mixed daily/weekly regression. Specifically, the k^{th} element of $\widehat{\boldsymbol{\beta}}_{weekly}$ is equal to the sum over the k^{th} set of 7 elements in $\underline{\widehat{\boldsymbol{\beta}}}$. In matrix notation:*

$$\Phi \underline{\widehat{\boldsymbol{\beta}}} = \widehat{\boldsymbol{\beta}}_{weekly}, \tag{C.5}$$

where $\Phi \equiv \mathbf{1}_{1\times 7} \otimes \boldsymbol{I}_{K\times K}$.

[91] This construct is analogous to $\boldsymbol{T}^k_{\underline{daily}}$. The only difference is that the 7 elements within a row of $\boldsymbol{T}^k_{\underline{weekly}}$ are identical.

Proof. As with Proposition C.2, we will prove the claim by contradiction. Suppose $\Phi\widehat{\underline{\boldsymbol{\beta}}} \neq \widehat{\boldsymbol{\beta}}_{weekly}$, which implies the following sequence of expressions:

$$\begin{aligned}
\Phi\widehat{\underline{\boldsymbol{\beta}}} &\neq \widehat{\boldsymbol{\beta}}_{weekly} && \Rightarrow \\
\Phi(\underline{\boldsymbol{T}}'\underline{\boldsymbol{T}})^{-1}(\underline{\boldsymbol{T}}'\underline{\boldsymbol{Y}}) &\neq (\boldsymbol{T}'_{weekly}\boldsymbol{T}_{weekly})^{-1}(\boldsymbol{T}'_{weekly}\boldsymbol{Y}_{weekly}) && \Rightarrow \\
\Phi(\underline{\boldsymbol{T}}'\underline{\boldsymbol{T}})^{-1}(\underline{\boldsymbol{T}}'\underline{\boldsymbol{Y}}) &\neq 49(\Phi\underline{\boldsymbol{T}}'\underline{\boldsymbol{T}}\Phi')^{-1}(\tfrac{1}{7})(\Phi\underline{\boldsymbol{T}}'\underline{\boldsymbol{Y}}) && \Rightarrow \\
\Phi(\underline{\boldsymbol{T}}'\underline{\boldsymbol{T}})^{-1} &\neq 7(\Phi\underline{\boldsymbol{T}}'\underline{\boldsymbol{T}}\Phi')^{-1}\Phi && \Rightarrow \\
\Phi\Phi' &\neq 7(\Phi\underline{\boldsymbol{T}}'\underline{\boldsymbol{T}}\Phi')^{-1}\Phi(\underline{\boldsymbol{T}}'\underline{\boldsymbol{T}})\Phi' && \Rightarrow \\
\Phi\Phi' &\neq 7\boldsymbol{I}_{K\times K} && ,
\end{aligned}$$

where the second line uses the formula for the least squares estimate, and the third line is obtained by noting that $\boldsymbol{T}'_{weekly}\boldsymbol{T}_{weekly} = \frac{1}{49}(\Phi\underline{\boldsymbol{T}}'\underline{\boldsymbol{T}}\Phi')$ and $\boldsymbol{T}'_{weekly}\boldsymbol{Y}_{weekly} = \frac{1}{7}(\Phi\underline{\boldsymbol{T}}'\underline{\boldsymbol{Y}})$. Noting that $\Phi\Phi' = 7\boldsymbol{I}_{K\times K}$ (see proof of Proposition C.2), we reach a contradiction. Therefore $\Phi\widehat{\underline{\boldsymbol{\beta}}} = \widehat{\boldsymbol{\beta}}_{weekly}$.

□

While Proposition C.3 demonstrates the necessary adjustments to the outcome and temperature variables when combining daily and weekly observations, Propositions C.4 and C.5 demonstrate the necessary adjustments for person-level control variables (e.g., age). Unlike temperature, these variables are not additive over days in the week.[92] In Proposition C.4 we show that coefficients on such control variables are 7 times larger in magnitude in a regression with weekly observations than in a regression with daily observations. This necessitates a rescaling adjustment when combining daily and weekly observations in a single regression (Proposition C.5).

Let $\boldsymbol{X}_i$ denote an L-element vector of control variables for person i. For notational parsimony, we define $\boldsymbol{X}_{daily}$ as the $N_{daily} \times L$ matrix of $\boldsymbol{X}_i$ vectors for all person-days and $\boldsymbol{X}_{weekly}$ as the $N_{weekly} \times L$ matrix of $\boldsymbol{X}_i$ vectors when observations are aggregated to person-weeks. Note that both $\boldsymbol{X}_{daily}$ and $\boldsymbol{X}_{weekly}$ are built from numerically identical $\boldsymbol{X}_i$ vectors, but these vectors are repeated over 7 observations in $\boldsymbol{X}_{daily}$ for every one observation in $\boldsymbol{X}_{weekly}$.

Let $\widehat{\boldsymbol{\lambda}}_{daily}$ refer to the $L \times 1$ vector of estimated coefficients from the least squares regression of $\boldsymbol{Y}_{daily}$ on $\boldsymbol{X}_{daily}$, and let $\widehat{\boldsymbol{\lambda}}_{weekly}$ refer to the $L \times 1$ vector of estimated coefficients from the least squares regression of $\boldsymbol{Y}_{weekly}$ on $\boldsymbol{X}_{weekly}$.

Proposition C.4. *Coefficient estimates on the vector of person-level control variables from a regression with weekly observations are 7 times larger in magnitude than those*

[92] For example, suppose a 30 year old's labor supply is observed on each of 7 days in a week. If aggregated to the weekly level, the individual's age remains 30 and does not become 210.

from a regression with daily observations. (i.e., $\widehat{\boldsymbol{\lambda}}_{weekly} = 7\widehat{\boldsymbol{\lambda}}_{daily}$).

Proof. Note that $\boldsymbol{Y}_{weekly} = \Psi \boldsymbol{Y}_{daily}$ and $\boldsymbol{X}_{daily} = \Psi' \boldsymbol{X}_{weekly}$, where $\Psi \equiv \mathbf{1}_{1\times 7} \otimes \boldsymbol{I}_{N_{weekly}\times N_{weekly}}$. By the formula for the least squares estimate.

$$\widehat{\boldsymbol{\lambda}}_{weekly} = (\boldsymbol{X}'_{weekly}\boldsymbol{X}_{weekly})^{-1}(\boldsymbol{X}'_{weekly}\Psi \boldsymbol{Y}_{daily}), \tag{C.6}$$

and

$$\widehat{\boldsymbol{\lambda}}_{daily} = (\boldsymbol{X}'_{weekly}\Psi\Psi'\boldsymbol{X}_{weekly})^{-1}(\boldsymbol{X}'_{weekly}\Psi \boldsymbol{Y}_{daily}). \tag{C.7}$$

Noting that

$$\begin{aligned}
\Psi\Psi' =& (\mathbf{1}_{1\times 7} \otimes \boldsymbol{I}_{N_{weekly}\times N_{weekly}})(\mathbf{1}_{1\times 7} \otimes \boldsymbol{I}_{N_{weekly}\times N_{weekly}})' \\
=& (\mathbf{1}_{1\times 7} \otimes \boldsymbol{I}_{N_{weekly}\times N_{weekly}})(\mathbf{1}_{7\times 1} \otimes \boldsymbol{I}_{N_{weekly}\times N_{weekly}}) \\
=& (7 \otimes \boldsymbol{I}_{N_{weekly}\times N_{weekly}}) \\
=& 7\boldsymbol{I}_{N_{weekly}\times N_{weekly}},
\end{aligned}$$

it is evident that $\widehat{\boldsymbol{\lambda}}_{weekly} = 7\widehat{\boldsymbol{\lambda}}_{daily}$.

□

Having established that the estimated coefficients on the person-level controls are equal up to a constant of proportionality in regressions with daily vs. weekly observations, we now consider a situation where labor supply for a part of the sample is reported at the daily level while labor supply for the rest of the sample is only reported as a weekly aggregate (as in Proposition C.3).

Define $\boldsymbol{X}_{\underline{daily}}$ as the $N_{\underline{daily}} \times L$ matrix of $\boldsymbol{X}_i$ vectors for all observations reporting daily labor supply, and $\boldsymbol{X}_{\underline{weekly}}$ as the $N_{\underline{weekly}} \times L$ matrix of $\boldsymbol{X}_i$ vectors for all observations reporting weekly labor supply. From these matrices, we construct the $\underline{N} \times L$ matrix $\underline{\boldsymbol{X}}$, containing the labor supply values for all $\underline{N}$ observations:

$$\underline{\boldsymbol{X}} = \begin{bmatrix} \frac{1}{\sqrt{7}}\boldsymbol{X}_{\underline{daily}} \\ \boldsymbol{X}_{\underline{weekly}} \end{bmatrix}.$$

Note that the vector of person-level controls for observations reporting daily labor supply is rescaled through multiplying by $\frac{1}{\sqrt{7}}$, a step that is necessary to recover coefficients that are proportional to those in Proposition C.4.[93] Let $\widehat{\underline{\boldsymbol{\lambda}}}$ represent the $L \times 1$ vector of

[93]Instead rescaling by $\frac{1}{\sqrt{7}}$ for observations reporting daily labor supply, one may instead rescale by $\sqrt{7}$ for observations reporting weekly labor supply. This alternative rescaling also maintains proportionality of coefficient estimates.

estimated coefficients on $\underline{\boldsymbol{X}}$ from the mixed daily/weekly regression of $\underline{\boldsymbol{Y}}$ on $\underline{\boldsymbol{X}}$.

Proposition C.5. *The coefficient estimates on the vector of person-level controls from the weekly regression (i.e., $\widehat{\boldsymbol{\lambda}}_{weekly}$) can be recovered by estimating the mixed daily/weekly regression of $\underline{\boldsymbol{Y}}$ on $\underline{\boldsymbol{X}}$. Specifically, $\underline{\widehat{\boldsymbol{\lambda}}} = \widehat{\boldsymbol{\lambda}}_{weekly}$.*

Proof. Note that $(\underline{\boldsymbol{X}}'\underline{\boldsymbol{X}})^{-1} = (\boldsymbol{X}'_{weekly}\boldsymbol{X}_{weekly})^{-1}$ and that $\underline{\boldsymbol{X}}'\underline{\boldsymbol{Y}} = \boldsymbol{X}'_{weekly}\boldsymbol{Y}_{weekly}$. From the least squares formula, it is thus evident that $\underline{\widehat{\boldsymbol{\lambda}}} = \widehat{\boldsymbol{\lambda}}_{weekly}$. □

D Labor supply-temperature relationship: Robustness

In this appendix, we demonstrate that labor-supply temperature relationships for high- and low-risk workers (Table 2 and Figure 3) are robust to alternative functional forms as well as to alternative classifications of high- and low-risk workers.

D.1 Robustness to alternative functional forms

Figure D.1 displays the results of estimating Equation 6 using a set of different functional forms of temperature (i.e., different formulations of the temperature vector $\boldsymbol{T}_{j,t}$). The functional forms displayed are bins of daily maximum temperature,[94] restricted cubic spline (with knots at 27° C, 37° C, and 39° C), and polynomials of second, third, and fourth order.[95]

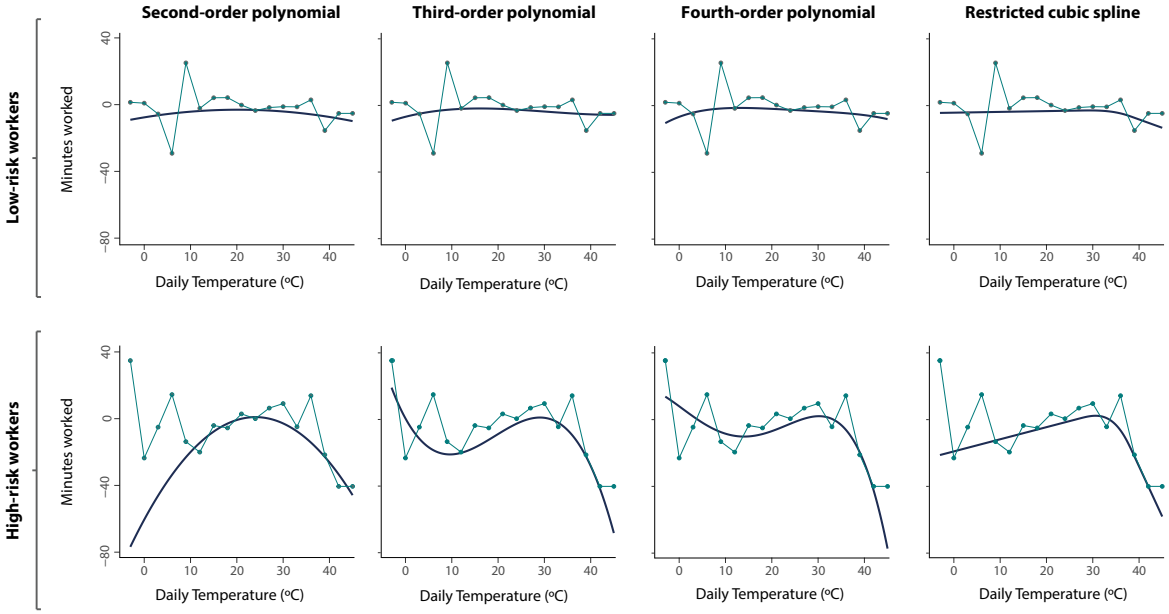

Figure D.1: Changes in weekly minutes worked per person due to daily temperature: Robustness to alternative functional forms. Labor supply-temperature response functions are estimated according to Equation 6 for low-risk workers (top row) and high-risk workers (bottom row). Each panel displays an estimate for a different parametric functional form of temperature (blue), along with the binned estimate (cyan). Points along each parametric curve represent the effect on weekly labor supply of a single day at the daily maximum temperature value shown on the x-axis, relative to a day with a maximum temperature of 27°C (81°F). Points in the binned estimate are relative to a day with a maximum temperature in the 24°C-27°C bin.

Table D.1 provides a quantitative comparison between the non-parametric, binned response and the parametric responses from the restricted cubic spline and polynomial.

[94] Bins are defined for temperatures below 0°C, above 42°, and for 3°C intervals between 0°C and 42°C.

[95] We estimated 3-knot restricted cubic splines with 336 sets of knot placements. Placing knots at 27°C, 37°C, and 39°C yielded the best fit to the data, as measured by the adjusted R^2.

We construct a root mean square error (RMSE) metric that compares each parametric response with the binned response. Specifically, for each bin's midpoint temperature, we take the square difference of the binned response and the parametric response. We then take a weighted average of the square differences across all bins, with weights determined by the global distribution of temperatures either in 2010 or 2099. Table D.1 shows the square root of this weighted average for each parametric functional form. For both high- and low-risk workers, the restricted cubic spline response has either the lowest or second lowest RMSE, depending on the weighting. Based on this evidence, we use the restricted cubic spline functional form for our main results, as it captures important nonlinearities recovered by the non-parametric binned response, while being parsimonious.

	Root mean square error relative to non-parametric, binned labor supply-temperature response			
	Low-risk workers		High-risk workers	
Functional form	Weighted by 2010 temperature	Weighted by 2090 temperature	Weighted by 2010 temperature	Weighted by 2090 temperature
Second-order polynomial	9.01	7.49	29.51	21.27
Third-order polynomial	9.16	7.38	16.49	17.02
Fourth-order polynomial	10.07	7.68	9.73	15.82
Restricted cubic spline	8.73	7.44	13.53	14.57

Table D.1: Comparison of labor supply-temperature response estimates under various parametric functional forms to non-parametric, binned estimates. This table displays values of a root mean square error (RMSE) metric that compares labor supply temperature response estimates of various functional forms with the non-parametric, binned response estimate. Specifically, for each bin's midpoint temperature, we take the square difference of the binned response and the parametric response at that temperature. We then take the square root of the weighted average of the square differences across all bins, with weights determined by the global distribution of temperatures either in 2010 or 2099.

D.2 Robustness to alternative classifications of high- and low-risk workers

In the labor supply-temperature responses shown in main text Figure 3 and Table 2, we classify whether workers are high or low risk based on the industry in which they are employed, with workers in agriculture, mining, construction, and manufacturing defined as high risk and all others as low risk. Here, we estimate labor supply-temperature responses using alternative classifications of high- and low-risk workers that take into account a worker's occupation. Specifically, we define protective services, maintenance, farming, fishing, forestry, construction, production, and transportation as high-risk occupations, and all others classified as low risk.

Based on these occupational categories, we consider two alternative classifications of workers by risk. In the first alternative, we classify workers as high or low risk based on whether their occupation is high or low risk. In the second alternative, we classify workers as high risk if both their industry and occupation is high-risk; all other workers are considered low risk. Table D.2 reports on the high-risk and low-risk labor supply-temperature responses estimated using the industry-based classification (Columns 1 and 4), and the two alternative classifications (by occupation in Columns 2 and 5, by industry and occupation in Columns 3 and 6). Responses are qualitatively similar under all three classifications.

	Weekly Minutes worked per worker					
	Low-risk workers			High-risk workers		
Daily maximum temperature	Industry	Occupation	Industry & Occupation	Industry	Occupation	Industry & Occupation
45°	-11.0	-13.5	-15.8	-58.6	-75.3***	-63.4***
	(11.8)	(12.6)	(12.3)	(22.4)	(19.6)	(22.7)
40°	-5.7	-7.2	-8.3	-28.7	-37.3***	-30**
	(6.2)	(6.6)	(6.5)	(12.1)	(10.6)	(12.7)
35°	-1.2	-1.8	-1.9	-3.8	-5.7	-2.5
	(2.1)	(2.1)	(2.1)	(4.9)	(3.7)	(6.0)
27°	–	–	–	–	–	–
	–	–	–	–	–	–
10°	-0.9	0.0	-0.7	-12.3	-13.2*	-18.1
	(4.9)	(4.8)	(4.8)	(12.0)	(7.7)	(14.8)
5°	-1.1	0.1	-0.9	-16.0	-17.1*	-23.4
	(6.3)	(6.2)	(6.2)	(15.6)	(10)	(19.2)
0°	-1.3	0.1	-1.1	-19.6	-20.9*	-28.7
	(7.7)	(7.7)	(7.6)	(19.1)	(12.3)	(23.6)
-5°	-1.6	0.1	-1.3	-23.2	-24.8*	-34.1
	(9.2)	(9.1)	(8.9)	(22.7)	(14.5)	(27.9)
-10°	-1.8	0.1	-1.6	-26.9	-28.7*	-39.4
	(10.6)	(10.5)	(10.3)	(26.2)	(16.8)	(32.3)
Adj R-squared	.56	.55	.56	.56	.55	.56
N	4,175,377	4,152,555	4,753,289	2,423,958	2,446,784	1,846,018

Table D.2: Labor supply response to temperature: Alternative classifications of high- and low-risk workers. This table shows estimates for labor supply-temperature responses that differ for low-risk (Columns 1-3) and high-risk (Columns 4-6) workers. All regression estimates are based on main text Equation 6 using a restricted cubic spline in daily maximum temperature; observations within each country are weighted by the sample weights specified in that country's survey, while across countries, observations are differentially weighted according to the country's total population of workers in the particular risk group. Point estimates indicate the effect on weekly labor supply of a single day at each daily maximum temperature value shown, relative to a day with a maximum temperature of 27°C (81°F). Standard errors (in parentheses) are clustered at the ADM1 (e.g., state) × month-of-sample level. Each column shows estimates using a different classification of high- and low-risk workers. Columns 1 and 4 use a classification by industry and reproduce the estimates from main text Table 2. Columns 2 and 5 use a classification by occupation, while Columns 3 and 6 limit the definition of high risk to workers who are employed in both a high-risk industry and occupation, with all other workers deemed low risk.

E Workforce composition in the present-day cross section of locations

In main text Equation 10, we estimate how the share of high-risk workers varies as a function of income and long-run average temperature in the present-day cross section of locations. In this appendix, we estimate alternative specifications of this regression that include different spatial and temporal fixed effects. The estimates and predictions from these alternative specifications are qualitatively similar to those from Equation 10.

Table E.1 reports the results for all specifications. Column 1 shows estimates from main text Equation 10; Column 2 adds fixed effects for census years; Column 3 adds fixed effects for continents;[96] Column 4 adds fixed effects for continents and census years; Column 5 adds fixed effects for countries; and Column 6 add fixed effects for countries and census years. The sample for Columns 1-5 only uses the most recent census year available for each country, while the sample for Column 6 uses all available years from 1980-2010.

The purpose of these estimates is to make out-of-sample predictions of the high-risk share, including in locations and (future) years that are not part of the estimation sample. As such, certain specifications are unsuitable for this purpose. For instance, models with country or year fixed effects cannot be used to predict the high-risk share in countries or years outside the estimation sample. Nevertheless, in Figure E.1 we show that the in-sample predictions of all specifications are similar to those of the Column 1 specification without fixed effects. Each scatter plot in Figure E.1 plots the in-sample high-risk share predictions from Table E.1 Columns 2, 3, 4, 5, or 6, against the predictions from Column 1, with the 45° line shown for comparison. In each panel, the pairs of predictions are generally aligned with the 45° line.

[96] Countries are grouped into four continents: Americas, Europe, Africa, and Asia. Our data contain one country in Oceania– Fiji. However, for purposes of defining the continent-specific fixed effects, we classify Fiji under Asia.

	Share of high-risk workers					
	(1)	(2)	(3)	(4)	(5)	(6)
Long-run Avg. Daily Maximum Temperature	−8.2e-03	1.5e-04	5.8e-04	3.9e-03	9.8e-03	6.6e-04
	(4.0e-03)	(4.0e-03)	(3.7e-03)	(3.8e-03)	(4.7e-03)	(3.0e-03)
Long-run Avg. Daily Maximum Temperature^2	−1.6e-03	−1.1e-03	−8.0e-04	−4.6e-04	−6.7e-04	−5.8e-04
	(2.6e-04)	(2.5e-04)	(2.5e-04)	(2.5e-04)	(2.6e-04)	(1.9e-04)
Long-run Avg. Daily Maximum Temperature^3	5.9e-05	3.6e-05	1.1e-05	−3.0e-06	−1.6e-05	1.3e-05
	(1.8e-05)	(1.7e-05)	(1.7e-05)	(1.7e-05)	(1.8e-05)	(1.4e-05)
Long-run Avg. Daily Maximum Temperature^4	−1.8e-07	−2.2e-07	3.0e-07	3.2e-07	8.4e-07	5.1e-08
	(4.1e-07)	(4.0e-07)	(3.8e-07)	(3.8e-07)	(4.3e-07)	(3.1e-07)
Log Income	−1.8e-01	−1.7e-01	−1.6e-01	−1.6e-01	−1.4e-01	−1.4e-01
	(4.6e-03)	(4.9e-03)	(4.7e-03)	(5.4e-03)	(7.5e-03)	(5.2e-03)
Continent fixed effects	No	No	Yes	Yes	No	No
Country fixed effects	No	No	No	No	Yes	Yes
Year fixed effects	No	Yes	No	Yes	No	Yes
N	1,073	1,073	1,073	1,073	1,073	1,917
Adj R-squared	0.62	0.68	0.69	0.71	0.77	0.81

Table E.1: Share of high-risk workers, income, and climate. This table shows estimates of the association between the share of high-risk workers (dependent variable) and explanatory variables log GDP per capita (averaged over the previous 15 years) and polynomials of daily maximum temperatures (averaged over the previous 30 years). Column 1 presents results from estimating the specification in Equation 10 in the main text, while subsequent columns add spatial and temporal fixed effects as indicated in the table. The sample for Columns 1-5 only uses the most recent census year available for each country, while the sample for Column 6 uses all available years from 1980-2010.

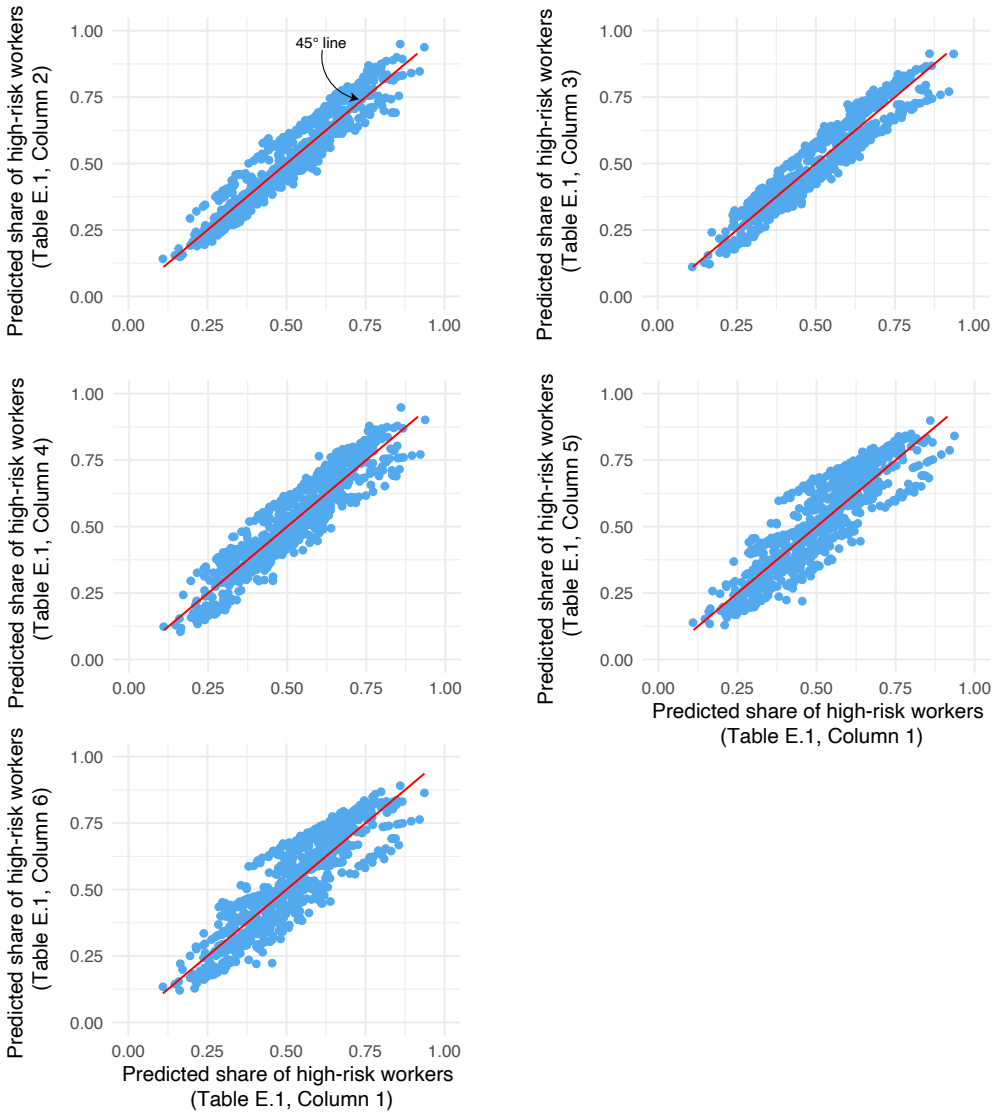

Figure E.1: Predicted share of high-risk workers from different empirical specifications. Each scatter plot compares the predicted share of high-risk workers from the empirical specification in one of the Columns 2-6 in Table E.1 (vertical axis), against the predicted share of high-workers from the empirical specification in Column 1 of Table E.1 (horizontal axis). The 45° line is indicated for reference. Each point corresponds to an in-sample observation (i.e., ADM1 unit).

F Worker disutility impacts of climate change: the role of economic development, climate-driven adaptation, and emissions mitigation

In this appendix, we first describe a set of calculations that illustrate how economic development and climate-driven adaptation shape the projected impacts of climate change. We then present results that illustrate the effect of emissions mitigation on the projected impacts of climate change.

F.1 Economic development and climate-driven adaptation

Our primary calculation is based on projected changes in labor supply due to a warmer future climate, accounting for projected future changes in the shares of high- and low-risk workers as economies develop and the climate warms. For an impact region c and future date t, this is expressed in Equation 11 in the main text:

$$\begin{aligned} \textit{Labor Supply Impact Of Climate Change}_{c,t,y} = & \underbrace{\left[\widehat{\rho}_{c,y}\widehat{f}_{high}(\boldsymbol{T}_{c,t,y}) + (1-\widehat{\rho}_{c,y})\widehat{f}_{low}(\boldsymbol{T}_{c,t,y})\right]}_{\substack{\text{Temperature-induced labor supply under climate change} \\ \text{(with economic development and climate-driven adaptation)}}} \\ & - \underbrace{\left[\widehat{\rho}_{c,\widetilde{y}}\widehat{f}_{high}(\boldsymbol{T}_{c,t,2015}) + (1-\widehat{\rho}_{c,\widetilde{y}})\widehat{f}_{low}(\boldsymbol{T}_{c,t,2015})\right]}_{\substack{\text{Temperature-induced labor supply without climate change} \\ \text{(with economic development)}}}, \end{aligned} \tag{F.1}$$

The labor supply-temperature response function estimate for each risk group r ($\hat{f}_r(\cdot)$) is evaluated at the daily temperature vector under a warmer climate projected for year y ($\boldsymbol{T}_{c,t,y}$), as well as a counterfactual daily temperature vector under a climate that is the same as that of 2015 $\boldsymbol{T}_{c,t,2015}$. The first bracketed term represents the total predicted labor supply under climate change, averaging across risk groups using predicted high and low-risk employment shares ($\widehat{\rho}_{c,y}$ and $1-\widehat{\rho}_{c,y}$ respectively) that account for shifts in workforce composition due to economic development and climate-driven adaptation.[97] In contrast, the second bracketed term represents the total predicted labor supply under a counterfactual with no climate change, where effects in each risk group are averaged using counterfactual employment shares in the absence of climate change. These counterfactual shares ($\widehat{\rho}_{c,\widetilde{y}}$ and $1-\widehat{\rho}_{c,\widetilde{y}}$) reflect changes in workforce composition due to economic development, but not due to climate-driven adaptation.[98] The difference between the two

[97] We predict the high-risk share in region c at year y using the fitted values of Equation 10, evaluated at the projected GDP per-capita and climate of year y: $\widehat{\rho}_{c,y} = \widehat{\gamma}\overline{LogGDPpc}_{c,y} + \widehat{h}(\overline{\boldsymbol{T}}_{c,y})$.

[98] We predict the counterfactual high-risk share in region c at year y using the fitted values of Equation 10, evaluated at the projected GDP per-capita of year y, but the climate of 2015: $\widehat{\rho}_{c,\widetilde{y}} = \widehat{\gamma}\overline{LogGDPpc}_{c,y} +$

bracketed terms in Equation F.1 expresses the impact of climate change on labor supply, accounting for shifts in workforce composition due to both economic development- and climate change-induced adaptation.

To illustrate the contribution of economic development and climate-driven adaptation, we also construct two alternative projections that ignore one or both of these mechanisms. The first of these is a "fixed workforce" (FW) projection in which each impact region's shares of high- and low-risk workers are held fixed through the century at their 2015 values (i.e., $\rho_{c,2015}$ and $1-\rho_{c,2015}$):

$$\textit{Labor Supply Impact Of Climate Change}^{FW}_{c,t,y} = \underbrace{\left[\widehat{\rho}_{c,2015}\widehat{f}_{high}(\boldsymbol{T}_{c,t,y}) + (1-\widehat{\rho}_{c,2015})\widehat{f}_{low}(\boldsymbol{T}_{c,t,y})\right]}_{\substack{\text{Temperature-induced labor supply under climate change}\\ \text{(without economic development or climate-driven adaptation)}}} - \underbrace{\left[\widehat{\rho}_{c,2015}\widehat{f}_{high}(\boldsymbol{T}_{c,t,2015}) + (1-\widehat{\rho}_{c,2015})\widehat{f}_{low}(\boldsymbol{T}_{c,t,2015})\right]}_{\substack{\text{Temperature-induced labor supply without climate change}\\ \text{(without economic development)}}}. \tag{F.2}$$

To decompose the contribution of economic development vis-a-vis climate-driven adaptation, we construct a second alternative, "no climate adaptation" (NCA) projection in which each impact region's high- and low-risk shares are allowed to change due to economic development but not due to climate-driven adaptation:

$$\textit{Labor Supply Impact Of Climate Change}^{NCA}_{c,t,y} = \underbrace{\left[\widehat{\rho}_{c,\widetilde{y}}\widehat{f}_{high}(\boldsymbol{T}_{c,t,y}) + (1-\widehat{\rho}_{c,\widetilde{y}})\widehat{f}_{low}(\boldsymbol{T}_{c,t,y})\right]}_{\substack{\text{Temperature-induced labor supply under climate change}\\ \text{(with economic development but no climate-driven adaptation)}}} - \underbrace{\left[\widehat{\rho}_{c,\widetilde{y}}\widehat{f}_{high}(\boldsymbol{T}_{c,t,2015}) + (1-\widehat{\rho}_{c,\widetilde{y}})\widehat{f}_{low}(\boldsymbol{T}_{c,t,2015})\right]}_{\substack{\text{Temperature-induced labor supply without climate change}\\ \text{(with economic development)}}}. \tag{F.3}$$

All three projections of labor supply impacts can be converted to disutility costs by multiplying by the ratio of the impact region's projected wage rate and the Frisch elasticity of labor supply.[99] Figure 8A in the main text plots these three projections of disutility costs of climate change under a very high emissions scenario (RCP8.5).

$\widehat{h}(\overline{\boldsymbol{T}}_{c,2015})$.

[99] In the map in main text Figure 6 Panel B, disutility estimates are aggregated over all workers and over all days in 2099, and expressed as a percentage of the impact region's projected 2099 GDP. We use impact region populations for this purpose. While an impact region's population would be larger than its number of workers, this does not affect our final calculation of total disutility costs, as these costs are valued using a wage that is calculated based on average per capita labor income rather than average per worker labor income. The larger number of individuals over which we are calculating the disutility costs (i.e. total population vs. workers) is exactly offset by the smaller wage value used for valuing the costs.

F.2 Emissions mitigation

Figure 8B in the main text illustrates that the projected impacts of climate change on labor disutility amount to 1.8% of 2099 global GDP under a very high emissions scenario (RCP8.5) but fall to 0.5% of 2099 global GDP under an intermediate scenario (RCP4.5). Here we present spatially disaggregated impacts under each of these emissions scenarios. Specifically, Figure F.1, Panels A and C, map changes to labor supply per worker for all impact regions at 2099 under RCP8.5 and RCP4.5 respectively. Figure F.1, Panels B and D map the total annual labor disutility costs for each impact region under RCP8.5 and RCP4.5 respectively, as a percentage of the impact region's projected 2099 GDP.[100]

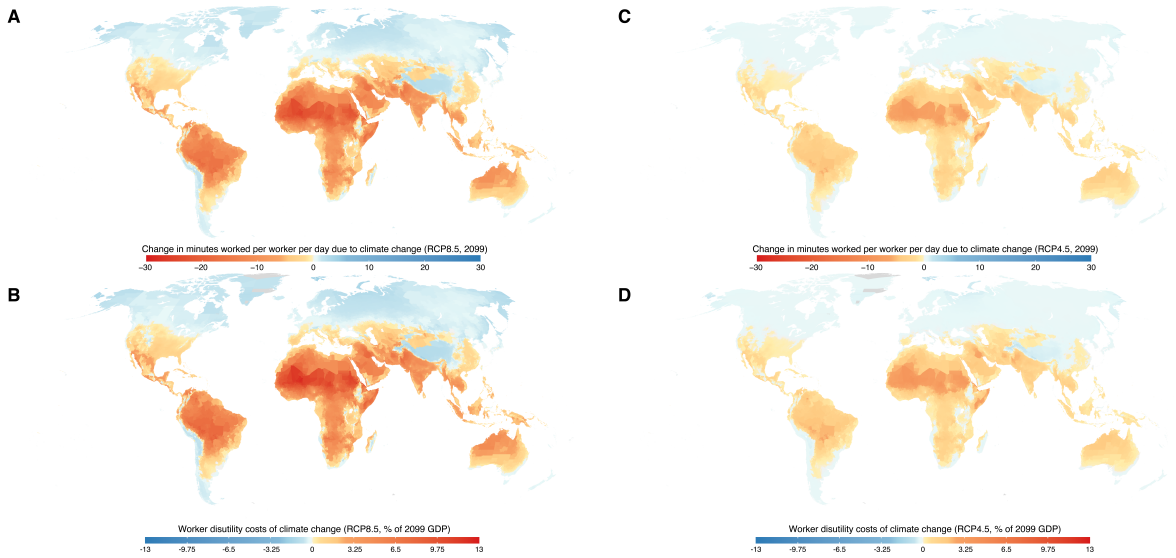

Figure F.1: Projected impact of climate change on labor supply and disutility at 2099, by emissions scenario. Panels A and C map the labor supply impacts of climate change in the year 2099 (minutes per worker per day) under a very high emissions scenario (RCP8.5) and an intermediate scenario (RCP4.5) respectively, across 24,378 impact regions. Panel B and D map the annual worker disutility costs of climate change in the year 2099, under a very high emissions scenario (RCP8.5) and an intermediate scenario (RCP4.5) respectively. Costs are calculated based on Equation F.1 with a labor share of income = 0.6 (Karabarbounis and Neiman, 2014) and elasticity of labor supply = 0.5 (Chetty et al., 2011), and are expressed as a percentage of each impact region's 2099 GDP. Estimates account for changes to workforce composition as incomes grow and the climate warms, and the maps show the climate model weighted mean estimate across Monte Carlo simulations conducted on 33 climate models. All values shown refer to the SSP3 socioeconomic scenario.

[100] Figure F.1, Panels A and B, respectively reproduce main text Figure 6, Panels A and B

G Heterogeneous labor supply-temperature responses within risk groups

In this appendix, we estimate a model in which the effect of temperature on labor supply can differ both across high-risk and low-risk workers as well as within each risk group. We then apply this model as a robustness check when estimating the hedonic value of thermal comfort offered by a low risk job and projecting the impacts of climate change on worker disutility.

G.1 Within-risk group differences in labor supply-temperature responses

Equation 6 in the main text allows the effect of temperature on labor supply to differ for high- and low-risk workers. Here we also allow the effect to vary across workers within the same risk group, allowing for the possibility that location-specific characteristics may influence the temperature sensitivity of each risk group's labor supply. Specifically, we estimate a richer version of main text Equation 6 that includes interactions of the nonlinear temperature response functions for each risk group with location-specific measures of income per capita and climate:[101]

$$Labor_{i,r,j,t} = f_r(\boldsymbol{T}_{j,t}, LogGDPpc_u, TMEAN_u) + g_r(\boldsymbol{P}_{j,t}) + \lambda_r \boldsymbol{X}_i + \alpha_{j,r} + \psi_{k,y,r} + \delta_{k,w,r} + \phi_{d,r} + \epsilon_{i,j,r,t}. \tag{G.1}$$

In Equation G.1, the labor supply-temperature response function for risk group r, $f_r(\cdot)$, depends on $TMEAN_u$, the sample period average annual daily maximum temperature in location u, and the natural logarithm of $GDPpc_u$, the sample period average of annual GDP per capita in location u. Importantly, the spatial units u for which we define these variables differ by country, because the surveys from which we obtain labor supply vary in the geographical resolution at which they are representative of the population. For the United States, the United Kingdom, and France, surveys are only representative at the national level. We therefore use national level measures of average income per capita and average annual temperature for these countries. For all other countries, surveys are representative at the ADM1 level, and we use ADM1 level measures of average income per capita and average annual temperature. To estimate Equation G.1, we interact $TMEAN$

[101] Income and long-run climate are widely used in the climate-economy literature to model heterogenous responses to temperature (Auffhammer and Aroonruengsawat, 2011; Carleton et al., 2022; Davis and Gertler, 2015; Heutel, Miller, and Molitor, 2021; Hsiang, Meng, and Cane, 2011; Moore and Lobell, 2014; Rode et al., 2021). A practical reason to focus on these two explanatory variables is that credible, global projections of their future evolution are readily available and can be used to predict the temperature sensitivity of labor supply across locations in the future.

and $LogGDPpc$ with each of the elements of the temperature vector $\boldsymbol{T}_{j,t}$, which contains terms of the three-knot restricted cubic spline.[102]

When estimating Equation G.1, we model the labor supply-temperature relationship as a restricted cubic spline in daily maximum temperature with knots at 27° C, 37° C, and 39° C. Table G.1 reports on some key features of the results, with each value representing the change in the temperature-sensitivity of labor supply associated with a marginal increase in the relevant covariate (i.e., $LogGDPpc$ or $TMEAN$), evaluated at the daily maximum temperature shown. All temperature sensitivities are shown relative to a day with a maximum temperature of 27° C. For example, a doubling of per capita income is associated with a lower sensitivity of high-risk labor supply to both cold temperatures (14.6 fewer lost weekly minutes per high-risk worker on a -10°C day), and to hot temperatures (7.0 fewer lost weekly minutes per high-risk worker on a 40°C day).[103] For climate, a 10° C increase in annual average daily maximum temperature is associated with a lower sensitivity of high-risk labor supply to cold temperatures (4 fewer lost weekly minutes per high-risk worker on a -10°C day) and to hot temperatures (14 fewer lost weekly minutes per high-risk worker on a 40°C day). Neither income nor climate are associated with substantial differences in the temperature sensitivity of low-risk labor supply.

Table G.1 does not provide clear evidence of within risk group heterogeneity that can robustly be statistically isolated, as the estimates are not found to be statistically significant by coventional criteria. In particular, we fail to reject that the labor supply-temperature response of low-risk workers differs by income or annual average temperature ($p = 59.0\%$ and 51.6%, respectively). We also fail to reject that the labor supply-temperature response of high-risk workers differs by annual average temperature ($p = 22.1\%$). The only borderline statistically significant difference is that high risk workers' labor supply responses to temperature vary with income ($p = 16.0\%$). In particular, the results in Table G.1 suggest that the labor supply losses from extreme temperatures may be mitigated in higher income locations.[104] To account for the possibility that this

[102]The exact form of the function $f_r(\boldsymbol{T}_{j,t}, LogGDPpc_u, TMEAN_u)$ is: $\boldsymbol{\beta}_r \cdot \boldsymbol{T}_{j,t} + \boldsymbol{\gamma}_{1,r} \cdot \boldsymbol{T}_{j,t} \cdot LogGDPpc_u + \boldsymbol{\gamma}_{2,r} \cdot \boldsymbol{T}_{j,t} \cdot TMEAN_u$, where $\boldsymbol{\beta}_r$ denotes the vector of coefficients on the uninteracted elements of the temperature vector $\boldsymbol{T}_{j,t}$, and $\boldsymbol{\gamma}_{1,r}$ and $\boldsymbol{\gamma}_{2,r}$ denote the vectors of coefficients on the elements of $\boldsymbol{T}_{j,t}$ interacted with $LogGDPpc_u$ and $TMEAN_u$, respectively. Note that there are no uninteracted terms for $LogGDPpc_u$ and $TMEAN_u$ because they would be collinear with the fixed effects. When estimating Equation G.1, observations within each country are weighted by the sample weights specified in that country's survey, while across countries, observations are weighted such that each representative spatial unit $u \times$ year carries equal weight. Unlike in Equation 6, we do not use populations weights because we are explicitly modeling heterogeneity in treatment effects rather than integrating over it.

[103]Because our covariates are linearly interacted with the full vector of temperature variables describing the nonlinear labor supply-temperature response, the effect of each covariate depends on the realized daily temperature.

[104]We also probed these results further by estimating separate responses by 4 subsamples of income *times* climate (above and below sample median income × above and below sample median annual average temperature), and the pattern of income-based heterogeneity in the high-risk response remains the same as in Table G.1. In contrast, while Table G.1 show some (imprecisely estimated) evidence that warmer locations suffer more high-risk labor supply losses on hot days, this pattern does not hold in the

Daily maximum temperature	Low-risk workers		High-risk workers	
	$LogGDPpc$	$TMEAN$	$LogGDPpc$	$TMEAN$
45°	2.3	0.3	15.6	-2.7
	(9.7)	(1.5)	(9.0)	(1.5)
40°	0.4	0.3	7.0	-1.4
	(4.9)	(0.8)	(4.6)	(0.8)
35°	-1.1	0.2	-0.1	-0.3
	(1.4)	(0.3)	(1.8)	(0.3)
27°	-	-	-	-
	-	-	-	-
10°	4.2	-0.6	6.7	-0.2
	(3.6)	(0.6)	(5.2)	(0.8)
5°	5.4	-0.8	8.7	-0.3
	(4.7)	(0.8)	(6.8)	(1.0)
0°	6.6	-1.0	10.7	-0.3
	(5.7)	(1.0)	(8.3)	(1.2)
-5°	7.8	-1.2	12.6	-0.4
	(6.8)	(1.2)	(9.9)	(1.5)
-10°	9.0	-1.3	14.6	-0.4
	(7.9)	(1.3)	(11.4)	(1.7)
Overall significance	$p = 59.0\%$	$p = 51.6\%$	$p = 16.0\%$	$p = 22.1\%$
Adj R-squared	0.33	0.33	0.33	0.33
N	4,175,377	4,175,377	2,423,958	2,423,958

Table G.1: Marginal effect of covariates on temperature sensitivity of labor supply. Estimates (standard errors) from Equation G.1 represent the marginal effect of increasing each covariate by one unit on the temperature sensitivity of labor supply, evaluated at each of the shown daily maximum temperatures. Temperature sensitivity is defined as the impact of a particular temperature on weekly labor supply, relative to a day with a maximum temperature of 27°C. The covariate $LogGDPpc$ is the logarithm of the average annual GDP per capita over the sample period, measured in constant 2005 dollars PPP, while the covariate $TMEAN$ is defined as the average annual daily maximum temperature over the sample period. All response functions are estimated jointly in a stacked regression model that is fully saturated with risk-group specific fixed effects. Regression is a restricted cubic spline in daily maximum temperature with knots at 27° C, 37° C, and 39° C; each term of the spline is interacted with each covariate.

result recovers true heterogeneity in the labor supply-temperature relationship, we conduct a robustness test where we estimate a modified version of Equation G.1, in which the labor supply-temperature response for low-risk workers does not differ by income or annual average temperature, while the response for high-risk workers differs by income only. Specifically, this modified estimating equation only includes interactions of the nonlinear temperature response function for high-risk workers with a location-specific measure of income per capita:

$$\begin{aligned} Labor_{i,r,j,t} = f_r(\boldsymbol{T}_{j,t}, LogGDPpc_u) * [\boldsymbol{I}_{r=high}] + f_r(\boldsymbol{T}_{j,t}) * [\boldsymbol{I}_{r=low}] \\ + g_r(\boldsymbol{P}_{j,t}) + \lambda_r \boldsymbol{X}_i + \alpha_{j,r} + \psi_{k,y,r} + \delta_{k,w,r} + \phi_{d,r} + \epsilon_{i,j,r,t}. \end{aligned} \tag{G.2}$$

The variables $\boldsymbol{I}_{r=high}$ and $\boldsymbol{I}_{r=low}$ are indicator variables for whether worker i is in the high or low risk group, respectively. Reflecting results in Table G.1, Equation G.2 does not include interactions of the high-risk response function with climate, or interactions of the low-risk response function with income or climate.

Figure G.1 presents the reponse functions for high-risk workers obtained from estimating Equation G.2.[105] Each panel displays a predicted high-risk labor supply-temperature response function evaluated at a particular point in the income space within the estimation sample. Response functions are ordered by *LogGDPpc* terciles of the estimation sample (increasingly rich from left to right), with each evaluated at the mean value of *LogGDPpc* within its respective tercile. The histograms at the bottom of each panel reveal the distribution of daily maximum temperatures in the relevant income tercile, with the inner pair of vertical lines indicating the 5^{th} and 95^{th} percentiles and the outer pair indicating 1^{st} and 99^{th} percentiles. Because the low-risk response function is not interacted with income or climate, it remains identical to the one estimated using the main text Equation 6 and displayed in main text Figure 3B.

Table G.2 reports on some key features of the high-risk response functions in Figure G.1, with each value representing the change in the temperature-sensitivity of labor supply associated with a marginal increase in *LogGDPpc*, evaluated at the daily maximum temperature shown. Although not statistically significant by conventional standards, we find evidence that higher incomes afford protection from labor supply losses at extreme temperatures, with a doubling of income associated with 15.7 fewer lost weekly minutes per high-risk worker on a -10°C day, and 7.3 fewer lost minutes on a 40°C day. These effects are similar in magnitude to those estimated from Equation G.1.

subsampled responses. We therefore, focus on heterogeneity in the high-risk response by income.

[105] Temperature is modeled with a restricted cubic spline in daily maximum temperature with knots at 27° C, 37° C, and 39° C.

Daily maximum temperature	High-risk workers
	LogGDPpc
45°	16.4
	(9.1)
40°	7.3
	(4.6)
35°	-0.2
	(1.8)
27°	-
	-
10°	7.2
	(5.3)
5°	9.3
	(6.9)
0°	11.4
	(8.4)
-5°	13.6
	(10.0)
-10°	15.7
	(11.5)
Overall significance	$p = 11.6\%$
Adj R-squared	0.33
N	2,423,958

Table G.2: Marginal effect of covariates on temperature sensitivity of labor supply. Estimates (standard errors) from Equation G.2 represent the marginal effect of increasing *LogGDPpc* by one unit on the temperature sensitivity of high-risk labor supply, evaluated at each of the shown daily maximum temperatures. Temperature sensitivity is defined as the impact of a particular temperature on weekly labor supply, relative to a day with a maximum temperature of 27°C. *LogGDPpc* is the logarithm of the average annual GDP per capita over the sample period, measured in constant 2005 dollars PPP. Response functions for high- and low-risk workers are estimated jointly in a stacked regression model that is fully saturated with risk-group specific fixed effects. Regression is a restricted cubic spline in daily maximum temperature with knots at 27° C, 37° C, and 39° C; each term of the spline is interacted with *LogGDPpc* for high-risk workers.

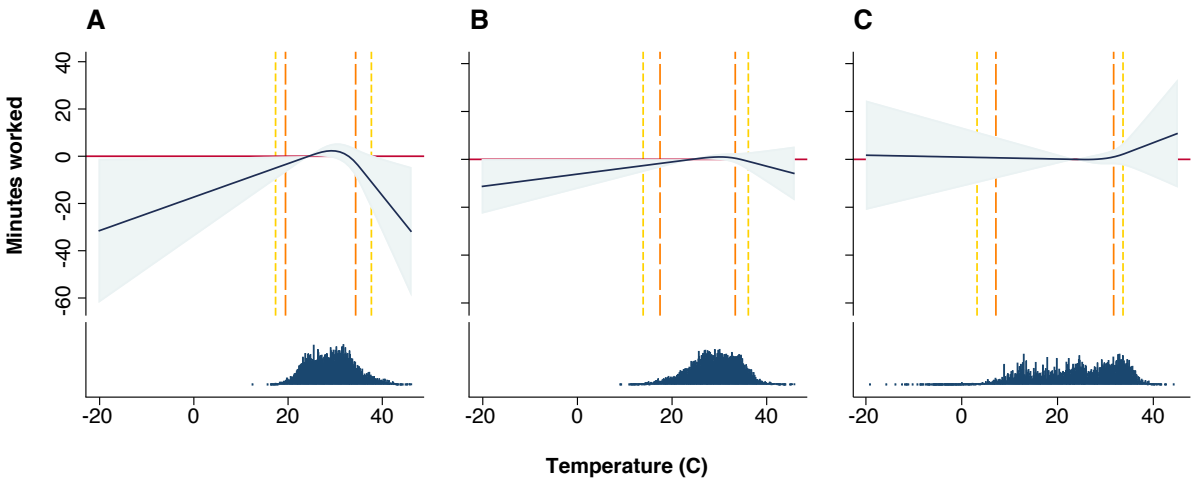

Figure G.1: Changes in weekly minutes worked per high-risk worker due to daily temperature, as a function of income. Labor supply-temperature response functions are estimated for high-risk workers as a function of income (Equation G.2). Each panel shows a predicted response function for an in-sample income tercile (increasing income from left to right). Points along each curve represent the effect on weekly labor supply of a single day at the daily maximum temperature value shown on the x-axis, relative to a day with a maximum temperature of 27°C (81°F). Shaded areas indicate 95% confidence intervals. Histograms show the distribution of daily maximum temperatures in each income tercile, with the inner pair of vertical lines indicating the 5^{th} and 95^{th} percentiles and the outer pair indicating 1^{st} and 99^{th} percentiles.

G.2 Hedonic value of thermal comfort accounting for within-risk group differences in labor supply-temperature responses

We use the estimates from Equation G.2 to calculate the hedonic value of thermal comfort offered by a low-risk job, allowing for the labor supply response of high-risk workers to vary with a region's income, but keeping the low-risk response constant as in main text Figure 3B. As in main text Section V.B, the hedonic value will vary by location because because locations vary in their distribution of the differences between daily temperatures and T_{opt} over the year. However, here there exists an additional source of variation across locations— the mitigated labor supply losses from extreme temperatures in higher income locations (as seen in Figure G.1 and Table G.2) reveal that the value of temperature-induced disutility in a high-risk job relative to a low-risk job would be lower in richer locations compared to poorer locations.

Following the general approach in main text Equation 9, we thus calculate the hedonic value of thermal comfort in a low-risk job in impact region c as:

$$\frac{\omega_c}{\epsilon}\sum_t\left(\left[\widehat{f}_{high}(\overline{\boldsymbol{T}}_{c,t,y}, LogGDPpc_{c,y}) - \widehat{f}_{high}(\boldsymbol{T}_{opt}^{high}(LogGDPpc_{c,y}), LogGDPpc_{c,y})\right] - \left[\widehat{f}_{low}(\overline{\boldsymbol{T}}_{c,t,y}) - \widehat{f}_{low}(\boldsymbol{T}_{opt}^{low})\right]\right), \tag{G.3}$$

where $\overline{\boldsymbol{T}}_{c,t}$ represents region c's 1950-2010 average temperature vector for each calendar date t, $LogGDPpc_c$ represents region c's 2010 log GDP per capita, and $\hat{f}_r(\cdot)$ represents

the fitted values from Equation G.2 for each of the two risk groups r.[106] In calculating Equation G.3, we use the empirically determined optimum temperatures for low- and high-risk labor supply. While $T_{opt}^{low} = 29.3°C$, T_{opt}^{high} varies by income and ranges between $28.4°C$ and $31.7°C$.[107] As in main text Equation 9, we construct a wage rate for each impact region (ω_c) based on its average per capita income in 2010 and use a Frisch elasticity (ϵ) of 0.5.

To implement Equation G.3, we impose a constraint on the income-varying high-risk responses to ensure that higher income does not mitigate any region's high-risk response to be less than the low-risk response. Specifically, we impose that at any given daily maximum temperature, the labor supply losses (relative to a day at $T_{opt}^{high}(LogGDPpc_{c,y})$) of a high-risk worker cannot be smaller than those of a low-risk worker (relative to a day at T_{opt}^{low}). In other words, we assume that temperatures farther from the optimum (either colder or hotter) must be at least as harmful to high-risk workers as they are to low-risk workers.[108] To operationalize this, we calculate impacts along an adjusted high-risk response function that is defined at each temperature as the minimum of the region- and year-specific high-risk response function and the low-risk response.[109]

Under this model, we find that the hedonic value of thermal comfort in a low-risk job amounts to 1.8% of annual income in 2010. This is roughly 40% less than hedonic value based on estimates from main text Equation G.3, where we find the hedonic value of thermal comfort to be worth 2.9% of annual income (main text Table 4). However, both estimates have wide and overlapping 5^{th} to 95^{th} percentile ranges (0.3% to 3.3% for the 1.8% estimate and -0.9% to 6.2% for the 2.9% estimate).

G.3 Impacts of climate change accounting for within-risk group differences in labor supply-temperature responses

We use the estimates from Equation G.2 to project the impacts of climate change, allowing for the labor supply response of high-risk workers to evolve into the future as regional incomes rise, but keeping the low-risk response constant as in main text Figure 3B. In this case, the labor supply impact of climate change is defined as:

[106] Note that for the low risk group, this fitted value is the same as the one from main text Equation 6.

[107] The vectors $\boldsymbol{T}_{opt}^{low}$) and $\boldsymbol{T}_{opt}^{high}(LogGDPpc_{c,y})$ contain the nonlinear transformations of these optimal temperatures.

[108] This assumption is important because Equation G.2 parameterizes the flattening of the inverted U-shaped high-risk response function such that, with sufficiently high income, it could become flatter than the low-risk response function, and even go so far as to take on a U-shape such that labor supply *increases* due to extreme temperature days. However, such behavior is inconsistent with prior literature documenting that high-risk workers experience greater labor supply losses on extreme temperature days than low-risk workers (Garg, Gibson, and Sun, 2019; Graff Zivin and Neidell, 2014).

[109] Specifically, we take the minimum of high-risk and low-risk response function, where each function is defined relative to its optimum. To accommodate this procedure when characterize uncertainty in Equation G.3 estimates, we construct confidence intervals by resampling parameters of the labor supply-temperature response functions.

$$
\begin{aligned}
&\textit{Labor Supply Impact Of Climate Change}_{c,t,y} = \\
&\underbrace{\Big[\widehat{\rho}_{c,y}\widehat{f}_{high}(\boldsymbol{T}_{c,t,y}, LogGDPpc_{c,y}) + (1-\widehat{\rho}_{c,y})\widehat{f}_{low}(\boldsymbol{T}_{c,t,y})\Big]}_{\substack{\text{Temperature-induced labor supply under climate change} \\ \text{(with economic development and climate-driven adaptation)}}} \\
&-\underbrace{\Big[\widehat{\rho}_{c,\widetilde{y}}\widehat{f}_{high}(\boldsymbol{T}_{c,t,2015}, LogGDPpc_{c,y}) + (1-\widehat{\rho}_{c,\widetilde{y}})\widehat{f}_{low}(\boldsymbol{T}_{c,t,2015})\Big]}_{\substack{\text{Temperature-induced labor supply without climate change} \\ \text{(with economic development)}}}, \qquad \text{(G.4)}
\end{aligned}
$$

where $\widehat{f}_r(\cdot)$ represents the fitted values from Equation G.2 for each of the two risk groups r.[110] As in the impact calculated in main text Equation 11, each impact region's share of high-risk workers is allowed to evolve as incomes grow and the climate warms. However, in contrast to main text Equation 11, the high-risk response $\widehat{f}_{high}(\cdot)$ is also allowed to evolve based on the value of log GDP per capita in impact region c and year y. The disutility costs of climate change are then calculated by multiplying the labor supply impact by the ratio of the impact region's projected wage rate and the Frisch elasticity of labor supply.

In implementing this projection, we impose a constraint on the evolution of high-risk responses to ensure plausible out-of-sample projections over the 21^{st} century. Specifically, we impose that at any given daily maximum temperature, the labor supply losses (relative to a day at 27° C) of a high-risk worker cannot be smaller than those of a low-risk worker. In other words, we assume that temperatures farther from 27° C (either colder or hotter) must be at least as harmful to high-risk workers as they are to low-risk workers.[111] To operationalize this, we calculate impacts along an adjusted high-risk response function that is defined at each temperature (relative to 27° C) as the minimum of the region- and year-specific high-risk response function and the low-risk response shown in main text Figure 3B.

Under this projection, we project that by 2099, the global disutility costs of climate change under RCP8.5 will amount to roughly 0.7% of 2099 global GDP (Figure G.2). This is slightly less than half of the projected costs based on estimates from main text Equation 6, where we projected global disutility costs at 2099 equal to 1.8% of 2099 global GDP (main text Figure 8A, green line).[112] However, both estimates have wide 5^{th} to 95^{th} percentile ranges with considerable overlap (-0.3% to 2.5% for the 0.7% estimate and 0.2%

[110] Note that for the low risk group, this fitted value is the same as the one from main text Equation 6.

[111] This assumption is important because Equation G.2 parameterizes the flattening of the inverted U-shaped high-risk response function such that, with sufficiently high income, it could become flatter than the low-risk response function, and even go so far as to take on a U-shape such that labor supply *increases* due to extreme temperature days. However, such behavior is inconsistent with prior literature documenting that high-risk workers experience greater labor supply losses on extreme temperature days than low-risk workers (Garg, Gibson, and Sun, 2019; Graff Zivin and Neidell, 2014).

[112] Similarly, the end-of-century disutility costs of climate change under RCP4.5 reduce from 0.5% to 0.2% of 2099 global GDP, with 5^{th} to 95^{th} percentile ranges 0.0% to 1.3% and -0.1% to 0.7%, respectively.

to 5.1% for the 1.8% estimate). Main text Table 6 also reports labor disutility partial SCC estimates based on disutility costs projected in Equation G.4. Allowing for heterogenous high-risk responses as a function of income roughly halves the SCC estimates, although the uncertainty ranges in both cases are wide and substantially overlapping.

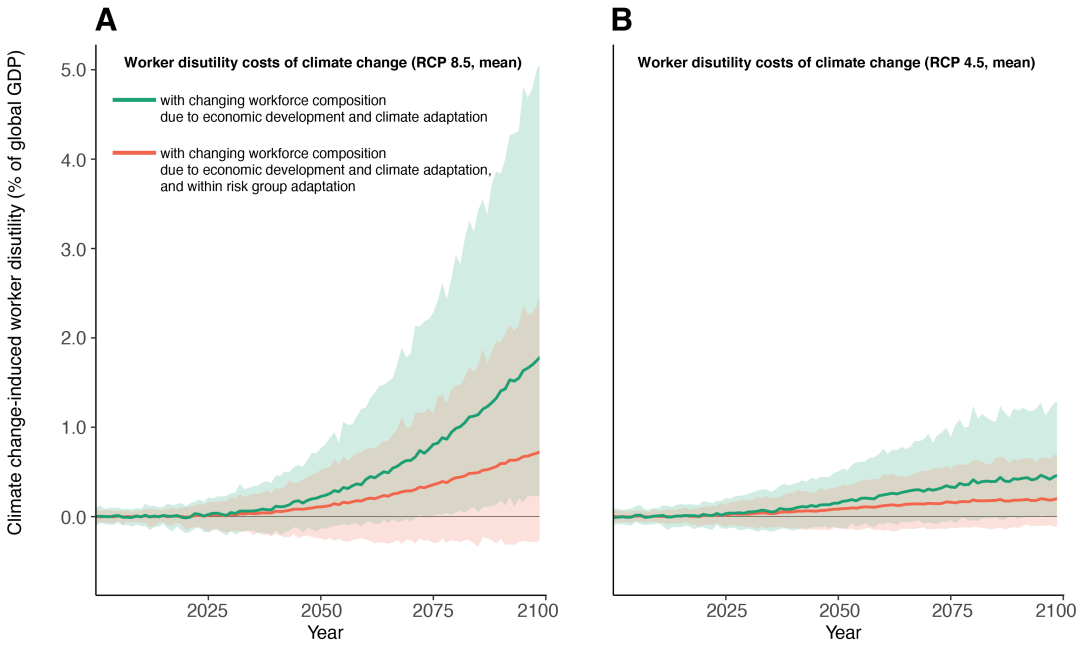

Figure G.2: Time series of projected climate change-induced worker disutility costs, accounting for within risk group adaptation. Costs in each year are calculated under a labor share of income = 0.6 (Karabarbounis and Neiman, 2014) and elasticity of labor supply = 0.5 (Chetty et al., 2011) and are expressed as a percentage of that year's global GDP. All estimates refer to the SSP3 socioeconomic scenario. Panels A and B respectively show globally aggregated worker disutility costs of climate change under the RCP 8.5 and RCP4.5 emissions scenarios. In each panel, the green line shows estimates that account for changes in each impact region's workforce composition as incomes grow and the climate warms (main text Equation 11), while the orange line additionally accounts for changes in the temperature sensitivity of high-risk labor supply as incomes grow (Equation G.4). Lines represent a mean estimate across a set of Monte Carlo simulations accounting for both climate model and statistical uncertainty; shaded areas indicate the range between 10^{th} and 90^{th} percentiles.

H Calculation of a labor disutility partial social cost of carbon

We compute the labor disutility costs imposed by a marginal ton of CO_2 in two key steps. First, we construct "damage functions" (Hsiang et al., 2017; Nordhaus, 1992), which describe labor disutility costs as a function of the change in the global climate. Second, we use a climate-carbon cycle model to simulate future warming trajectories that result from the marginal emission today, which we combine with estimated damage functions to calculate the temporal trajectory of global costs. The present discounted value of these costs represents the labor disutility component of the SCC. Both steps of this process involve uncertainty, deriving both from econometric uncertainty in the labor disutility costs imposed by a given level of climate change, as well as from physical uncertainty in the sensitivity of the global climate to greenhouse gas emissions. We quantify the uncertainty from both these sources, as well as value its contribution to the partial SCC when individuals are risk averse. In this Appendix, we describe these two steps and our treatment of uncertainty, and then present ranges of partial SCC estimates that decompose uncertainty into its component parts. Lastly, we present partial SCC estimates under alternative baseline socioeconomic scenarios. We note that the methodology used here is nearly identical to that developed and described in Rode et al. (2021) and Carleton et al. (2022); for further methodological details, we refer the reader to these prior publications.

H.1 Constructing damage functions for labor disutility

We construct empirical damage functions that express global labor disutility costs of climate change as a function of the change in global mean surface temperature relative to the 2001-2010 average level (ΔGMST). Damage functions through 2099 are built from projections of global disutility costs (D_{ylps}) in each year (y) using 33 climate models (l), two emissions scenarios (p), and a resampling of estimates (s) that captures uncertainty in the estimation of Equations 6 and 10. These multiple projections lead to an empirically-derived distribution of potential outcomes that are conditional on the ΔGMST value for the year, climate model, and emissions scenario used to generate that projection. Using these outcomes and their associated ΔGMST values, we separately estimate a quadratic damage function in each year, as follows:

$$D(\Delta GMST, y)_{ylps} = \psi_1^y \Delta GMST_{ylp} + \psi_2^y \Delta GMST_{ylp}^2 + \varepsilon_{ylps}, \tag{H.1}$$

using all simulations within a 5-year window of year y, thereby allowing the shape of the function $D(\Delta GMST, y)$ to evolve flexibly and smoothly over the century. Such time-varying damage functions are estimated in order to account for changes over time in the underlying global population distribution and workforce composition, which shape the

sensitivity of labor supply to temperature (Carleton et al., 2022; Rode et al., 2021).

Figure H.1A illustrates this exercise for for $y = 2097$, with D_{ylps} values from all Monte Carlo simulations shown as points situated along the horizontal axis based on their corresponding $\Delta GMST_{ylp}$. This scatterplot includes realizations under RCP4.5 and RCP8.5 scenarios over the years 2095-2099, for all projections in our 33-member ensemble. The median end-of-century warming relative to 2001-2010 under RCP8.5 (red points) across our climate models is +3.7°C, while under RCP4.5 (blue points) it is +1.6°C. The black line is the quadratic damage function estimated for the year 2097, the latest year for which a full 5-year window of damage estimates can be constructed. We recover a convex damage function, indicating that the marginal disutility costs of warming increase with ΔGMST.

Analogous curves are constructed for all years, 2015 to 2099. To obtain damage functions for the year 2100 onwards, years for which high-resolution climate and socioeconomic projections are not available, we extrapolate the estimated coefficients of the 2099 damage function at the annual growth rate of GDP per capita from 2098 to 2099.[113] The resulting damage functions are shown in Figure H.1B, where damage functions in later years are shown to be steeper than those in earlier years, reflecting trends in income and population.

H.2 Computing damages from a marginal carbon dioxide emissions pulse

The partial SCC at year y_0 is defined as the marginal social cost from increased labor disutility imposed by the emission of a marginal ton of CO_2 at y_0, holding all other factors fixed, including the forecast trajectory of baseline greenhouse gas emissions.[114] Formally, for a discount rate δ, this is expressed as:

$$Partial\ SCC_{y_0} = \sum_{y_0}^{2300} e^{-\delta y} \frac{d\hat{D}(\Delta GMST, y)}{d\Delta GMSTy} \frac{d\widehat{\Delta GMST}_y}{dCO2_{y_0}}. \tag{H.2}$$

The values $\frac{d\hat{D}(\Delta GMST,y)}{d\Delta GMST_y}$ are the marginal damages at each year that occur as a result of the small change in future global temperatures caused by the marginal emission.[115] They are computed using the differentiable damage functions described in Equation H.1. The

[113]Specifically, for $y > 2100$ and $k \in \{1, 2\}$, $\widehat{\psi}_k^y = \widehat{\psi}_k^{2099} * (1 + g)^{(y-2099)}$, where g denotes the growth rate of GDP per capita from 2098 to 2099 under a given socioeconomic scenario.

[114]We use CO_2 to represent changes in all global greenhouse gas (GHG) emissions as it is the most abundant GHG and the warming potential of all other GHGs are generally reported in terms of their CO_2 equivalence.

[115]We assume that discounted damages from an emissions pulse at $y_0 = 2020$ become negligible after 2300.

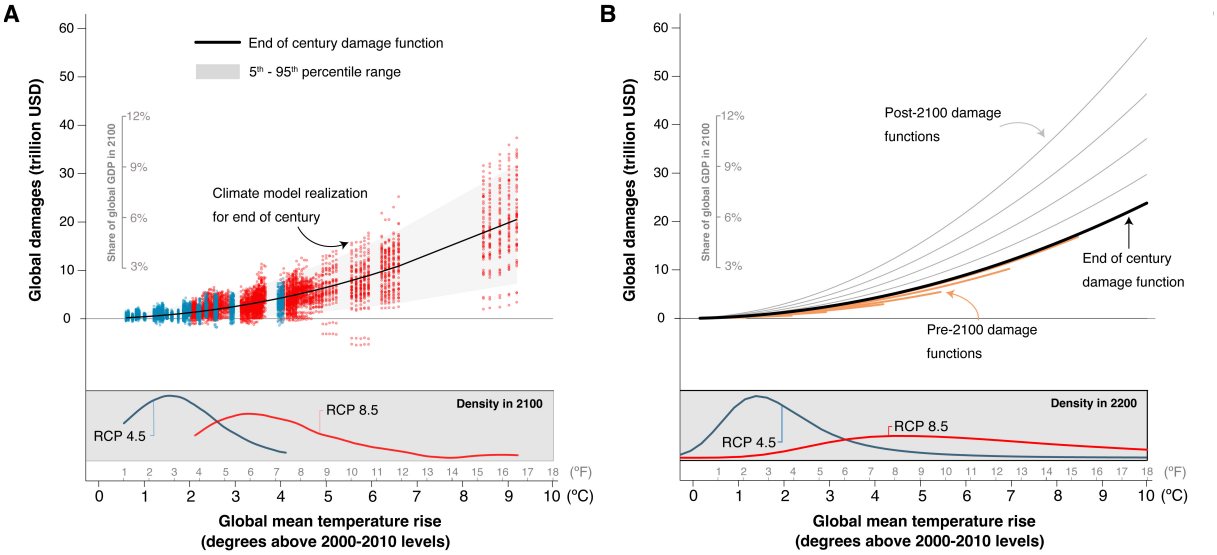

Figure H.1: Global labor disutility damages. The damage function in Panel **A** relates empirically-derived total global labor disutility damages to anomalies in global mean surface temperature (ΔGMST) at end-of-century. Each point (red = RCP8.5, blue = RCP4.5) indicates the global labor disutility costs of climate change in a single year (ranging from 2095 to 2099) for a single simulation of a single climate model, accounting for changes to workforce composition as incomes grow and the climate warms. The black line represents the end-of-century quadratic damage function, which is estimated through the points shown. Shaded areas indicate the range between 5^{th} and 95^{th} quantiles. Damage functions that evolve over time (Panel **B**) are estimated up to 2100, and their continuing evolution extrapolated forward to 2300 at the annual growth rate of GDP per capita from 2098 to 2099. Orange curves depict damage functions for every 10 years pre-2100; the black curve depicts the end-of-century damage function; grey curves depict damage functions for every 50 years post-2100. Probability density functions below display the distribution of GMST anomalies at 2100 (Panel **A**) and 2200 (Panel **B**) in each emissions scenario across our 33 climate models. Damages are calculated under a labor share of income = 0.6 (Karabarbounis and Neiman, 2014) and elasticity of labor supply = 0.5 (Chetty et al., 2011). All values refer to the SSP3 socioeconomic scenario.

term $\frac{d\widehat{\Delta GMST_y}}{dCO2_{y_0}}$ is the increase in ΔGMST that occurs at each year along a baseline climate trajectory as a result of a marginal unit of emissions at y_0, which we approximate with an "infinitesimally small" pulse of CO_2 emissions occurring at year $y_0 = 2020$.

Estimating $\frac{d\widehat{\Delta GMST_y}}{dCO2_{y_0}}$ requires a climate model capable of estimating the global temperature response in each year to a single pulse of CO_2 emissions. We adopt a version of the Finite Amplitude Impulse Response (FAIR) simple climate model that has been developed especially for this type of calculation (Millar et al., 2017; Smith et al., 2018). Specifically, we use FAIR to calculate $\Delta GMST_y$ trajectories for emissions scenarios RCP4.5 and RCP8.5, both with and without an exogenous impulse of 1Gt C (equivalent to 3.66Gt CO2) in the year 2020, an approximation of an infinitesimal emission for which the model numerics are stable (Carleton et al., 2022; Rode et al., 2021). In FAIR, this emissions impulse perturbs the trajectory of atmospheric CO_2 concentrations and $\Delta GMST_y$ for 2020-2300, with dynamics that are influenced by the baseline RCP scenario. In each scenario, the trajectory of $\Delta GMST_y$ in the "RCP + pulse" simulation is differenced from the baseline RCP simulation to compute $\frac{d\widehat{\Delta GMST_y}}{dCO2_{y_0}}$, and the resulting damages are converted

into USD per 1t CO_2. Details on our use of FAIR are provided in Carleton et al. (2022) and Rode et al. (2021). Figure 9D plots the discounted (2% discount rate) stream of labor disutility damages in future years due to the marginal pulse of emissions today, using the median values of FAIR's four key parameter distributions and the mean global damage function. The shaded area represents the inter-quartile range of each years damages, reflecting uncertainty in the climate system as well as uncertainty in the damage function, as detailed in the next section.

H.3 Accounting for uncertainty and its value in the partial SCC for labor disutility

We compute labor disutility partial SCCs accounting for both damage function uncertainty and uncertainty over climate sensitivity. Here, we briefly describe our implementation of uncertainty in the SCC calculation, as well as our approach to valuing uncertainty in the SCC when individuals are risk averse.

H.3.1 Labor disutility partial SCC estimates accounting for both damage function and climate sensitivity uncertainty

As described in Section H.1, damage functions are computed using estimates of the global monetized damages in each year generated from 33 climate models, two emissions scenarios, and a resampling of damage estimates that captures uncertainty in the estimation of Equations 6 and 10. These multiple simulations (we draw 15 realizations of global damages for each climate model, emissions scenario, SSP trajectory, and year) give us an empirically-derived distribution of potential economic outcomes that are conditional on the ΔGMST value for the year, emissions scenario, and climate model used to generate that projection. To account for uncertainty in a single year's damage function, we pool these realizations for the associated 5-year window (see Section H.1). We then run quantile regressions to fit quantile-specific damage functions for 19 quantiles (i.e., every 5^{th} percentile from the 5^{th} to 95^{th}). As in the mean damage function estimation, damage function quantiles for years after 2099 are obtained by extrapolation; estimated coefficients of each 2099 damage function quantile are extrapolated at the annual growth rate of GDP per capita from 2098 to 2099.

We run each quantile-specific damage function through each of $\sim$100,000 sets of distinct parameter combinations in the FAIR climate-carbon cycle model; these parameter combinations together represent uncertainty in the climate's sensitivity to carbon emissions (Carleton et al., 2022; Rode et al., 2021).[116] We then report moments (e.g., 1^{st}-99^{th}

[116]The sets of FAIR parameter combinations are identical to Rode et al. (2021) and Carleton et al. (2022), except we apply an additional constraint here to rule out simulations with unrealistically high equilibrium climate sensitivity (ECS) that yield unrealistic future temperature changes. Specifically,

percentile ranges) of the resulting distribution of partial SCC estimates, up-weighting runs in order to reflect probability mass in the damage function uncertainty space. This process reflects a joint sampling from the full space of damage function uncertainty and climate sensitivity uncertainty.

In Table H.1, we isolate uncertainty in the labor disutility partial SCC that arises from uncertainty in the damage function versus that arising from uncertainty in climate sensitivity. To isolate uncertainty arising from the damage function, we run the set of quantile-year damage functions through FAIR with each climate parameter fixed at its median value and up-weight runs in order to reflect probability mass in the damage function uncertainty space. The corresponding SCC 1^{st}-99^{th} percentile range is resolved from the resulting distribution of labor disutility partial SCCs. To isolate uncertainty in the labor disutility partial SCC that arises from climate sensitivity uncertainty, we run the mean damage function through each of the ∼100,000 sets of FAIR parameters. The corresponding SCC 1^{st}-99^{th} percentile range is resolved from the resulting distribution of energy partial SCCs.

H.3.2 Calculating a certainty equivalent partial SCC for labor disutility

Here we demonstrate how we incorporate damage function and climate sensitivity uncertainty into the calculation of a "certainty equivalent" partial SCC for labor disutility, accounting for the fact that individuals are risk averse and therefore value reducing uncertainty. This takes place in two steps. First we calculate "certainty equivalent" global damage functions for labor disutility that reflect uncertainty within each of the 24,378 impact regions for which we project damages. Second, we use these damage functions to calculate a certainty equivalent partial SCC, using the distribution of parameters in the climate model FAIR to value the uncertainty in the sensitivity of the global climate to additional emissions.

Certainty equivalent global damage functions for labor disutility The building blocks of a certainty equivalent global damage function are projections of labor disutility costs in each of 24,378 impact regions under each of 33 climate models and two emissions scenarios. As discussed above, these projections are resampled to capture uncertainty in the estimation of Equations 6 and 10 and are denoted D_{cylps} for impact region c, year y, climate model l, emissions scenario p, and resampling s.

In the absence of climate change, individual consumption in impact region c in future year y is defined to be equal to GDP per capita ($GDPpc_{cy}$) (derived following Appendix B.3.3), plus an uncertain component that captures fluctuations in labor disutility due to variability in the local climate around its historical mean. This term, which we denote $\widetilde{D}_{cys}$

we exclude ECS values above the 99^{th} percentile and symmetrically exclude ECS values below the 1^{st} percentile, which results in 1,928 simulations being ruled out, leaving a total ensemble of 94,378 members.

for resampling s, is necessary in order to avoid conflating weather variability in our future projections with uncertainty caused by climate change.[117] Thus in the absence of climate change, individual consumption under resampling s is $C_{cys}^{NoClimateChange} = GDPpc_{c,y} - \widetilde{D}_{cys}$. While under the climate change projected for climate model l and emissions scenario p, individual consumption after subtracting labor disutility costs under resampling s is $C_{cylps}^{ClimateChange} = GDPpc_{c,y} - D_{cylps}$.

To convert these uncertain levels of individual consumption into a certainty equivalent, we use a constant relative risk aversion utility function $V(\cdot)$ with a coefficient of relative risk aversion set equal to 2.[118] We then compute certainty equivalent consumption with and without climate change. For consumption in the absence of climate change, we take the certainty equivalent over all resampled consumption values for a given impact region and year:

$$C_{cy}^{NoClimateChangeCE} = V^{-1}\Big(\frac{1}{S}\sum_{s=1}^{S} V(C_{cys}^{NoClimateChange})\Big), \tag{H.3}$$

where S denotes the total count of resampled values. For consumption under the climate change projected for a given climate model l and emissions pathway p, we similarly take the certainty equivalent over all resampled values:[119]

$$C_{cylp}^{ClimateChangeCE} = V^{-1}\Big(\frac{1}{S}\sum_{s=1}^{S} V(C_{cylps})\Big). \tag{H.4}$$

The certainty equivalent labor disutility costs of climate change are thus the difference between individual certainty equivalent consumption under no climate change and certainty equivalent consumption under climate change:

$$D_{cylp}^{CE} = C_{cy}^{NoClimateChangeCE} - C_{cylp}^{ClimateChangeCE}. \tag{H.5}$$

Total global labor disutility damages D_{ylp}^{CE} are obtained through a population-weighted sum of per capita labor disutility costs across all impact regions c.[120] Using these certainty

[117] To construct $\widetilde{D}_{cys}$, we calculate the change in annual labor disutility costs due to a given year's daily temperatures— where those daily temperatures are drawn from the 1981-2005 time period— relative to the mean temperature for each day over that same period.

[118] A large literature generally estimates that this coefficient is approximately equal to 2 (Arrow, 2007; Dasgupta, 2007, 2008; Weitzman, 2007, 2009).

[119] At this stage, we do not take a certainty equivalent over future climate uncertainty (i.e., across climate models) because the variation in global climate provided by the climate models is necessary to construct a global damage function for calculating damages from a marginal emission. Hence Equation H.4 only takes a certainty equivalent over resampled values *within* a climate model.

[120] National population projections are taken from the Shared Socioeconomics Pathways (SSP) and are

equivalent global damages and their associated $\Delta GMST$ values based on the year, climate model, and emissions scenario, we separately estimate a quadratic damage function in each year in the same manner as described in Section H.1, Equation H.1:

$$D^{CE}(\Delta GMST, y)_{ylp} = \psi_1^y \Delta GMST_{ylp} + \psi_2^y \Delta GMST_{ylp}^2 + \varepsilon_{ylp}. \tag{H.6}$$

The only difference between the estimation of Equation H.1 and Equation H.6 is that the latter is estimated through fewer points, as the multiple resampled realizations of damages for a given year, climate model, and emissions scenario are collapsed to a single certainty equivalent. However, it should be noted that this certainty equivalent damage function only values *econometric* uncertainty, and not physical uncertainty in the sensitivity of the global climate to emissions. To calculate a certainty equivalent partial SCC that reflects both econometric and physical sources of uncertainty, it is necessary to apply our certainty equivalent damage functions to the full distribution of parameters in the FAIR simple climate model, and value the resulting uncertain stream of damages from the marginal emission, as we do in the next subsection.

Certainty equivalent damages from the marginal emission The certainty equivalent partial SCC at year y_0 is defined as the certainty equivalent marginal social cost from increased labor disutility imposed by the emission of a marginal ton of CO_2 at y_0, holding all other factors fixed, including the forecast trajectory of baseline greenhouse gas emissions. Formally, for a discount rate δ, this is expressed as:

$$Partial\ SCC_{y_0}^{CE} = \sum_{y_0}^{2300} e^{-\delta y} \Big[\frac{d\hat{D}^{CE}(\Delta GMST, y)}{d\Delta GMST_y} \frac{d\widehat{\Delta GMST}_y}{dCO2_{y_0}} \Big]^{CE}. \tag{H.7}$$

Equation H.7 expresses the present discounted value of the certainty equivalent labor disutility damages imposed by the marginal emission at y_0, and differs in two important ways from the partial SCC expression in Equation H.2. In particular, the certainty equivalent partial SCC calculation: (i) uses the estimated certainty equivalent damage function estimated in Equation H.6, i.e., $\hat{D}^{CE}(\Delta GMST, y)$; and (ii) accounts for uncertainty in the FAIR simple climate model of how $\Delta GMST$ is perturbed by the marginal emission, i.e., $\frac{d\widehat{\Delta GMST}_y}{dCO2_{y_0}}$. Importantly, the trajectories with and without the impulse are both uncertain, due to uncertainty in the sensitivity of the global climate to emissions, and we characterize this uncertainty by resampling the parameters of FAIR to generate K pairs of realized trajectories (i.e., with and without the impulse). We use $\Delta GMST_{baseline^+,yk}$ and $\Delta GMST_{baseline,yk}$ to denote the realization $k \in \{1, \ldots, K\}$ in year y, with and without

allocated to impact regions based on current satellite-based within-country population distributions from Bright et al. (2012) (see Appendix B.3.4).

the impulse, respectively.

In the absence of climate change, total global consumption in future year y is assumed to be deterministic and equal to total global GDP ($GlobalGDP_y$). However, under climate change, consumption will be equal to GDP less the labor disutility damages associated with a given level of warming. Let $GlobalC_{baseline^+,yk}$ and $GlobalC_{baseline,yk}$ denote total global consumption under climate change with and without the impulse, respectively, at year y in realization k. Formally:

$$\begin{aligned} GlobalC_{baseline^+,y,k} &= GlobalGDP_y - \hat{D}^{CE}(\Delta GMST_{baseline^+,yk}); \\ GlobalC_{baseline,y,k} &= GlobalGDP_y - \hat{D}^{CE}(\Delta GMST_{baseline,yk}). \end{aligned} \tag{H.8}$$

Certainty equivalent (CE) consumption in year y, with and without the pulse, is thus:[121]

$$\begin{aligned} GlobalC^{CE}_{baseline^+,y} &= V^{-1}\Big(\tfrac{1}{K}\textstyle\sum_{k=1}^{K} V(GlobalC_{baseline^+,yk})\Big); \\ GlobalC^{CE}_{baseline,y} &= V^{-1}\Big(\tfrac{1}{K}\textstyle\sum_{k=1}^{K} V(GlobalC_{baseline,yk})\Big), \end{aligned} \tag{H.9}$$

where the certainty equivalent here is taken over climate sensitivity uncertainty, which is captured by the K resampled realizations of FAIR parameters.

Finally, subtracting $GlobalC^{CE}_{baseline^+,y}$ from $GlobalC^{CE}_{baseline,y}$ yields the certainty equivalent labor disutility damages at year y imposed by the marginal emission at y_0:

$$GlobalC^{CE}_{baseline,y} - GlobalC^{CE}_{baseline^+,y} = \Big[\frac{d\hat{D}^{CE}(\Delta GMST, y)}{d\Delta GMST_y}\frac{d\widehat{\Delta GMST}_y}{dCO2_{y_0}}\Big]^{CE}. \tag{H.10}$$

Taking the net present value of these certainty equivalent damages (i.e., Equation H.7) yields the certainty equivalent partial SCC for labor disutility.

H.4 Decomposing estimates of the partial social cost of carbon due to labor disutility by source of uncertainty

In the main text, Table 5 reports point estimate labor disutility partial SCCs, 1^{st}-99^{th} percentile ranges over a distribution of SCCs accounting for both damage function and climate sensitivity uncertainty, and certainty equivalent SCCs. In Table H.1, these results are expanded to include a decomposition of uncertainty into its two component parts. Specifically, Panel I shows the same point estimates and full uncertainty 1^{st}-99^{th} percentile ranges as in Table 5, but additionally includes 1^{st}-99^{th} percentile ranges accounting only

[121] Note that with a constant relative risk aversion utility function, only the percent loss from global GDP will matter for risk aversion. Hence the utility function can be directly applied to global consumption, without needing to first convert to per capita terms.

for damage function uncertainty (using a deterministic climate sensitivity) and 1^{st}-99^{th} percentile ranges accounting only for climate sensitivity uncertainty (using a deterministic damage function). We note that because the estimated damage function relationships between labor disutility costs and ΔGMST are nonlinear, and because the distributions of FAIR model parameters are not normal, the full uncertainty 1^{st}-99^{th} percentile ranges will not necessarily contain the corresponding ranges derived from one source of uncertainty alone. Panel II replicates the certainty equivalent partial SCC estimates also shown in Panel II of Table 5.

As is evident in Table H.1, uncertainty in climate sensitivity tends to dominate overall uncertainty in the labor disutility partial SCC, especially on the top end of the distribution. In contrast, while damage function uncertainty plays an important role, it is more influential over lower quantiles of the partial SCC distribution. This finding is consistent across distinct discount rates and emissions scenarios.

Discount rate	$\delta = 1.5\%$	$\delta = 2\%$	$\delta = 2.5\%$	$\delta = 3\%$	$\delta = 5\%$
			I. Partial SCC estimates		
RCP 8.5	\$28.8	\$16.7	\$10.6	\$7.2	\$2.4
Damage function uncertainty	[\$4.9,\$49.9]	[\$1.1,\$30.9]	[-\$0.7,\$21.0]	[-\$1.5,\$15.3]	[-\$2.1,\$6.5]
Climate sensitivity uncertainty	[\$4.3,\$222.9]	[\$2.6,\$132.0]	[\$1.8,\$83.9]	[\$1.3,\$56.1]	[\$0.5,\$14.5]
Full uncertainty	[\$0.2,\$215.3]	[-\$0.5,\$125.1]	[-\$0.9,\$77.7]	[-\$1.1,\$50.6]	[-\$1.4,\$12.1]
RCP 4.5	\$17.5	\$10.6	\$7.0	\$5.0	\$1.9
Damage function uncertainty	[-\$3.3,\$41.9]	[-\$3.6,\$26.9]	[-\$3.5,\$18.9]	[-\$3.3,\$14.3]	[-\$2.6,\$6.7]
Climate sensitivity uncertainty	[\$3.4,\$235.8]	[\$2.1,\$130.0]	[\$1.5, \$78.3]	[\$1.1,\$50.3]	[\$0.5,\$12.3]
Full uncertainty	[-\$2.4,\$229.8]	[-\$2.3,\$125.5]	[-\$2.3,\$74.4]	[-\$2.2,\$46.9]	[-\$2.0,\$10.7]
			II. Partial SCC estimates (certainty equivalent)		
RCP 8.5	\$50.8	\$29.1	\$18.0	\$11.9	\$3.2
RCP 4.5	\$39.7	\$22.5	\$13.9	\$9.3	\$2.7

Table H.1: Estimates of a partial social cost of carbon for labor disutility. All partial SCC values are for the year 2020, measured in PPP-adjusted 2019 USD, and are calculated from damage functions estimated from projected results under the socioeconomic scenario SSP3. Values shown assume a Frisch elasticity of labor supply of 0.5 (Chetty et al., 2011) and a labor share of income of 0.6 (Karabarbounis and Neiman, 2014). Point estimates displayed in Panel I rely on the median values of the four key input parameters into the climate model FAIR and a conditional mean estimate of the damage function; 1^{st}-99^{th} percentile ranges [in brackets] reflect damage function uncertainty, climate sensitivity uncertainty, or both damage function and climate sensitivity uncertainty (i.e., full uncertainty). Panel II displays certainty equivalent values of the partial SCC, which account for risk aversion using a constant relative risk aversion utility function with a coefficient of relative risk aversion equal to 2.

H.5 Alternative socioeconomic scenarios

In the main text, we display climate change impact projections and estimates of the partial social cost of carbon under the socioeconomic scenario SSP3. Each Shared Socioeconomic

Pathway (SSP) scenario models a different possible pathway of economic development, population growth, and demographics. In Table H.2, we show estimates of the labor disutility partial social cost of carbon under two alternative scenarios (SSP2 and SSP4, alongside SSP3). While results from these alternative scenarios are similar in magnitude to those from SSP3, we emphasize SSP3 in the main text because its historic global growth rates in GDP per capita and population match observed global growth rates over the 2000-2018 period much more closely than either SSP2 or SSP4 (Carleton et al., 2022).

Discount rate	$\delta = 1.5\%$	$\delta = 2\%$	$\delta = 2.5\%$	$\delta = 3\%$	$\delta = 5\%$
			I. Partial SCC estimates		
			SSP2		
RCP 8.5	\$85.0	\$40.0	\$21.3	\$12.6	\$3.2
	[\$4.5,\$593.7]	[\$1.3,\$284.3]	[\$0.0,\$151.9]	[-\$0.5,\$88.5]	[-\$1.2,\$16.8]
RCP 4.5	\$51.6	\$24.9	\$13.8	\$8.6	\$2.6
	[-\$2.0,\$741.2]	[-\$2.1,\$327.2]	[-\$2.1,\$162.4]	[-\$2.0,\$89.3]	[-\$1.8,\$15.5]
			SSP3		
RCP 8.5	\$28.8	\$16.7	\$10.6	\$7.2	\$2.4
	[\$0.2,\$215.3]	[-\$0.5,\$125.1]	[-\$0.9,\$77.7]	[-\$1.1,\$50.6]	[-\$1.4,\$12.1]
RCP 4.5	\$17.5	\$10.6	\$7.0	\$5.0	\$1.9
	[-\$2.4,\$229.8]	[-\$2.3,\$125.5]	[-\$2.3,\$74.4]	[-\$2.2,\$46.9]	[-\$2.0,\$10.7]
			SSP4		
RCP 8.5	\$27.8	\$15.8	\$9.9	\$6.7	\$2.2
	[-\$0.2,\$202.5]	[-\$1.0,\$113.3]	[-\$1.4,\$68.0]	[-\$1.6,\$42.9]	[-\$1.9,\$9.3]
RCP 4.5	\$18.5	\$11.0	\$7.2	\$5.1	\$1.9
	[-\$3.5,\$224.3]	[-\$3.2,\$117.7]	[-\$3.0,\$67.1]	[-\$2.8,\$40.7]	[-\$2.4,\$8.6]
			II. Partial SCC estimates (certainty equivalent)		
			SSP2		
RCP 8.5	\$143.4	\$67.0	\$35.1	\$20.3	\$4.1
RCP 4.5	\$123.2	\$55.8	\$28.6	\$16.3	\$3.4
			SSP3		
RCP 8.5	\$50.8	\$29.1	\$18.0	\$11.9	\$3.2
RCP 4.5	\$39.7	\$22.5	\$13.9	\$9.3	\$2.7
			SSP4		
RCP 8.5	\$45.1	\$25.3	\$15.4	\$10.0	\$2.4
RCP 4.5	\$38.2	\$21.0	\$12.6	\$8.2	\$2.1

Table H.2: Estimates of a partial social cost of carbon for labor disutility under alternative socioeconomic scenarios. All partial SCC values are for the year 2020, measured in PPP-adjusted 2019 USD, assuming a Frisch elasticity of labor supply of 0.5 (Chetty et al., 2011) and a labor share of income of 0.6 (Karabarbounis and Neiman, 2014). Estimates are calculated using constant annual discount rates ranging from 1.5% to 5%, either a very high (RCP8.5) or intermediate (RCP4.5) baseline emissions scenario, and socioeconomic scenario SSP2, SSP3, or SSP4. Point estimates displayed in Panel I rely on the median values of the four key input parameters into the climate model FAIR and a conditional mean estimate of the damage function; 1^{st}-99^{th} percentile ranges [in brackets] reflect climate sensitivity and damage function uncertainty. Panel II displays certainty equivalent values of the partial SCC, which account for risk aversion using a constant relative risk aversion utility function with a coefficient of relative risk aversion equal to 2.